

1-1-2015

Dna Aptamers Selected Against Wild-Type Helix 69 Ribosomal Rna And Their Implications In Combating Antibiotic Resistance

Sakina Miriam Hill
Wayne State University,

Follow this and additional works at: http://digitalcommons.wayne.edu/oa_dissertations

Recommended Citation

Hill, Sakina Miriam, "Dna Aptamers Selected Against Wild-Type Helix 69 Ribosomal Rna And Their Implications In Combating Antibiotic Resistance" (2015). *Wayne State University Dissertations*. Paper 1140.

This Open Access Dissertation is brought to you for free and open access by DigitalCommons@WayneState. It has been accepted for inclusion in Wayne State University Dissertations by an authorized administrator of DigitalCommons@WayneState.

**DNA APTAMERS SELECTED AGAINST WILD-TYPE HELIX 69 RIBOSOMAL RNA AND THEIR
IMPLICATIONS IN COMBATING ANTIBIOTIC RESISTANCE**

by

SAKINA MIRIAM HILL

DISSERTATION

Submitted to the Graduate School

of Wayne State University

Detroit, Michigan

in partial fulfillment

for the degree of

DOCTOR OF PHILOSOPHY

2015

MAJOR: CHEMISTRY (Biochemistry)

Approved by:

Advisor

Date

DEDICATION



I dedicate this to all seekers of truth.

ACKNOWLEDGEMENTS

I am indebted to the unwavering love and support of my family. I especially thank my mom, Audrey Renaye Allison, "Ummie", and my dad, Robert Stewart Allison for nurturing my curiosity through frequent visits to The Detroit Science Center (now Michigan Science Center), Belle Island Nature Center, and granting permission to travel for various state-wide internships and summer research science programs. Without their sacrifices and honesty, my longing to become a scientist would have only been a dream. I am also grateful for the encouragement and wisdom of my brother, Lateef Jamal Calloway, who taught me how important interpersonal skills are in life, and the love and strength of my great grandparents, Oscar "Moses" and Ruby Calloway, as well as their son, Lewis Ray Calloway and wife, Gloria Hill-Calloway. Their courage and strength to persevere against all odds helped to instill valuable qualities to last a lifetime. Next, destiny lead me to my patience and understanding husband, Clifford Samuel Simpson, and our four sons, Khalee Linzy Simpson, Clifford "Ajany" Simpson, Robert Taha Simpson, and Atta Aalee Simpson. They all have earned a doctorate for going through the ropes with me for the many years of sacrifices and summers at the lab. They have been a huge source of inspiration and motivation, even when juggling graduate school and family-life seemed to be a sweet dream trapped in a nightmare. Their importance is immeasurable, and I have undying love and appreciation for them all. I would also like to acknowledge Omar Mason for his thought provoking conversations on the properties of the universe and our roles within it, Adolf Allen Jr. (Abdul Fattah) and his daughter and nephew, Burujah Ismail and Fard Elijah Karim for their support, advice and encouragement. In their own special ways, my family has placed themselves in my shoes to provide their best advice and much appreciated support.

I emphatically acknowledge and thank my advisor, Professor Christine S. Chow, for spreading her love for scientific exploration of the nucleic acid world, patience, professionalism and motivation to seek scientific excellence and integrity. I respect her drive to encourage her students to challenge themselves, search in-depth for new approaches to solving problems, and seek answers to meaningful questions. I also appreciate her for allowing me to "roost" in her research laboratory nest the longest. Next, I am thankful to the scientists and professors of my dissertation committee, Louis J. Romano, Ph.D., Mary T. Rodgers, Ph.D. and Timothy L. Stemmler, Ph.D. for accepting my dissertation committee invitation, extending their time, understanding, professionalism and scientific expertise. Although I did not remain a graduate student of Dr. Pushpalatha Murthy at Michigan Technological University's Department of Chemistry, I am thankful for being accepted within her lab and being afforded the opportunity to simultaneously explore the RNA world, begin the challenges of graduate level scientific research, and learn the responsibilities of a chemistry teaching assistant. As a transfer student from MTU, my new dissertation research at WSU was supported by the chemistry department and the National Institutes of Health, GM058905-6, and the King, Chavez, Parks Future Faculty Fellowship (KCP Fellowship). Acknowledgements and gratitude are also due to both Joseph Dunbar Ph.D., and Rasheeda Zafar Ph.D., for challenging me to seek a greater understanding of the fundamentals of quality scientific research. After selecting me to become a fellow of the National Institutes of Health's Initiative for Minority Student Development Program, they were both instrumental in helping me effectively teach key concepts of chemistry to incoming undergraduate WSU freshmen students as well as present original research through professional presentations. Furthermore, I appreciate Philip Cunningham, Ph.D., and Andrew

Feig, Ph.D., for allowing me to use their DNA sequencing stations, even when it cost them additional money and time. Gail Richmond, Ph.D., and Thomas Deits, Ph.D., of Michigan State University's Department of Biochemistry are scientists that I am grateful for their mentorship within the MSU's High School Honors Program. They exposed me to an amazing hands-on approach to the world of nucleic acids and proteins and new software programs to explore their structures and functions. I am especially thankful to Dow Chemical Company's Toxicologist, William T. Stott, Ph.D., and Usha Vedula for unhesitatingly welcoming and mentoring me as a Dow Premier Scholarship from high school and throughout my undergraduate studies at Alma College. Alma College chemistry professors that I am indebted to for their support and opportunities to conduct independent research (*e.g.*, molecular biology, physical chemistry, and environmental chemistry in Egypt) are, Steven Wietstock, Ph.D., James Hutchinson, Ph.D., El-Maazawi, Ph.D., and Melissa Strait, Ph.D. I am also thankful to have been given professional and spiritual guidance and many laughs from my dear colleague from my internship at Dow Chemical in Freeport Texas, Sheikh Yasir Qadhi, Ph.D., before he successfully pursued Islamic studies after his academic career in Chemical Engineering. Mrs. Betty Chavis of Michigan Technological University is greatly appreciated for also being very instrumental in my financial ability to pursue a higher education through introducing me to the KCP Fellowship. Her encouraging words reminded me of the importance of caring for others and applying both values and principles of education and equality taught by Martin Luther King Jr. Ph.D., Rosa Parks, and Mr. Cesar Chavez.

Wayne State University has done an excellent job of admitting wonderful students that I feel fortunate to have shared meaningful scientific conversations, equipment, reagents, great

food, and laughter with. Firstly, past and present members of Professor C. Chow's lab members that I would like to thank are, Jean-Paul Desaulniers, Ph.D., Mina Sumita, Ph.D., Jason Kieltyka, Ph.D., Leo Lamsen, M.D., and especially Yogo Sakakibara Ph.D. for his patience whenever I began to extend our conversations into new dimensions. Furthermore, Papa Nii Asare-Okai, Ph.D., Moninderpaul Kaur Ph.D., Pei Wen Chao, Ph.D., and Mei Li, Ph.D., are colleagues that I would like to thank for bringing a human element to the countless optimization experiments that we each tried to perfect. I also appreciated the kindness and professionalism of dearly departed Chow Lab Group students, Uzo Azuh, for his gentle nature and sincerity, and Johannes Ghatnekar, for his bold personality and deep scientific conversations during our "tea-time" breaks. Most recently, I would like to thank current and former Chow Lab members, Hyosuk Seo, Gayani Dedduwa, Prabuddha Dodanduwa, Danielle Dremann, Daya Kharel, Bett Kimutai, Nisansala Muthunayake, Supuni Thalalla Hysok, Xun Bao, Yuqin Shang, M.S., Faddy Matti, Malak Abbas, and Mariem Alnaed, and enjoyed mentoring guest students, Desmond Parker and Alecia M. McCall, Ph.D., as they brought much positivity and enthusiasm for our dissertation research. Furthermore, I am very appreciative for Wayne State University post doctorates, Jay Herath, Ph.D., Jun Jiang Ph.D., and Alfonso Brenlla Ph.D., for extending their time and advice. Most importantly, I am forever indebted to The Creator of everything, The First, The Last, The Most Merciful, The Most Beneficent, The All Knowing, The Redeemer, The Greatest, and source of all knowledge and The Truth. Alhamdulillah. Ameen.

TABLE OF CONTENTS

DEDICATION.....	ii
ACKNOWLEDGEMENTS.....	iii
CHAPTER 1 - INTRODUCTION TO MODIFIED HELIX 69 RIBOSOMAL RNA AND ITS IMPORTANCE IN COMBATING ANTIBIOTIC RESISTANCE	1
1.1. Introduction: DNA, RNA, ribosomes, and protein synthesis.....	1
1.1.1. Deoxyribonucleic acids vs. ribonucleic acids	2
1.1.2. Basic structure and function of ribosomes.....	7
1.1.3. Protein synthesis.....	12
1.2. Pseudouridine and 3-methylpseudouridine: significance of modified nucleotides	16
1.3. Helix 69 (H69) motif of <i>Escherichia coli</i> 23S ribosomal RNA.....	19
1.3.1. Proposed roles of pseudouridine in H69.....	21
1.3.2. H69: significant contacts and functions	21
1.5. H69 as a viable biological target	29
CHAPTER 2 - SELECTING DNA APTAMERS	30
2.1. Background of SELEX and aptamers	30
2.2. Using systematic evolution of ligands by exponential enrichment (SELEX) for generating highly specific target-binding ligands.....	31
2.2.1. Experimental rationale of SELEX	32
2.2.2. Basic parameters and design.....	33
2.2.3. SELEX generated aptamers as highly specific binding ligands	33
2.3. Aptamers: novel therapeutics generated by <i>in vitro</i> selection	35
2.3.1. Basic properties and applications	35
CHAPTER 3 – PURPOSE: ISOLATION AND ANALYSIS OF DNA APTAMERS BY SELEX FOR H69..	37
3.1. Research proposal and thesis statement.....	37
3.2. Purpose and specific aims	40
CHAPTER 4 – EXPERIMENTAL APPROACH: SELECTION AND CHARACTERIZATION OF DNA APTAMERS FOR H69	42
4.1. Experimental design and methodologies	42

4.2. Approach to isolate and characterize DNA aptamers for H69 by monitoring diversity and percentage of library bound	42
4.3. Experimental procedures.....	45
4.3.1. Preparation of a randomized 84-nt oligonucleotide ssDNA library and DNA primers for SELEX	45
4.3.2. Preparation of H69 and biotin-H69	46
4.3.3. Preparation of Dynal® magnetic beads for immobilization of 5'-biotinylated $\Psi m^3 \Psi \Psi$ H69 rRNA	47
4.3.4. Preparation of single-stranded DNA library	47
4.3.5. Direct-bead PCR.....	49
4.3.6. Cloning and sequencing	52
4.3.7. Identification of sequence consensus by Clustal W and Mfold structure prediction.	54
4.3.8. Radiolabeling of wild-type H69 for electrophoretic mobility shift assays (EMSAs)....	54
4.3.9. Preparation of FAM-DNA	55
4.3.10. Fluorescence experiments and determining dissociation constants (K_d s)	56
CHAPTER 5 – RESULTS: CHARACTERIZATION OF DNA APTAMERS FOR H69.....	59
5.1. Biotin-strand capturing for separation of sense strand and non-sense strands confirmed by agarose gel analysis and super-shift assays	59
5.2. SELEX generated DNA aptamers against H69 with streptavidin-coated 96-well plates and Dynal® magnetic beads	60
5.3. Inverse proportionality of reduced diversity to increased percent DNA bound confirmed with each successive round.....	63
5.4. Sequencing and cloning results.....	63
5.6. Clustal W sequence analysis identified consensus sequences	65
5.7. Mfold analyses predicted diverse secondary structures for consensus sequences.....	67
5.8. Diversity of DNA structures.....	73
5.9. Dissociation constants for H69DNAapt18: binding to wild-type H69 observed by EMSA and fluorescence titration experiments.....	74
5.10. Fluorescence titration comparison binding studies: DNA aptamer #18 binding results.	79
6.1. SELEX optimization and DNA aptamer consensus sequences	85
6.2. Determination of selectivity and affinity of DNA aptamers for wild-type H69	86
6.3. Mfold structural analysis of DNA aptamers and potential kissing-kissing loop interactions between H69DNAapt18 and H69.....	89

CHAPTER 7 - FUTURE DIRECTIONS.....	95
7.1. Future directions: H69-DNA aptamer drug development	95
7.2. Applications of selected DNAs as probes.....	99
7.3. Counter-selection aptamers: SELEX against human H69 analog with DNA aptamers	100
APPENDIX.....	102
REFERENCES	150
AUTOBIOGRAPHICAL STATEMENT	170

LIST OF TABLES

Table 1.1 General properties of A-form, B-form and Z-form helices.....	6
Table 1.2 Nomenclature for pseudouridine family of post-transcriptionally modified nucleosides.....	17
Table 1.3 Antibiotic classes and modes of action.....	26
Table 4.1 Direct-bead PCR amplifications of H69-bound DNA library.....	51
Table 5.1 SELEX round diversity as a result of DNA pools challenged with 5'-biotinylated- $\Psi m^3\Psi\Psi$	64
Table 5.2 Average number of colonies and average efficiency of transformation of plasmid clones from select SELEX generated DNA ligands rounds.....	68
Table 5.3 Thermodynamic analysis of cloned and sequenced H69-aptamers.....	71
Table 5.4 Summary of apparent dissociation constants (K_d s) from EMSA binding experiments.....	79
Table 6.1 Comparison of dissociation constant K_d values of aptamer #18 binding to wild-type H69 and various rRNA motifs.....	88
Table 6.2 Comparison of dissociation constant K_d values of aptamer #18 binding to wild-type H69 and various rRNA motifs to H69 binding phage display generated heptapeptide, NQVANHQ-NH2 and aminoglycoside, neomycin.....	89
Table 6.3 Proposed base pairing of hairpin apex region of DNA aptamers duplexed with H69.....	93

LIST OF FIGURES

Figure 1.1 Purines present in both DNA and RNA	3
Figure 1.2 Schematic representation of the Watson-Crick (B form) DNA	4
Figure 1.3 Definition of sugars/furanoses puckering conformations in nucleic acids	5
Figure 1.4 Both DNA and RNA have structural diversity demonstrated by various motifs	8
Figure 1.5 Schematic representation of the Central Dogma of Molecular Biology	9
Figure 1.6 General features of ribosomal RNA	10
Figure 1.7 Eukaryotic versus bacterial ribosomal complexes	12
Figure 1.8 Overview of function of the ribosome during transcription and translation within a cell	14
Figure 1.9 Translocation within the ribosomal 50S and 30S subunits	15
Figure 1.10 Illustration of Isomerization of 1-ribosyluracil to pseudouridine	17
Figure 1.11 A schematic of the secondary structure of the 3' half of <i>E. coli</i> 23S RNA and locations of pseudouridine (Ψ) and 3-methylpseudouridine ($m^3\Psi$)	20
Figure 1.12 Significant ribosomal contacts by H69	22
Figure 1.13 Three different model views of H69	23
Figure 1.14 Continued emergence of antibiotic resistance	27
Figure 2.1 Overview of standard SELEX method	32
Figure 2.2 Example of DNA/RNA kissing complex motif	34
Figure 4.1 Experimental summary of research approach in eleven steps	43
Figure 4.2 Application of biotin linker for immobilization of H69	47
Figure 4.3 Confirmation of biotinylated DNA library by super-shift assay	50

Figure 4.4 Summary of SELEX procedure	52
Figure 4.5 Model analysis of electrophoretic mobility-shift assays (EMSA) for DNA ligands	56
Figure 5.1 Super-shift assay for biotin-strand capture for separation of the sense and antisense-strand	61
Figure 5.2 Results of preliminary binding of DNA library pools from SELEX rounds	62
Figure 5.3 Sequence results for DNA library	65
Figure 5.4 Clustal W multiple sequence alignment data report reveals consensus sequences of DNA library	66
Figure 5.5 <i>Mfold</i> family grouping results from SELEX with magnetic beads for aptamers #1-20	70
Figure 5.6 Conserved hairpin motifs of aptamers #8 and 18	72
Figure 5.7 <i>Mfold</i> structural analysis of untruncated aptamer #18	73
Figure 5.8 <i>Mfold</i> structural analysis of truncated aptamer #18	74
Figure 5.9 Preliminary EMSA binding results for DNA aptamer #16	76
Figure 5.10 Preliminary EMSA binding results for DNA aptamer #17	77
Figure 5.11 Preliminary EMSA binding results for DNA aptamer #18	78
Figure 5.12 Relative binding affinities of fluorescently labeled DNA aptamer #18 to A-site rRNA	81
Figure 5.13 Relative binding affinities of fluorescently labeled DNA aptamer #18 for UUU	82
Figure 5.14 Relative binding affinities of fluorescently labeled DNA aptamer #18	

for $\Psi\Psi\Psi$	83
Figure 5.15 Relative binding affinities of fluorescently labeled DNA aptamer #18	
for $\Psi m^3\Psi\Psi$	84
Figure 6.1 Conserved hairpin motifs and proposed interactions of H69 and truncated H69DNAapt18 and truncated H69DNAapt8	91
Figure 6.2 Hairpin motifs of aptamer versus target with kissing loop structure	92
Figure 6.3 Possible complementary base pairs of the proposed kissing-kissing loop-loop RNA/DNA duplexes of aptamers #8 and #18 bound to the apex region of H69	94
Figure 7.1 Structural comparison of bacterial versus human H69	101

CHAPTER 1 - INTRODUCTION TO MODIFIED HELIX 69 RIBOSOMAL RNA AND ITS IMPORTANCE IN COMBATING ANTIBIOTIC RESISTANCE

1.1. Introduction: DNA, RNA, ribosomes, and protein synthesis

Deoxyribonucleic acid (DNA) works in concert with polymerases, proteins, ribosomes, ribosomal RNA (rRNA), messenger RNA (mRNA), and transfer RNA (tRNA) to enable expression of genetic information, translation of proteins, and performance of essential cellular processes. Less than three decades following the deciphering of the structure of DNA, Thomas Cech and Sidney Altman were awarded the 1989 Nobel Prize in Chemistry for their ground-breaking discoveries of auto-catalytic RNAs, ribozymes isolated from *Tetrahymena thermophila*.¹ Cech *et al.* uncovered significant properties of RNAs after isolating and characterizing the complex structures of ribozymes and their abilities to self-splice their introns. Ribozymes changed the conventional view that only proteins performed enzymatic functions. Altman *et al.* demonstrated the broader implications of catalytic activity of RNA through observations of another ribozyme, ribonuclease P (RNase P), in catalytic splicing reactions without the assistance of ribo-proteins.² These breakthroughs suggested novel applications of nucleic acids within drug discovery, and the development of biomarkers, probes, diagnostics, and therapeutics. They have sparked greater interest in structure-function relationships of nucleic-acid-based motifs and their potential applications as novel therapeutics and in diagnostic technologies. As an introduction to this dissertation and its focus to develop novel applications of nucleic acids, it is important to first review the current knowledge of nucleic acids and ribosome structure-function roles *in vivo*, as well as the process of protein synthesis.

1.1.1. Deoxyribonucleic acids vs. ribonucleic acids

Nucleic acids were first discovered by F. Miescher in 1868,³ but it wasn't until more than eight decades later that a crystal structure of deoxycytidine, representing the first published molecular structure of a DNA nucleoside, was presented in 1951 by Furberg.⁴ This work laid the groundwork for subsequent nucleic acid structure studies, leading to our current understanding of the geometries of deoxy- and ribonucleosides.⁴ Two years later, the correct double-helical structure for deoxyribonucleic acid (DNA) was proposed by J. Watson and F. Crick, marking a new era for chemical and biological sciences.⁵ Analysis of DNA macro-molecular structures through X-ray crystallography diffraction maps generated by M. Watkins, and R. Franklin,⁶ the renowned Watson and Crick model of two anti-parallel chains of repeating subunits participating in intra-strand hydrogen bonding was proposed (**Fig. 1.1 and Fig. 1.2**).^{5,6} These hydrogen-bonding, base-pairing, and base stacking interactions of deoxy- and ribonucleotides were later explained as London dispersion forces⁷ attributed to hydrophobic effects within the intra-strands having stabilizing forces within pyrimidine and purine bases of DNA and ribonucleic acid (RNA) (**Fig. 1.1**). In addition to London dispersion forces, the Watson-Crick base-pairing model includes repeating molecular subunits of nucleotides, consisting of pentose sugars, phosphate groups, and heterocyclic amines, or nucleobases (**Fig. 1.1**).⁸

The nucleobases of DNA are derived from six-membered ring pyrimidines and five-membered ring purines. The most common purines of DNA are adenine (A) and guanine (G) that interact with the following major pyrimidines: cytosine (C) and thymine (T) (**Fig. 1.2**). Notably, a second group of nucleic acids of similar structure, ribonucleic acids (RNA), were later

characterized and found in abundance within the cytoplasm of the cells and viruses. The chemical structure of RNA is very similar to that of DNA, with two very important differences: (a) RNA contains the sugar ribose, while DNA contains deoxyribose (**Fig. 1.3**), and (b) RNA has the nucleobase uracil (U) whereas DNA contains thymine. Both DNA and RNA are vital cellular macromolecules that provide both structural and informational diversity. They are essential molecules for all kingdoms of life, and work synergistically to execute replication, translation, transcription, and even catalysis.⁹

guanine (G)	adenine (A)	cytosine (C)	thymine (T)	uracil (U)
(DNA and RNA)	(DNA and RNA)	(DNA and RNA)	(DNA)	(RNA)

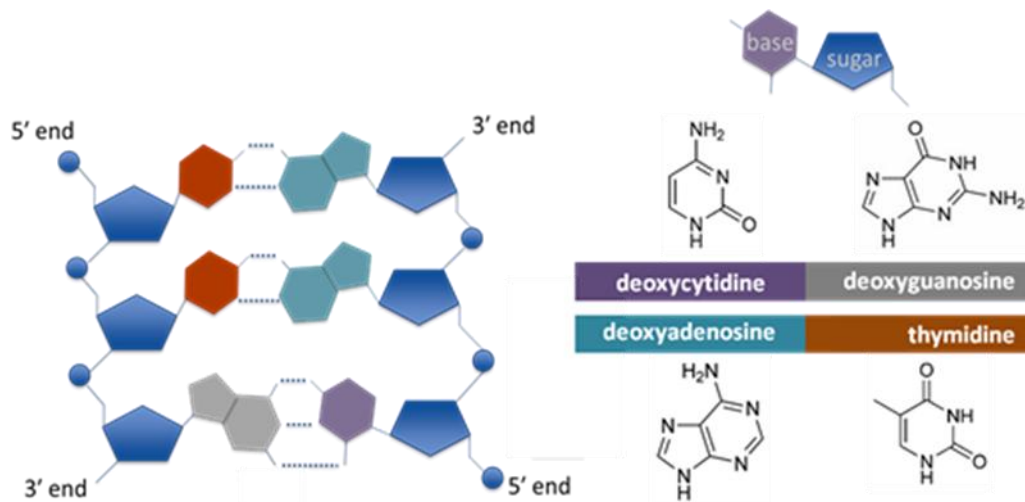


Figure 1.1. Purines present in both DNA and RNA. Adenine (A) and guanine (G) are present in both DNA and RNA. Cytosine (C) is the only pyrimidine present in both DNA and RNA. Thymine (T) is present in DNA, whereas uracil (U) is present only in RNA. The basic structural components of ribonucleic and deoxyribonucleic acid chains are shown. Watson-Crick base pairing by deoxyguanosine (gray) forms a triple hydrogen-bond base pair with deoxycytosine (purple), and deoxyadenosine (turquoise) forms a double hydrogen-bond base pair with thymidine (orange).

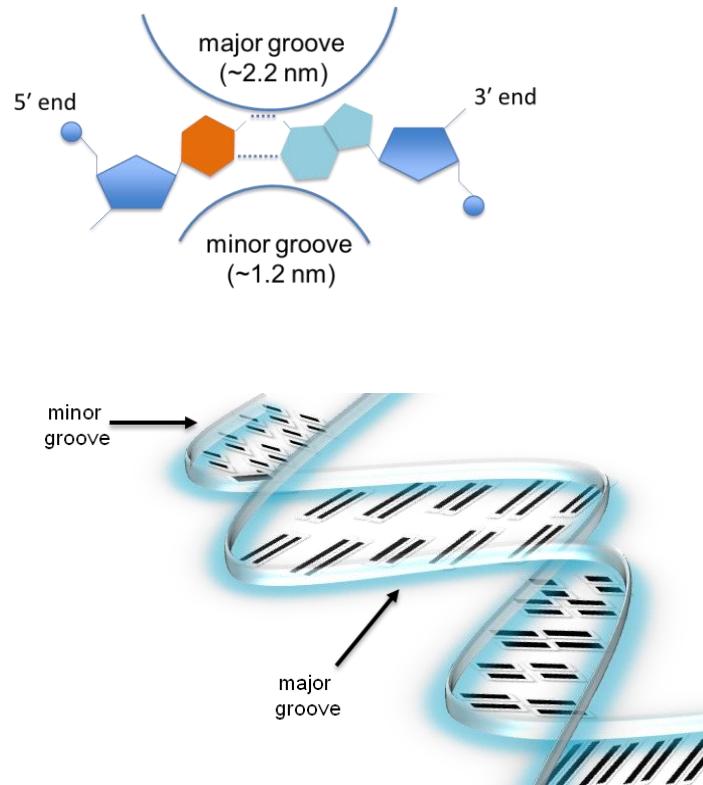


Figure 1.2. Schematic representation of Watson-Crick (B form) DNA. A double helical DNA cartoon model shows the major and minor grooves of the polynucleotide chains connected by complementary base pairing (double helix). The distance traveled along the helix axis for one complete helix turn, or 360° rotation, is the pitch (10 base pairs per turn), in which each base pair is twisted 36° clockwise with respect to the previous base pair. Grooves between the two sugar-phosphate backbones of the double helix have uneven spacing along the double helix and are labeled as the major and minor groove sides of the base pairs.¹⁰

In contrast to DNA, RNA molecules are typically single stranded and can adopt complex three-dimensional structures. Devoid of 2'-hydroxyl groups in its sugar moieties, RNA is stable against oxidative damage; however, DNA intrinsically has more chemical stability than RNA with regard to hydrolysis. Ribo- and deoxyribonucleosides furanose sugars (**Fig. 1.3a** and **Fig. 1.3b**) have two main non-planar modes of puckered rotations in envelope or twist forms, C3'-*endo*

(Fig. 1.3c) and C2'-endo (Fig. 1.3d), in contrast to the planar ring systems of pyrimidines and purines.¹¹

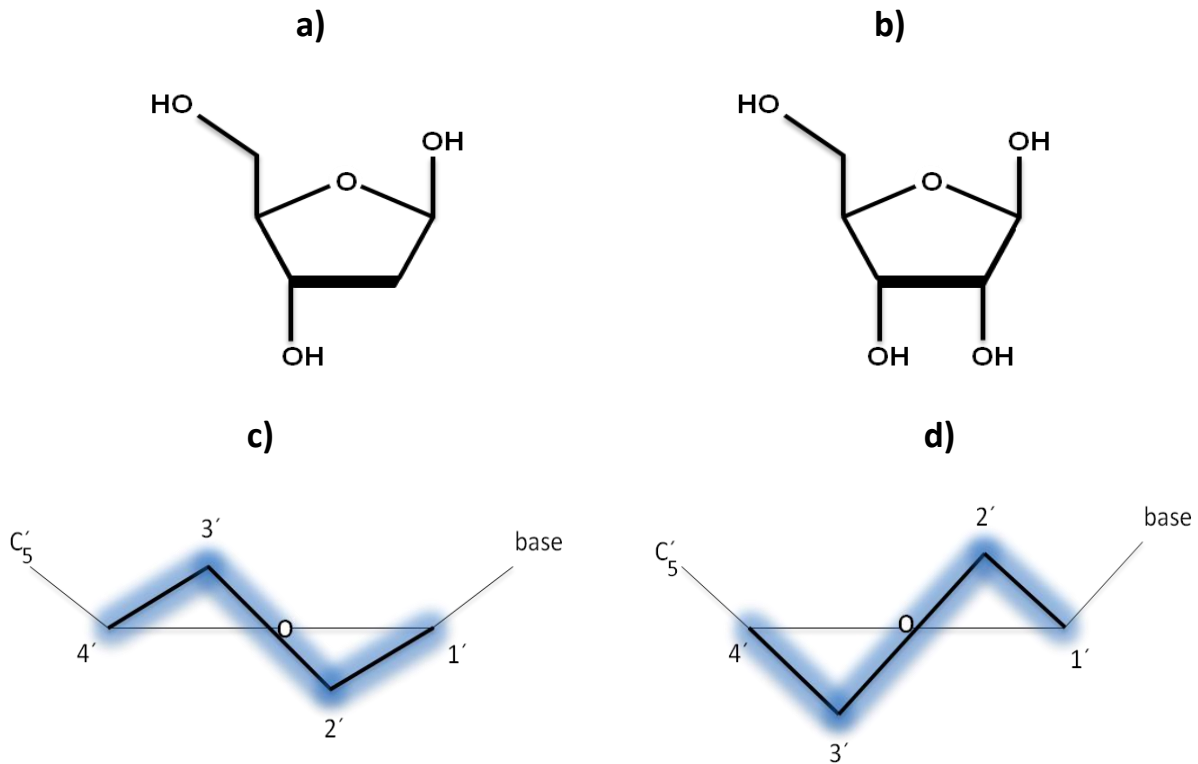


Figure 1.3. Definition of sugar/furanose puckering conformations in nucleic acids. These variations of sugar puckering are modes of pseudorotations of phase angles and torsion angles of furanose crystallographically determined by analysis of data of the most frequent modes of puckering.¹² This figure is a representation of the most frequently observed furanose pseudorotation angles, and they are commonly referred to as dominant puckering modes of deoxy- (a) and ribonucleosides (b), C3'-endo (c) and C2'-endo (d). Four of the five atoms are in a single plane and the fifth atom (c) C3'-endo or (d) C2'-endo positions are either on the same or opposite side of the plane relative to the C5' atom.

Molecular constraints of pentose sugars and phosphodiester linkages of the backbone chains of both DNA and RNA help to form complex secondary and tertiary structures often identified in

single- and double-stranded DNA and RNAs (**Fig. 1.4**). Notably, the presence of a 2'-hydroxyl group can hinder RNA from exhibiting long stretches of double-helical structures as seen in Z-, B-, and A-DNA (**Table 1.1**). Despite this fact, A-form RNA can mimic the structures of DNA helices by folding short stretches of single strands. Once various sensitive spectroscopic techniques were employed to further characterize RNA structures, unique three-dimensional motifs attributed to distinct biochemical processes emerged. Studies on RNA revealed an impressive array of structural variations and flexibilities.¹³

Table 1.1. General properties of A-form, B-form and Z-form helices.

Feature (DNA) ^[c]	A-form (DNA) ^[a]	A-form (RNA)	B-form (DNA) ^[b]	Z-form
Helical sense (handedness)	right	right	right	left
Sugar pucker conformation (purines)	C3'-endo	C3'-endo	C2'-endo	C3'-endo
Helix rise/ bp (Å)	2.6	2.8	3.4	3.7

Experimental conditions can give rise to different forms of helices in DNA and RNA. ^[a]A-form DNA formed under hydrated conditions. ^[b]B-form DNA formed under hydrated conditions. ^[c]Z-form DNA is observed under high-salt conditions.

Extensive and diverse tertiary structures emerged from studies to explore novel biomolecular interactions. A variety of structural motifs in both DNA and RNA, such as hairpin loops and stems that form between nearby self-complementary sequences, double/single-stranded regions, loop-loop kissing hairpin interactions, internal loops, junctions, bulges, and pseudo-knots (**Fig.1.4**).¹⁴

1.1.2. Basic structure and function of ribosomes

Although DNA and RNA are intrinsic components of eukaryotic and bacterial cells, it is important to note that they do not work alone in the processes of translating and transcribing genes into proteins; rather, macromolecular warehouses, such as ribosomes, house collective cellular processes with the ultimate goal of generating essential proteins for proper growth and function of an organism.¹⁵ Ribosomes are synthesized within the nucleolus of cells and can concentrate within the cytoplasm, chloroplasts, and mitochondria, and function as the backbone for many molecules during translation. The complex has room for binding protein-synthesis-enhancing molecules of various structures.¹⁶ Ribosomes, tRNA, and mRNA use the information of the genetic code to assemble thousands of functional proteins from amino acids. These protein products ultimately govern the function and metabolic activities of cells and performance of an organism.¹⁷ The ribosome houses a myriad of RNA-RNA and RNA-protein contacts that are critical for its function.

Ribosomes were first observed in the mid-1950s by cell biologist George Palade. He used electron microscopy to characterize cellular granules. The term *ribosome* was proposed by

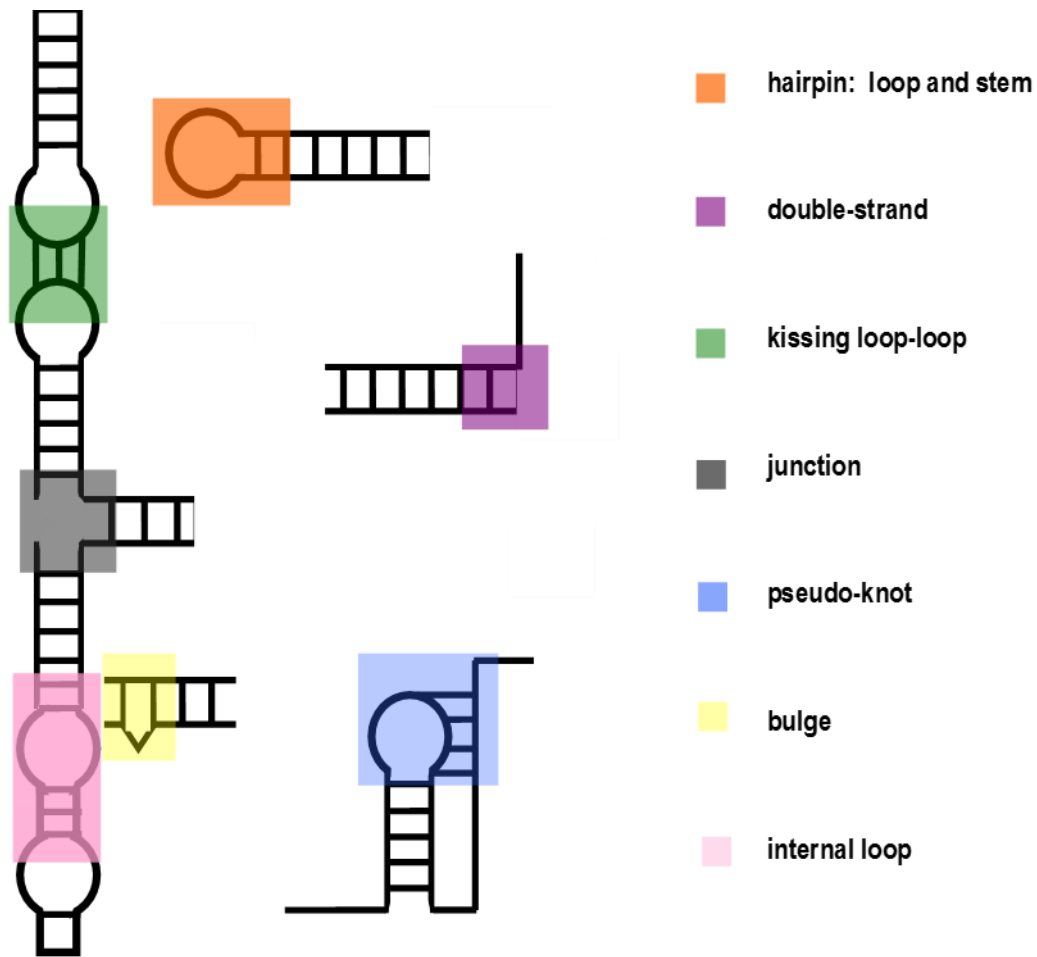


Figure 1.4. Both DNA and RNA have structural diversity demonstrated by various motifs.¹⁴

Richard B. Roberts in 1958.¹⁸ Since then, advancements in X-ray crystallography,¹⁹ electron cryomicroscopy (cryo-EM) techniques,²⁰ site-directed mutagenesis,²¹ immunoelectron microscopy²² and probing studies,²³ have provided a better analysis of the structures and functions of key components of ribosomes.²⁴ Assembled ribosomes comprise up to three rRNA molecules, and a variable number of proteins. Combinations of rRNAs and proteins form two unequally sized subunits characterized by Svedberg units of sedimentation rates (S) after centrifugation and are detailed by cryo-EM interpretations of the atomic structures of the

ribosome at moderate levels of resolution ($< 3.5\text{-}5.5 \text{ \AA}$) of *E. coli* 50S subunits.^{25,26} Probing studies with hydroxyl radicals assisted in the development of model systems of bacterial ribosomes.²³ The significance of ribosomes was suggested by Brenner, Jacob and Meselson,²⁷ and their key role in the Central Dogma of Molecular Biology was first proposed by Francis Crick.¹⁵ The Central Dogma of Molecular Biology (**Fig. 1.5**) summarizes the key processes of transcription and translation, which are essential for the replication and viability of eukaryotic and bacterial cells.



Figure 1.5. Schematic representation of the Central Dogma of Molecular Biology.¹⁵ An arrow from RNA to protein represents protein sequences being determined by RNA templates.

Early X-ray crystallographic data revealed the basic outlining shape of the bacterial and eukaryotic ribosomes. Structurally, an assembled ribosome displays a series of small grooves, tunnels, and platforms with the basic components of the large and small subunits (**Fig. 1.6**).²⁸ Ribosomal anatomy has been structurally categorized to include the following regions: (1) the central protuberance or head located on the 5S RNA; (2) a ridge; (3) the peptidyl-transferase center (PTC) for peptide-bond formation; (4) the stalk of the 30S subunit of the 23S RNA, composed of the ribosomal proteins and functioning as the binding site for ribosomal factors involved in translation; (5) the base of the stalk (containing proteins that function to simultaneously bind to RNA helices 43 and 44 (H43/44)); (6) the platform of the small subunit

and mRNA binding site; (7) the head of the 50S subunit with a groove containing translocation factors, peptidyl-transferase center, and the 5S RNA; and (8) the back and the front regions, representing the surface areas of the large and small subunits, respectively.²⁸

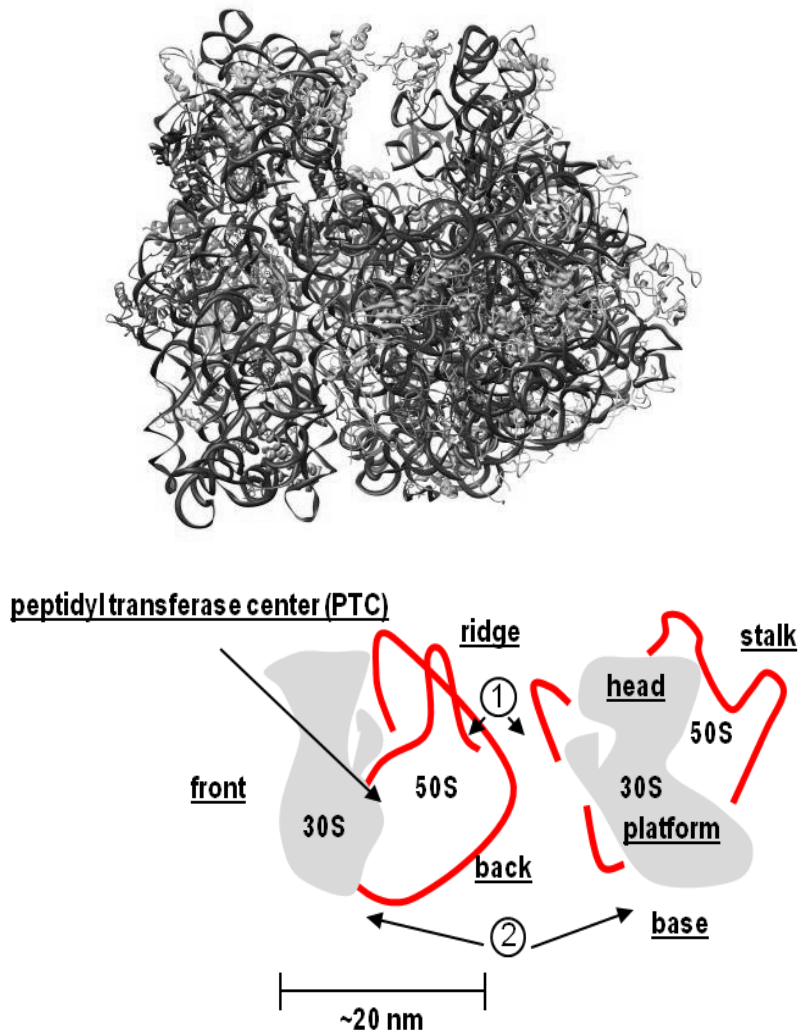


Figure 1.6. General features of ribosomal RNA. Roughly 20 to 30 nanometers in diameter, ribosomes are large RNA-protein complexes. A detailed X-ray crystallography view of the interface between the small and large ribosomal subunits and the conformation of the peptidyl-transferase center in the context of the intact bacterial ribosome (70S) from *Escherichia coli* is shown at a resolution of 3.5 Å (PDB ID 4V4Q). Below this figure is an image outlining the following key ribosomal components: ridges (circled 1), stalk, head, platform, back (circled 2), front, base, and peptidyl-transferase center of this complex.²⁸

As a separation tool to analyze ribosomal components, ultracentrifugation yields intact or whole ribosomes (70S) as well as the separated large (50S) and small subunits (30S) (**Fig. 1.7**).²⁹ Early X-ray crystallographic data revealed the basic outlining shape of the bacterial and eukaryotic ribosomes and included their basic components. Various atomic-resolution ribosome structures have been solved for the 30S and 50S subunits as well as the whole 70S ribosome. The ribosomes from diverse species, including *Escherichia coli*,³⁰ *Haloarcula marismortui*,³¹ and *Thermus thermophilus* have been crystallized.^{32,33} Noller and colleagues published results with complete bacterial ribosomes with more than 50 different proteins.³⁴ The laboratories of Steitz, Noller, Ramakrishnan, Yonath, Cate, and Yusupov, have revolutionized our understanding of the ribosome through X-ray crystallography.^{33-38,40} Yusupov *et al.* solved a 5.5-Å resolution structure of the complete ribosome incorporating tRNA and mRNA.³⁴ High-resolution structure studies provided the opportunity to more closely examine other features within the ribosome such as the aminoacyl (A), peptidyl (P), and exit (E) sites (**Fig. 1.8**). Ribosomal structural studies using cryo-electron microscopy, X-ray crystallography, and scanning microscopy, lead to refined structures and deeper insights into their remarkable structures and functions,³⁵ resulting in researchers V. Ramakrishnan,³⁶ T. Steitz,³⁷ and A. E. Yonath³⁸ being awarded the Nobel Prize in Chemistry (2009) for significant advancements in the knowledge of structure and function of ribosomes from X-ray crystallography maps of the positions for hundreds of thousands of ribosomal atoms at the atomic level.

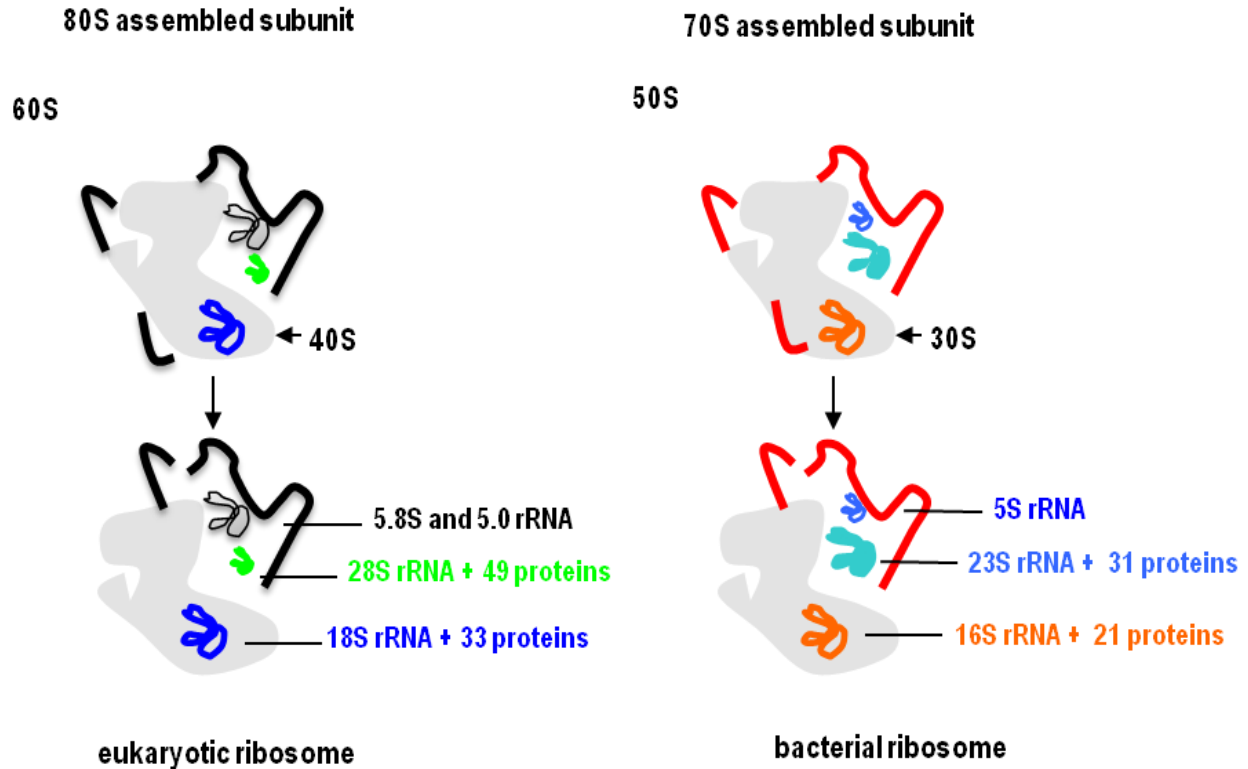


Figure 1.7. Eukaryotic versus bacterial ribosomal complexes. The large and small subunits of the ribosome form inter-subunit bridges to create an assembled ribosome. Eukaryotes have a complete assembled 80S monosome comprising a 40S small subunit (SSU) that includes the 18S rRNA of 1900 nucleotides (nt), and a 60S large subunit (LSU) composed of 120-nt 5S rRNA, and a 4718-nt 28S RNA, and a 160-nt 5.8S subunit that is bound to ~49 proteins.³⁶ The two units comprising the bacterial 70S ribosome are the small (30S) and large (50S) subunits. The 30S subunit has a RNA subunit of 1540-nt bound to 21 proteins, whereas the 50S subunit consists of a 120-nt 5S rRNA and a 2900-nt 23S rRNA bound to 34 proteins.³⁹

1.1.3. Protein synthesis

Collectively, S. Brenner, F. Jacob, and M. Meselson determined through radioactive tracing methods, or “pulse-chasing” basic mechanisms of how ribosomes enable protein synthesis (**Fig. 1.8**), the “missing link” of the Central Dogma of Molecular Biology.²⁷ Noller was the first to show that rRNA plays a crucial role in the catalysis of peptide-bond formation.⁴⁰ The ribosomes,

are the hosts for the translation process within cellular organelles. The average number of ribosomes within growing *E. coli* cells is ~20,000;⁴¹ and protein synthesis on one *E. coli* ribosome occurs at an impressive rate of 21 amino acids/second.⁴² Overall, the intrinsic components of eukaryotic and bacterial cells have been identified and extensively studied through atomic-scale resolution of the ribosome, as mentioned in the previous section; however, there are additional specialized features found within the ribosome complex that scientists are still studying in order to gain greater insight into their proposed roles, dynamics, structures, and key interactions with other macromolecules (*i.e.*, proteins, tRNA, mRNA).

RNA polymerase directs the process by which mRNA copies a gene. The process of translation can be summarized in five general steps: (1) activation of transfer RNA with *N*-formyl-methionine, (2) initiation, (3) elongation, (4) termination, and (5) post-translational processing.⁴³ This process begins with mRNA molecules copying instructions from chromosomal DNA, followed by various amino acids as building blocks of proteins, being carried to the ribosome by tRNA thereby initiating polypeptide chains synthesis in a specific sequence and order. From high-resolution structures of the *E. coli* ribosome, translocation events can be monitored, subsequently involving movement of mRNA and tRNAs over a distance of ~50 Å in crystal structures on the ribosomal subunits⁴⁴ providing data from directed hydroxyl radical probing and cryo-EM studies.^{45,46} Initiating protein synthesis, tRNA has an *N*-formyl-methionine (fmet) that recognizes the AUG codon through its UAC anticodon. The tRNA^{fmet} binds in the

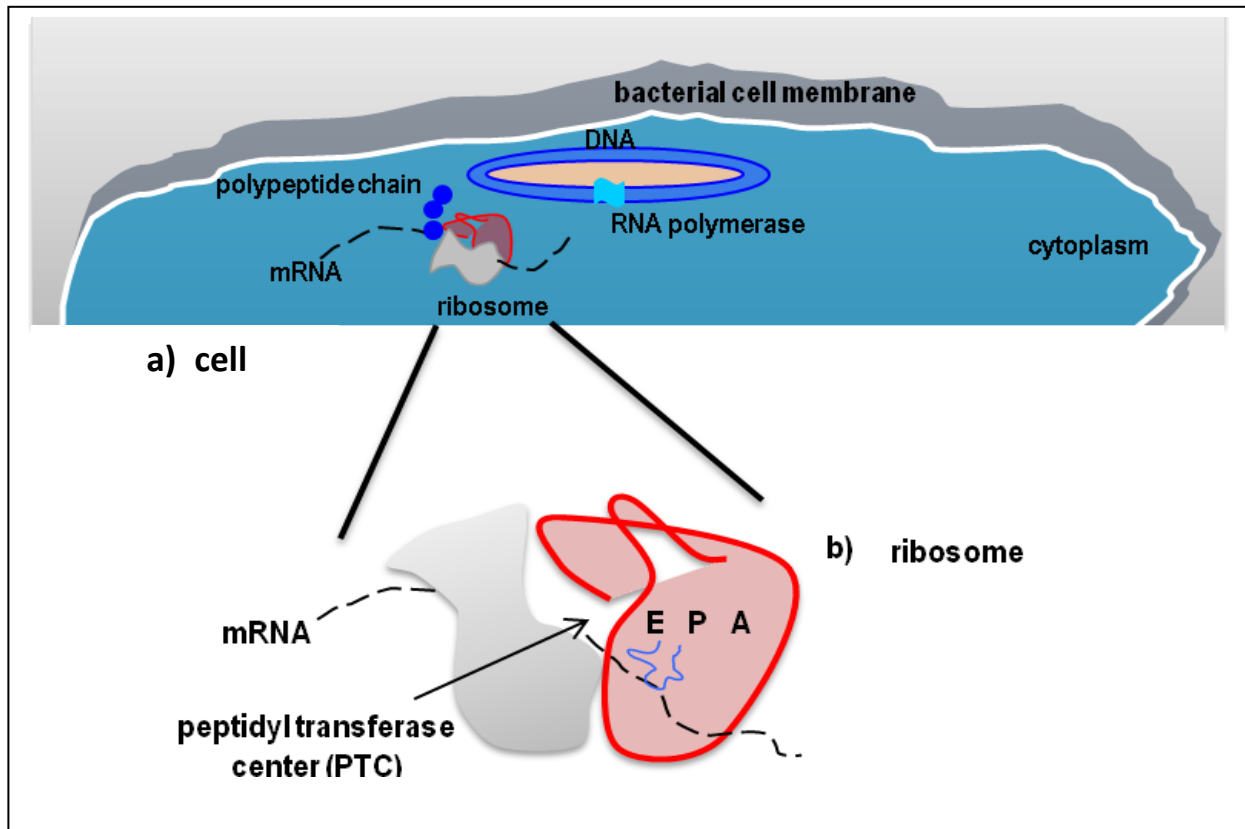


Figure 1.8. Overview of the function of the ribosome during transcription and translation within a cell. (a) Transcription and translation are shown in a bacterial cell. (b) The large and small ribosomal units at the beginning of protein translation in the peptidyl-transferase center and E, P, and A represent the exit, peptidyl, and acceptor sites of the ribosomal RNA, respectively. The clover-leaf structure of the initiating tRNA is shown in blue with its anticodon binding to the starting codon of the messenger mRNA.

P site.⁴⁷ The next step is for a second tRNA to approach the mRNA in the A site and start growth of the peptide chain.⁴⁷ The A site needs to be vacated in order to bind the next aminoacyl-tRNA to the ribosome.⁴³ In the final stage, the newly formed peptide chain dissociates from the ribosome upon hydrolysis at the last amino acid. Throughout these aforementioned steps, the ribosome holds the tRNAs in different conformations within its binding sites, to subsequently

pass through the A, P, and E sites located at the interface between the two subunits of the ribosome.⁴⁸

Processes of initiation, elongation, and termination are repeated to allow more proteins to be synthesized (**Fig. 1.9**). First, a correct match with the anticodons of a tRNA needs to be identified to form a peptide bond, thus initiating the formation of a peptide chain to encode for a protein. Next, elongation of the peptide begins and an appropriate tRNA reads the next codon. The translocation, or movement of tRNA within the ribosomal 50S and 30S subunits, includes a peptidyl-transferase reaction and movement of a peptidyl tRNA to the large subunit from the P and A sites to the E and P sites, respectively, while their anticodon ends remain bound to the small subunit (**Fig. 1.9**).^{49,50} Finally, termination of protein synthesis occurs when a stop signal codon is reached on the mRNA.

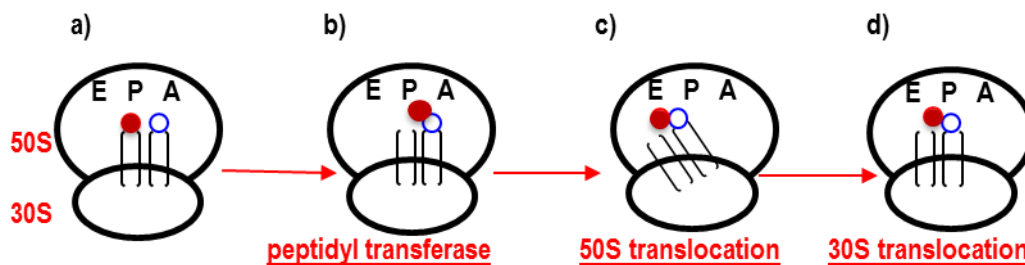


Figure 1.9. Translocation within the ribosomal 50S and 30S subunits. A peptidyl tRNA is located in the P site (solid red circle) and aminoacyl tRNA is in the A site (open blue circle) (**a**). The colored circles represent the amino acids attached to the 3' ends of the tRNAs. After peptide-bond formation, deacylated tRNA is in the P/P state and peptidyl tRNA extended by one amino acid is in the A/A state (**b**). The acceptor ends of the deacylated tRNA and the peptidyl tRNA are spontaneously translocated relative to the 50S subunit, resulting in P/E and A/P hybrid states, respectively (**c**) followed by movement of the anticodon and deacylation of the tRNA becomes deacylated (**d**).^{51,52} Note abbreviations: aminoacyl (A), peptidyl (P), and exit (E) sites.

1.2. Pseudouridine and 3-methylpseudouridine: significance of modified nucleotides

Database entries of more than 100 published naturally occurring modified nucleotides⁵³ are frequently updated; however, many of their biological functions are just beginning to be elucidated.⁵⁴ An array of structural diversity of post-transcriptional modifications for RNA exist (**Table 1.2**). Nearly all functionally important RNA molecules, including rRNAs, tRNAs, and mRNAs, contain nucleotide modifications.⁵⁵ Evidence of the importance of methylation within RNA was acknowledged in recent studies on *N*⁶-methyladenosine (m⁶A), the most prevalent internal (non-cap) modification present in the mRNA of all higher eukaryotes.⁵⁶ The exact role(s) of m⁶A modification remains to be determined; however, recently published work highlights its importance in basic biological functions, disease, cell viability, and development, including newly discovered roles in translation status and lifetimes of mRNA.⁵⁴ Furthermore, both natural and synthetically produced modified nucleosides and nucleotides such as 5'-*O*-(1-thio)-nucleoside triphosphate^{57,58} and 2-aminopurine ribonucleoside⁵⁷ have significance in biochemical regulation and applications in chemistry, pharmacology and biochemistry as probes to study RNA structure, function and conformational changes, respectively.⁵⁹

Of the known naturally occurring modified nucleotides, pseudouridine (5-β-D-ribofuranosyluracil; Ψ; psi) constitutes 8% of the uridines found in the large subunit rRNAs (**Fig. 1.10**).⁶⁰ Although detailed structural and functional dynamics of the ribosome, its role in protein synthesis, and the locations of modified nucleotides in the rRNA have been extensively reported, further deciphering of the importance of nucleotide modifications and their impact on eukaryotic and bacterial translation still remains.⁶¹ As nature's most abundant modified

base, Ψ has been identified in many different types of RNAs.⁶² Discovered by Davis and Allen in 1957, Ψ is the C-glycosidic isomer of uridine⁶³ and was structurally characterized by Cohn.⁶⁴ Despite its known presence for many decades, the biological roles of Ψ have remained poorly understood.^{65,66} Notably, Ψ was the first modified nucleoside identified in cellular RNA, and later shown to be broadly distributed in all kingdoms of life,⁶⁷ including archaeobacteria, eubacteria, and eukaryotes (RNA Modification Database and Modomics Database).⁶⁷

Table 1.2. Nomenclature for pseudouridine family of post-transcriptionally modified nucleosides.

Common Name	Symbol
pseudouridine ⁶⁷	Ψ
1-methylpseudouridine ⁶⁸	$m^1\Psi$
2'-O-methylpseudouridine ⁶⁹	Ψm

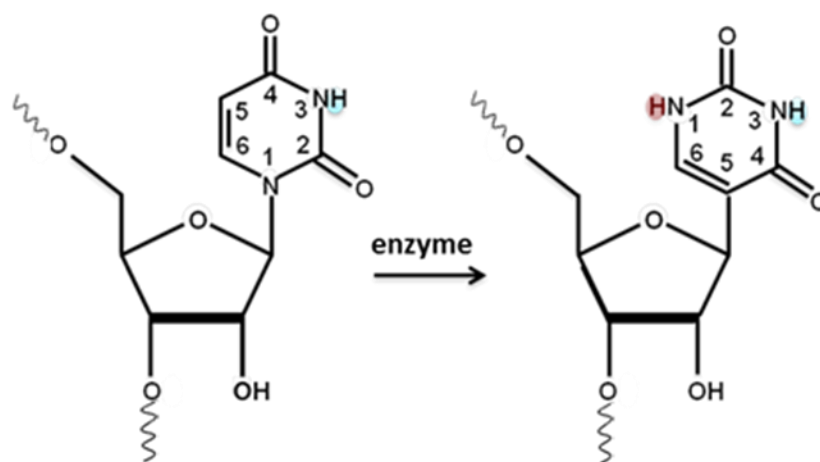


Figure 1.10. Illustration of isomerization of 1-ribosyluracil to pseudouridine.⁶⁷

Typical of most modified nucleotides, Ψ arises by site-specific, enzymatically catalyzed modification of uridine within RNA by Ψ synthases (*i.e.*, enzymes responsible for isomerization).⁷⁰ This post-transcriptional process is termed pseudouridylation.⁶² Derivatives of

Ψ , such as 3-methylpseudouridine ($m^3\Psi$), are also found in nature.⁷¹ In comparison to uridine, Ψ shows inherent structural differences; more specifically, Ψ typically has a 3'-*endo* sugar pucker and can participate in more extensive base-stacking interactions.⁷² The C-C glycosidic linkage also gives Ψ more conformational flexibility and rotational freedom.⁷³ Furthermore, Ψ has an extra hydrogen-bond donor ($\Psi N1H$) that can participate in interactions with neighboring groups.⁷⁴ Within an RNA helix, a $\Psi N1H$ H-bond can also form with a water molecule to bridge with the preceding phosphate group.⁷⁵ Such an interaction could alter RNA stability and impact its functions *in vivo*.

Although some functional roles have been attributed to modified RNAs, the majority of them appear to serve in fine-tuning and regulating RNA structure.⁷⁶ The locations of modified nucleotides tend to cluster at sites of functional biological importance, *e.g.*, the anticodon loop of tRNA,⁷⁷ the PTC of the large subunit rRNA,⁷⁸ and the decoding region of the small ribosomal subunit.⁷⁸ Naturally found RNAs (*i.e.*, tRNAs, rRNAs, and spliceosomal small nuclear RNAs (snRNAs)) have been reported to contain Ψ s; and it appears abundantly clustered within the PTC with conservation over a broad range of organisms, originally suggesting its potential significance with respect to protein synthesis.⁶⁵

1.3. Helix 69 (H69) motif of *Escherichia coli* 23S ribosomal RNA

There are six large domains within *E. coli* 23S rRNA that form intricate, compact, and unique secondary and tertiary structures (**Fig. 1.11**).³² Of great importance to this study is the 1920-stem-loop region of domain IV of *E. coli* 23S rRNA, commonly referred to as helix 69 (H69), which has been found to be a highly conserved motif localized at the inter-subunit bridge region of the ribosome (**Fig. 1.11**).³⁵ Inter-subunit bridges were identified by footprinting and chemical modification experiments and later confirmed by cryo-EM and crystallographic studies of the domains that undergo molecular motion during protein synthesis and participate in both RNA-RNA and protein-RNA contacts between the large and small ribosomal subunits.^{79,80}

The inter-subunit bridge known as B2a in *E. coli* 70S ribosomes involves both the large (50S) and small (30S) subunit rRNAs, with H69 positioned directly at the interface of the two subunits (**Fig. 1.12a**). There are nine Ψ s in *E. coli* 23S rRNA (**Fig. 1.12b**). This dynamic region of the 23S ribosome contains two Ψ s at positions 1911 and 1917 and an $m^3\Psi$ at position 1915 (**Fig. 1.12b**).⁸¹ H69 also contains a G•U mismatch in the stem region, which displays greater base-stacking overlap on the 5' side of U than with the Watson-Crick base pairs (**Fig. 1.12b**).

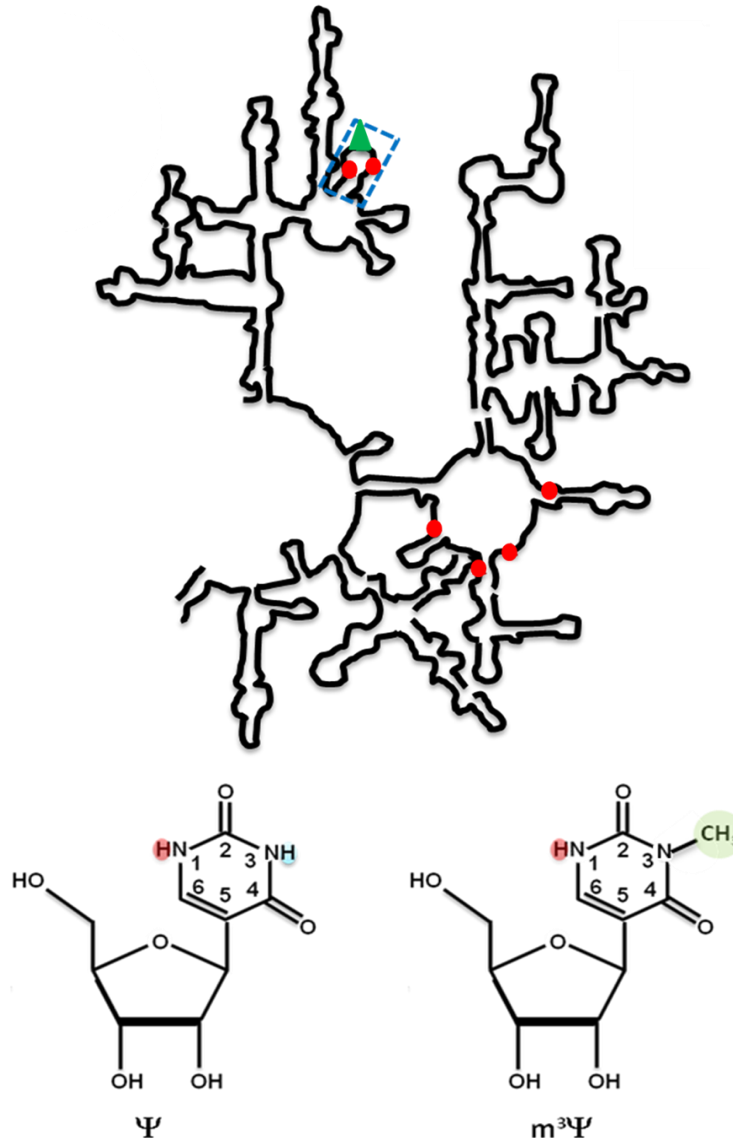


Figure 1.11. A schematic of the secondary structure of the 3' half of *E. coli* 23S rRNA and locations of pseudouridine (Ψ) and 3-methylpseudouridine ($m^3\Psi$). A map of domain IV of *E. coli* 23S rRNA is shown with the location of the H69 stem-loop region enclosed by a dotted rectangular blue box (the 5' half is not shown). The positions of the pseudouridines and 3-methylpseudouridine are labelled as follows: Ψ (red circle) and $m^3\Psi$ (green triangle). The image is adapted from (<http://www.rna.icmb.utexas.edu>).⁸⁰

1.3.1. Proposed roles of pseudouridine in H69

Ofengand noted that Ψ 1917 is likely to have a unique function, because results from the deletion of the three conserved Ψ s in H69 showed only position 1917, which is universally conserved, to have a strong effect.⁸¹ Similar studies by Liiv *et al.* revealed that *E. coli* ribosomal activity is affected by modifications in the loop region of H69; mutation of Ψ 1917C, but not Ψ 1911C or Ψ 1915C, caused inhibition of polysome formation and translation.⁸² Their findings implied that pseudouridylation of U1917 might have a special role in ribosome synthesis. These studies highlight the significance of Ψ in bacteria. A similarly important role of Ψ in eukaryotic systems was highlighted in yeast mutational studies by Liang *et al.*⁸³ Their results showed that blockage of one to two of H69's five Ψ s have no detectable effects on cellular growth; however, loss of three to five modifications impaired growth and caused ribosomal defects. In the absence of Ψ , levels of rRNA and amino-acid incorporation *in vivo* were reduced to a range of 20 to 60%.⁸⁴ Consequently, the observed major effects of loss of modification in H69 indicate that the modified bases influence both ribosome synthesis and function in synergistic ways.⁸⁴

1.3.2. H69: significant contacts and functions

The ribosome has subunits that connect through inter-subunit bridges, offering a channel for mRNA to flow through and tRNA to dock to the acceptor (A), peptidyl-transferase (P), and exit (E) sites (**Fig. 1.12 and 1.13**). As one of the 12 known inter-subunit bridges studied by Yusopov and co-workers, bridge B2a of the large subunit protrudes and makes contact with helix 44 (h44) of the smaller subunit, also referred to as the decoding region.⁷⁹

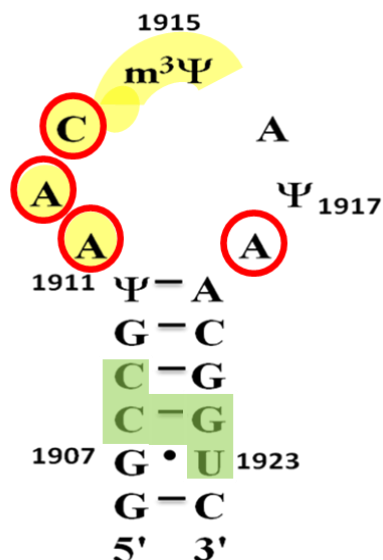


Figure 1.12. Significant ribosomal contacts of H69. Universally conserved H69 contacting the A-site region known to be the acceptor site (yellow) and P-site (green) tRNAs. Four residues of H69 have contact with the 30S subunit (red).⁸⁴

Schuwirth *et al.* revealed additionally important subunit contacts by H69 in crystal structures of the *E. coli* 70S ribosome at 3.5 Å.⁸⁵ Consequently, this work supports a view that H69, as a part of bridge B2a, has significant structural flexibility and may be involved in signal transmission between the two subunits at different stages of translation.⁸⁸ Another major finding is that H69 can function as what appears to be a molecular relay mechanism or communication pathway between the large and small subunits. H69 dynamics includes movement between two different conformations while protruding from the surface of the large subunit to interact with the small subunit and simultaneously participating in subunit association (**Fig. 1.13a**).⁸⁶

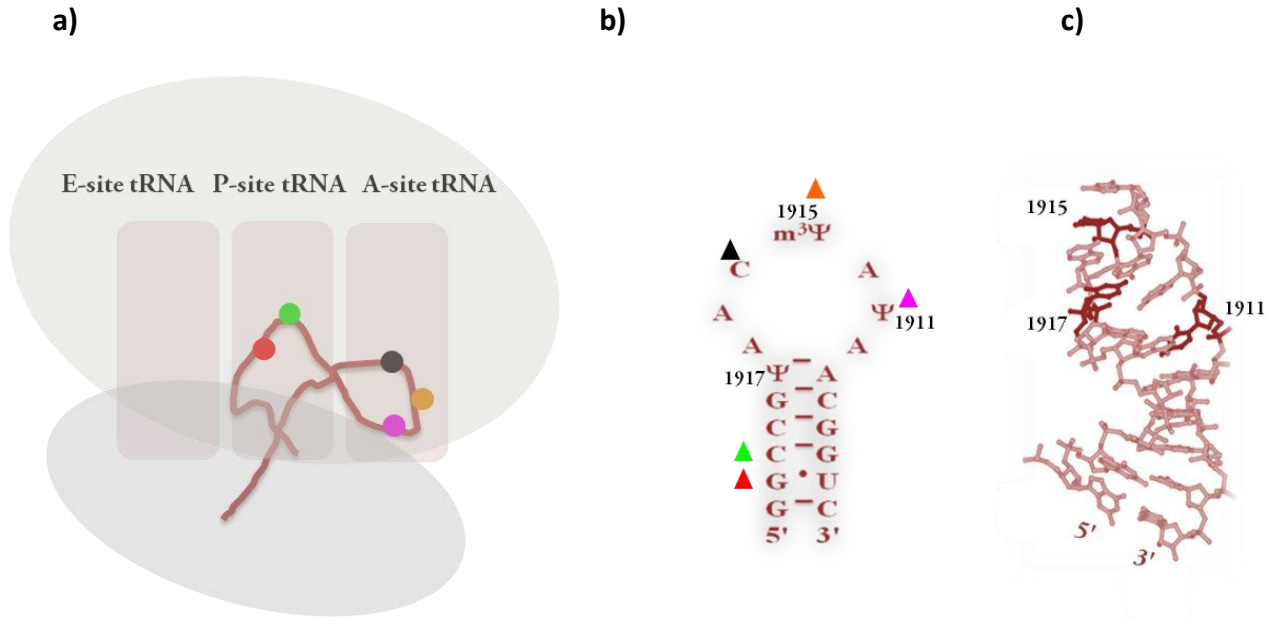


Figure 1.13. Three different model views of H69. (a) A closer view of H69 within the ribosome. Cryo-EM studies of *E. coli* ribosomes revealed that H69 is a component of both the A- and P-tRNA binding sites within the large 50S subunit where the inter-subunit bridge B2a is located.^{87,88} Important nucleotide contacts are shown as colored circles; H69 simultaneously contacts the P-site tRNA (red and green), and the A-site tRNA (black, orange, and pink).⁹¹ The D-stem junction of the A-site tRNA by the loop residues 1913 - 1915 as well as the P-site tRNA binding site by backbone-backbone interactions with stem nucleotides 1908, 1909, and 1922, corresponding colored triangles match colored circles in the P-site and A-site tRNA binding sites of the ribosome.¹⁰³ Triangles indicate Ψ or m³Ψ (b). H69 from the structure of the 50S ribosomal subunit of *Deinococcus radiodurans* (identical to that of *E. coli*), (c) generated with PyMOL (DeLano Scientific), modelled with unmodified uridines (PDB entry 1NKW).⁸⁹

Additional dynamic shifting movements of H69 were observed by Ramakrishnan and co-workers in a 2.8-Å-resolution structure of *T. thermophilus* 70S ribosomes.³³ Complexed with mRNA and tRNA, H69 was observed to be dynamic as it shifted toward the 30S subunit with outward base flipping of residue A1913, thus forming a hydrogen bond to the 2' hydroxyl of

ribose 37 of the A-site-bound tRNA anticodon stem–loop.⁹⁰ These conformational changes included the displacement of H69 during the dissociation step of protein synthesis.⁹⁰ Specific pH-dependent changes in synthetic, modified H69 constructs were observed through circular dichroism spectroscopy, thermal melting analysis, and NMR spectroscopy, providing further evidence that H69 is both structurally and functionally dynamic in solution.^{33,90}

Studies conducted by Wilson *et al.* helped to further reveal the essential roles of H69 in subunit association through RNA-RNA and RNA-protein interactions when they reported their findings of both H69-RNA and H69-protein contacts during translation termination.⁹¹ Specifically, ribosome structures have also revealed H69 interactions with proteins required for the final release step of protein translation, and recycling factors (RRF)⁹¹ necessary for promoting the dissociation of the large and small ribosomal subunits.^{92,93,94} Wilson *et al.* published their findings of RRF contacting H69 and the subsequent resulting conformational changes in the bridge B2a.⁹¹ Their study revealed contacts between H69 and RRF involving highly conserved amino acid residues E122 and V126 as they interacted with m³Ψ1915 of H69, and as V130 interacted with A1916.⁹¹ Ultimately, these H69-protein and H69-RNA interactions emphasize the importance of H69 in proper functioning of the ribosome during protein synthesis. Thus, continued structural and dynamics studies will provide insight into the biological function of H69.⁹¹

1.4. Antibiotic resistance and implications

Bacterial and eukaryotic ribosomes both house cellular processes with the ultimate goal of generating essential proteins for proper growth and function of an organism,¹⁵ but their

evolutionarily conserved structural features vary enough to be exploited for the development of effective drugs, such as anti-infectives or antibiotics⁹⁵ and effectively interfere with important cellular processes in bacteria (**Table 1.3**).⁹⁶ Antibiotics can selectively target either the small or large subunits of the invading microbe through mechanisms that involve the A or P sites of the decoding region or PTC, without targeting the ribosome function in the host.⁹⁷ For example, the large ribosomal subunit (50S) is targeted by many classes of antibiotics (*e.g.*, erythromycin, clarithromycin and roxithromycin, chloramphenicol, and clindamycin) that can block peptide-bond formation.^{95,97}

Infectious microbes have the ability to adapt through changes in an effort to survive and replicate.⁹⁸ Development of resistance in the antibiotic target site is an acquired mechanism for excluding or inactivating antibiotics. Other changes include modifications of the antibiotic to preclude binding, or alterations that affect the ability of antibiotics to reach their target.⁹⁹ For example, cephalosporinase-resistant bacteria modify their peptidoglycan cell wall and often use pump systems fueled by ATP to filter and eliminate specific antibiotics out of their cells.¹⁰⁰ Alternatively, some antibiotic-resistant microbes have developed the ability to chemically or structurally modify their target so that the antibiotic no longer has a recognizable target or ability to bind the target and otherwise cause a bactericidal and bacteriostatic effect.¹⁰⁰

The Centers for Disease Control and Prevention (CDC)¹⁰¹ monitored and reported emergence of antibiotic resistance in bacterial pathogens from 1980 to 2000 (**Fig. 1.14**) for methicillin-resistant *Staphylococcus aureus* (MRSA), *Vancomycin-resistant enterococci* (VRE) and fluoroquinolone-resistant *Pseudomonas aeruginosa* (FQRP), and their data analysis

illustrates the alarmingly rapid spread of antibiotic resistant microbes exposed to common antibiotics.

Table 1.3. Antibiotic classes and modes of action

Class	Example	Condition	Cellular target
beta-lactams	penicillin	skin	cell walls/inhibition of cellular walls
	ampicillin	ear	
	amoxicillin	urinary tract	
macrolides	erythromycin	respiratory tract	ribosome/inhibition of protein synthesis
aminoglycosides	gentamicin		ribosome/inhibition of protein synthesis
	kanamycin		
	streptomycin		
flouroquinolones	floxacin	respiratory tract	nucleus/inhibition of DNA synthesis
tetracyclines	doxycycline	skin	ribosome/inhibition of protein synthesis
	demeclocycline	urinary tract	ribosome/inhibition of protein synthesis
cyclic peptides	vancomycin	fever	ribosome/inhibition of protein synthesis
		gonorrhea	

Adapted from Physician's Desk 59th ed. Montvale, N.J. Thomson PDR, 2005.

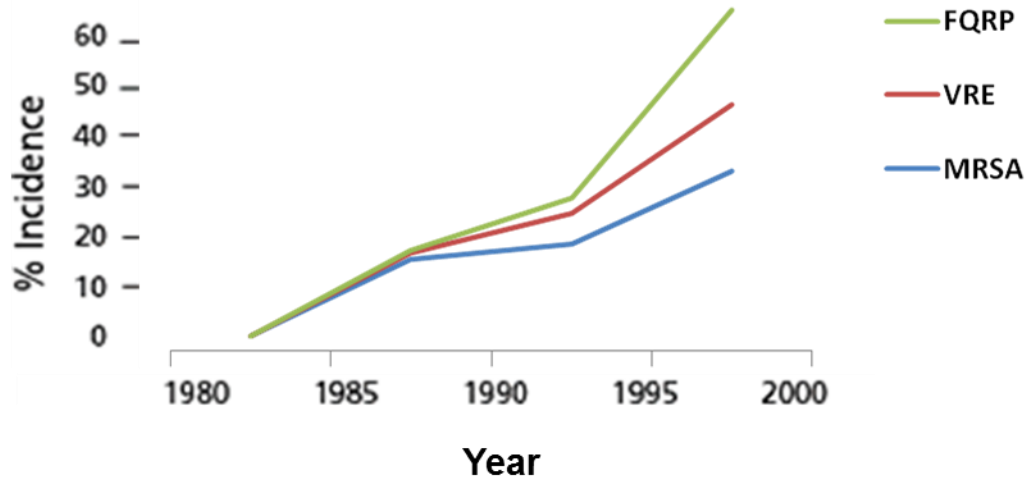


Figure 1.14. Continued emergence of antibiotic resistance. CDC National Survey Data (2013) data of resistant strains of infectious microbes. MRSA = methicillin-resistant *Staphylococcus Aureus*. VRE = vancomycin-resistant *Enterococci*. FQRP = fluoroquinolone-resistant *Pseudomonas aeruginosa*. Data graph adapted from CDC's 2013 report, "Resistant Strains Spread Rapidly".^{101,102}

The Centers for Disease Control and Prevention released their 2013 report of bacterial strains that have "concerning", "serious" or "urgent threat" levels in the United States and included as infectious microbes that have caused adverse health effects in more than two million people each year exhibiting antibiotic-resistant strains of bacteria and have been attributed to more than 23,000 deaths in 2013.¹⁰¹ The CDC continues to report the emergence of antibiotic resistance, and this information has been useful for the development of new ideas for combating the alarming rate of antibiotic resistance.¹⁰² As of 2013, greater than half of the antibiotics produced in the United States are disproportionately used in agricultural applications such as livestock and agricultural feed rather than human use, contributing to the emergence of accelerated rates of antibiotic resistant strains of human and animal pathogenic microbes.¹⁰³ Most strains of the staphylococcal infections in the United States have been

reported to be resistant to penicillin.¹⁰⁴ The CDC has listed the most “serious” antibiotic resistant microbial threats to include vancomycin-resistant *Enterococcus* (VRE) and methicillin-resistant *Staphylococcus aureus* (MRSA).¹⁰³ Finally, reported as “urgent threats” were *Clostridium difficile*, carbapenem-resistant *Enterobacteriaceae* (CRE), and *Neisseria gonorrhoeae*. Fluoroquinolone-resistant strains of *Clostridium difficile* have been reported by the CDC to be responsible for 250,000 infections, 14,000 mortalities, and excess medical costs of more than \$1 billion each year.¹⁰⁵ Carbapenem-resistant *Enterobacteriaceae* (*i.e.*, *Klebsella* and *E. coli* bacteria), or CRE, cause 9,000 infections and 600 deaths each year and are resistant to multiple antibiotics. Half of hospital patients who acquire CRE bloodstream infections die.¹⁰⁶ Listed by the CDC as the second most commonly reported notifiable infection, drug-resistant *Neisseria gonorrhoeae* is another microbe of urgent threat in the U.S. Approximately one-third of the 820,000 *Neisseria gonorrhoeae* infections reported in 2011 were resistant to at least one antibiotic (*i.e.*, tetracycline, cefixime).^{103,104}

Consequently, scientists are focusing on a long-term solution to address the emergence of antibiotic resistance in bacterial pathogens. For example, a potential solution was presented by the U.S. Food and Drug Administration (FDA) on December 11, 2013 through the release of “Guidance #213”,¹⁰⁷ a document listing recommendations designed to give direction to drug companies to voluntarily revise FDA-approved labeled use and conditions of common antimicrobials applied in medical health for humans. They desired more regulated use outside of human medical applications (*i.e.*, agricultural applications, such as livestock and agricultural feed). Ultimately, the Guidance #213 document requests 26 major manufacturers of antibiotics (~60% of American pharmaceutical drug producing companies) to change antibiotic product

labeling so that they cannot be marketed and used for livestock and agriculture to reduce incidences of antibiotic resistance.¹⁰⁷

1.5. H69 as a viable biological target

The general requirements for effective anti infectives have been extensively reported and can be summarized to have the following five properties: (1) ability to reach its target; (2) ability to retain its active form; (3) appropriate binding affinity once bound to the target site; (4) selectivity and binding specificity to the target; and (5) ability to interfere with important and essential functions carried out by the target and/or key biomolecular systems.⁹⁹ Helix 69 has been targeted by aminoglycoside antibiotics that have been shown to negate subunit dissociation and recycling of H69 bacterial ribosomes.^{91,94,108,109} Aminoglycoside binding to chemically synthesized motifs representing the *E. coli* and human H69 was detected and quantified by Agris *et al.* using thermal denaturation, circular dichroism spectroscopy, and isothermal titration calorimetry.¹¹⁰ Their findings suggest bacterial H69 as a viable target for neomycin, tobramycin, and paromycin, with a significantly lower affinity for human H69.¹¹⁰ Interestingly, Agris *et al.* also found that the presence of conserved modified nucleotides, Ψ 1911, Ψ 1915, and Ψ 1917, did not significantly affect the binding of paromomycin.¹¹⁰ Despite this, the higher affinity of the bacterial H69 for aminoglycosides over eukaryotic H69 supports the hypothesis that H69 is a viable target for new anti infectives. The aforementioned studies examine the different responses of a key rRNA motif RNA, which is highly conserved between bacterial and eukaryotic ribosomes and is already known as a target for anti-microbials. Helix 69 may potentially be a valid target for the development of more effective antibiotics.¹¹⁰

CHAPTER 2 - SELECTING DNA APTAMERS

2.1. Background of SELEX and aptamers

In vitro selection by systematic evolution of ligands by exponential enrichment (SELEX) is a combinatorial chemistry technique used to discover novel biomolecules with useful functionalities.¹¹³ SELEX was first described by Tuerk and Gold¹¹¹ as a technique to develop ligands for protein targets, and within the same year, Ellington and Szostak¹¹² reported SELEX of nucleic acids for small molecules targets. Ellington and Szostak coined the term “aptamers”, merging the Latin word "aptus" and the Greek word "meros", which mean "suitable, adjusted, or to fit" and "particle", respectively.¹¹⁴ SELEX enriches nucleic acid libraries by using the polymerase chain reaction (PCR), and generates ligands with diverse secondary and tertiary structures to function as specific binders for a given target.¹¹³ Other pioneers of *in vitro* selection were Robertson and Joyce.¹¹⁴ All three groups explored complex libraries of randomized sequences of oligonucleotides with $\sim 10^{15}$ in population diversity for screening of high-affinity, ligand-binding RNA molecules against various targets.^{113,114,116} Today, many variations of SELEX have been reported that generate aptamers against new biomolecular and small molecular targets, taking advantage of varying selection and counter-selection conditions.¹¹⁵ Famulok *et al.* have demonstrated the ability of aptamers to show high levels of affinity and selectivity of an RNA/L-arginine aptamer ($K_d = 330$ nM) with nearly a 200-fold improvement over the tightest binding arginine ligand known to date.¹¹⁶

2.2. Using systematic evolution of ligands by exponential enrichment (SELEX) for generating highly specific target-binding ligands

The standard experimental method of SELEX consists of iterative rounds of selection of sequences that bind to a target molecule through oligonucleotide library-target binding, washing, elution, and amplification, resulting in a gradual enrichment of the library with sequences exhibiting increased affinity for the target molecule.^{113-117,119} Iterative rounds of standard SELEX consist of the following four main stages: (1) incubation of the library with the target molecule; (2) separation of the complexes with the target from non-bound oligonucleotides; (3) amplification of the bound oligonucleotides by PCR for successive rounds; and (4) cloning of the enriched library and sequencing of select rounds for characterization and structural analyses (**Fig. 2.1**).^{113-117,119} Typically, during the initial rounds of SELEX, individual sequences are not highly represented, and the process should therefore be performed under low stringency conditions first (*e.g.*, low salt concentration, fewer washes, etc.) to ensure recovery of unique functional sequences. The stringency conditions are increased in subsequent rounds to help achieve higher frequency tighter binding of ligands to the target.¹¹⁷ Ultimately, rounds of *in vitro* selection are performed to reduce the number of weakly functional sequences, and increasing stringency during this process helps further enrich the library pool and obtain the best sequences. Finally, SELEX is complete when the activity of the DNA pool reaches a plateau, showing that a further increase in stringency will not result in an increased DNA pool activity.¹¹⁹

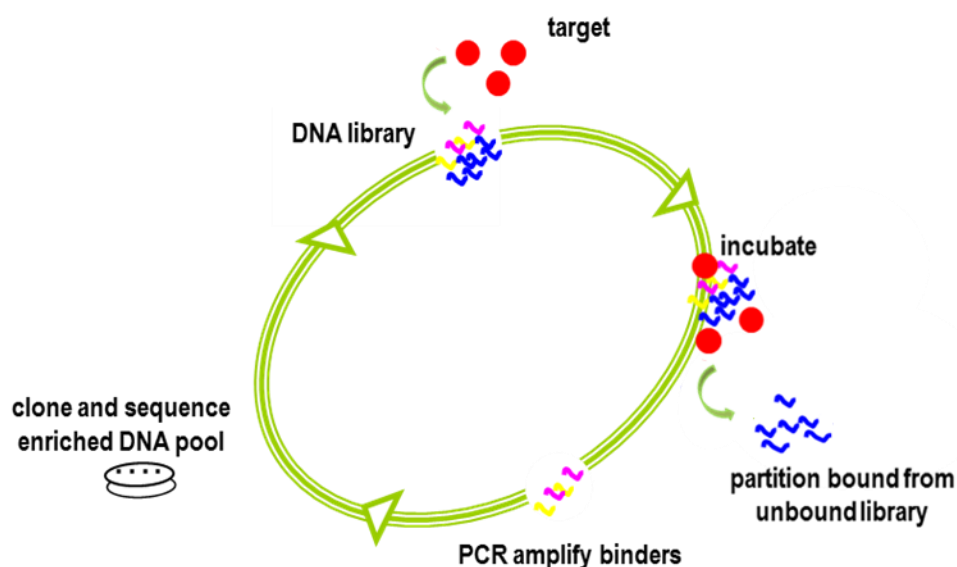


Figure 2.1. Overview of standard SELEX method. Following incubation of a target molecule with a library of randomized DNA sequences, target-DNA complexes are separated and amplified, and those with affinity to the target are recovered for repeated cycles of incubation, separation, and amplification until the sample is enriched with sequences that display high affinity for the target. Select nucleic acid library molecules are cloned and sequenced between cycles, or alternatively after the final cycle of SELEX.¹¹⁸

2.2.1. Experimental rationale of SELEX

Random sequence libraries generate molecular diversity necessary to isolate unique and rare aptamers that can interact with the target. When designing the initial DNA library, the randomized sequences chemically synthesized will have molecular diversity dependent on the number of randomized nucleotide positions (*i.e.*, a library containing a 20-nt random region has 1.2×10^{24} individual sequences) and the sample size (volume) selected for use within the experiments. For example, a 1.2×10^{24} oligonucleotide library from a 1 μmol -scale, solid-phase

DNA synthesis would actually be limited to 10^{14} to 10^{15} individual sequences because of practical reasons.

2.2.2. Basic parameters and design

Crystal structures or NMR solution structures of aptamers bound to their targets help provide information about the scaffolds and arrangement of aptamer chemical surfaces that are favorable for specific target binding interactions.¹¹⁹ Aptamers generated by the SELEX method can form complex three-dimensional structures and have various chemical properties, leading to selective binding towards their target, in which correctly positioned hydrogen-bonding and phosphate-group interactions dictate sequence-specific binding.¹¹⁴ Aptamers can be designed from single-stranded RNA or DNA for binding to a variety of targets including small molecules/proteins to whole cells.^{115,120} Aptamer target binding affinities and specificities have been reported in the range from μM to nM.^{113,114,118,119} Basic properties of aptamers include complex three-dimensional structures that have electrostatic interactions with their targets¹²¹ (*e.g.*, van der Waals; hydrogen bonding; and base stacking).^{114,115,119,121}

2.2.3. SELEX generated aptamers as highly specific binding ligands

Interestingly, nucleic-acid-based aptamers can exhibit multiple folded structures and unusual conformations, including double-stranded regions, non-standard base pairs, hairpin loops, triplexes, quadruplexes, multi-stem junctions, pseudoknots, nucleotide bulges, and loop-loop “kissing” interactions¹²⁰ between two hairpin structures or involving internal loops and

bulges (see **Fig. 1.4**).¹²¹ Consequently, oligonucleotides have been proposed as potential drugs¹²² that can bind tightly to targets based on complementarity of their three-dimensional structures and functional group display rather than just their sequences.¹²³ A well-known example of loop-loop “kissing” interactions between two hairpin structures has been observed and reported by Toulme *et al.* with DNA aptamers selected to bind to other RNA targets such as human immunodeficiency virus type-1 trans-activation-responsive (TAR) RNA element (**Fig. 2.2**).¹²⁴

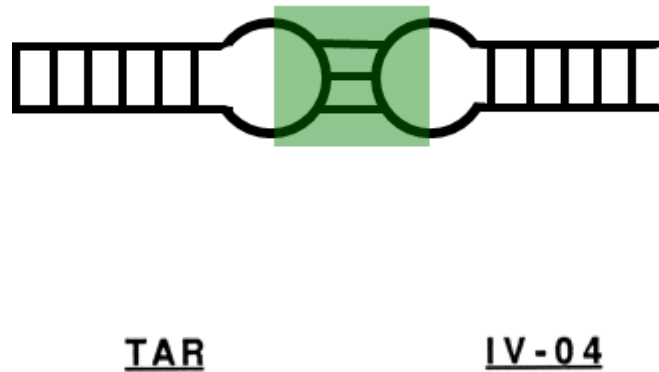


Figure 2.2. Example of DNA/RNA kissing complex motif.¹³⁷ Hairpin-hairpin or loop-loop “kissing” interactions between two hairpin structures have been observed and reported by Toulme *et al.* with DNA aptamers selected to bind human immunodeficiency virus type-1 trans-activation-responsive (TAR) RNA. Only the apical regions of TAR and IV-04 (25–46 nt) are represented. The consensus region of DNA aptamer (IV-04) the apical loop binds with the apical region of HIV TAR RNA (20–42 nt).¹⁴⁰

Aptamers have the potential to achieve a higher degree of specificity for their targets than antibodies.¹²² Aptamers have been noted for their remarkable specificity, discriminating on the basis of subtle target structural differences such as the presence or absence of hydroxyl and

methyl groups.¹²⁵ Amazingly, theophylline aptamers were characterized with greater than 10,000-fold binding preference for the target over caffeine, which differs from the theophylline structure by only one methyl group.¹²⁷

2.3. Aptamers: novel therapeutics generated by *in vitro* selection

The application of aptamers as therapeutics and diagnostics within the global market has grown rapidly since 2009 (valued at \$10 million), and was projected to have a value of \$1.8 billion by 2014.¹²⁶ The first FDA clinically approved aptamer based drug, Pegaptanib (Macugen), was developed for treatment of age-related macular degeneration (AMD).¹²⁷ In addition to this nanochemical application of aptamers, recent advancements with applications within electrochemical sensors for environmental pollutants have been reported.¹²⁸ Since the commercialization of aptamers, many biotechnological companies have designed aptamers or Aptabodies™ modified with sugars, fatty acids, amino acids, synthetic compounds, cofactors, and metal ions.¹²⁹

2.3.1. Basic properties and applications

Aptamers offer advantages over antibodies as functional, high-affinity, specific binders or inhibitors, as they require only a small quantity of pure target for the selection process.¹²⁴ Traditional rational drug discovery typically consumes large amounts of time and resources, as well as extensive information about the exact binding site or target. However, aptamers elicit

little or no immunogenicity in therapeutic applications and can be engineered completely *in vitro* with highly discriminating molecular recognition.¹³⁰ Thus, these intrinsic properties have shown promise as an alternative for food safety control.¹³¹ Furthermore, in cell-culture experiments and animal studies, aptamers do not exhibit intrinsic toxicity.¹³² For these reasons, aptamers have the potential to be used as novel drugs.¹³³

Unfortunately, limitations exist for obtaining in-depth structural information on aptamers. Often, aptamer structures are limited to secondary structure predictions from software analysis programs such as *Mfold*.¹³⁴ These computer-predicted secondary structures have a high degree of uncertainty, with even less information about the aptamer-target interactions. Further advancements in structure determination based on nucleic acid sequences could render more value and utility to aptamers as commercially viable biomolecular tools.

CHAPTER 3 – PURPOSE: ISOLATION AND ANALYSIS OF DNA APTAMERS BY SELEX FOR H69

3.1. Research proposal and thesis statement

Ribosomes are promising target macromolecules with functional importance for novel drug development. This importance has become increasingly clear because the ribosome is the heart of essential cellular functions, namely protein synthesis, and the rRNA is already a known target for anti-infectives. We propose that bacterial wild-type H69 rRNA would be a viable biological target for the development of DNA ligands or aptamers as novel anti-infectives. Importantly, the general requirements for effective anti-infectives have been reported extensively¹³⁵ and can be summarized to have the following five desired properties: (1) ability to reach the target; (2) ability to retain an active form; (3) have appropriate binding affinity once bound to the target site; (4) selectivity and binding specificity to the target; and (5) ability to interfere with important and essential functions carried out by the target and/or key biomolecular systems. Importantly, DNA molecules have been proven to be stable both *in vitro* and *in vivo*, and nucleic acid-based aptamers would be ideal ligands due to their diversity of structures and ability to build in chemical stability or new recognition motifs. Notably, H69 has already been targeted by aminoglycoside antibiotics, which negate subunit dissociation and recycling of bacterial ribosomes.^{136,137} Specifically, aminoglycoside binding to chemically synthesized RNA motifs representing *E. coli* and human H69 was detected and quantified by Agris *et al.* using thermal denaturation, circular dichroism spectroscopy, and isothermal titration calorimetry. Their findings are significant, because they suggest bacterial H69 as a viable target for neomycin, tobramycin, and paromycin, with a significantly lower affinity for human H69.¹³⁸

Furthermore, Agris and coworkers also found that the presence of conserved modified nucleotides, Ψ 1911, Ψ 1915, and Ψ 1917, did not significantly affect the binding of paromomycin. Despite this finding, the higher affinity of aminoglycosides for H69 over eukaryotic H69 supports the hypothesis that H69 is a viable target for new anti-infectives. Also of note is the fact that bacterial 70S ribosomes are more vulnerable to aminoglycoside antibiotics than eukaryotic 80S ribosomes because of differences in drug uptake.¹⁵¹ Consequently, results from the aforementioned studies examining the different responses to anti-microbials between bacterial and eukaryotic ribosomes suggest the ability to identify highly selective antibiotics. The multiple biological functions of H69 have also generated interesting and as of yet unanswered questions. In particular, can tightly bound molecules with high specificity and affinity for specific RNA conformational states inhibit or reduce binding and dynamics of H69 necessary for basal levels of protein synthesis and proper functioning of bacterial cells? An answer to this question would provide significant contributions to the understanding of a broader scope of the role of H69 in protein synthesis and vital cellular processes, as well as further insight into the significance of the abundance of modified bases (*i.e.*, pseudouridine and methylpseudouridine) within the hairpin and stem regions of H69.

This dissertation work approaches H69 as a highly conserved region of the ribosomal large subunit with importance for protein synthesis,¹³⁹ because H69 has been implicated in key intermolecular contacts between ribosomal subunits. H69 is also of interest because it has an abundance of conserved modified nucleotides. Understanding the role of pseudouridine within the sequence-conserved H69 rRNA motif may provide additional insight into the functional roles of H69 and strengthen its potential as a target for the development of DNA-based

therapeutics. Through an *in vitro* selection approach, our desire is to generate specific ligands for H69, commonly classified as "aptamers". Our specific aim is to generate and test DNA aptamers for their effectiveness to bind to H69, and evaluate their usefulness as potential replacement molecules of currently ineffective antimicrobials for resistant pathogenic microorganisms.

The proposed target for this study, bacterial H69, is structurally unique from the human analogue. Our research focus is to identify promising new ligands that specifically recognize and bind with high affinity to such key regions of bacterial ribosomes. Identification of aptamers that are specific for H69 may assist in the confirmation of this modified RNA motif as a new antimicrobial drug target site.

Expanding upon our current knowledge of the H69 motif and the role of Ψ s, this study seeks to explore potential binding interactions of H69 with a randomized DNA library containing ligands that may potentially serve as tools for structure and function regulation, such as disruption of essential protein synthesis processes. Because our library is designed to generate a large number of DNA aptamers, we hypothesize that these ligands will display both sequence and structural diversity. Ultimately, as DNA aptamer candidates emerge, we seek to characterize their interactions with the synthetic H69 motif as a model for the natural molecular target. This work will address the question of whether selected DNA ligands generated against H69 will bind with high specificity and affinity. The long-term goal of this project is inhibiting or reducing the functionality of H69 in bacterial protein synthesis and

possibly provide greater insight into the effectiveness of nucleic-acid-based molecules as highly specific ligands for rRNAs.

3.2. Purpose and specific aims

DNA aptamers have been applied for diagnostic and therapeutic applications. Our specific aim was to generate and characterize DNA aptamers for their efficacy in binding to H69. The focus of this dissertation was to develop aptamers through *in vitro* selection methods using a synthetic RNA construct representing bacterial H69 as the target and closely related RNAs in counter-selection experiments. Our primary short-term goal was to first isolate aptamers with affinity and selectivity for wild-type H69 from a random DNA library and immobilized RNA target. The aptamers were identified through cloning and sequencing, secondary structure analysis, and determination of their theoretical thermodynamic stabilities. In this approach, DNA consensus sequences and common secondary structural motifs for H69 targeting were discovered. In the last step, the aptamers were characterized for their binding affinities and selectivities for the modified H69 construct as well as unmodified and unrelated RNA sequences. As a future goal, the potential of these DNA aptamers to inhibit ribosome function and to serve as novel therapeutics will be explored, applying the resultant aptamers to counter antibiotic resistance in pathogenic organisms. Furthermore, we anticipate future applications to include validation of H69 as a viable target and increasing our understanding of the role of modified nucleotides in the ribosome. Finally, as a secondary goal, generated DNA aptamers may also function as potential probes for modified nucleotides. As such, DNA aptamers may be

employed experimentally to characterize H69 modification states and to probe their significance in RNA structure and function within cellular systems.

CHAPTER 4 – EXPERIMENTAL APPROACH: SELECTION AND CHARACTERIZATION OF DNA APTAMERS FOR H69

4.1. Experimental design and methodologies

DNA aptamers have shown great promise as functional single-stranded biomolecules that exhibit tight binding and high specificity for various targets.¹⁴⁰ In this study, we optimized a series of methods (**Fig. 4.1**) to generate DNA aptamers that fold into three-dimensional structures and bind to bacterial H69.

4.2. Approach to isolate and characterize DNA aptamers for H69 by monitoring diversity and percentage of library bound

The focus of the work described in this chapter is generation, isolation, and characterization of specific and H69-binding DNA ligands through SELEX. The following methods were utilized: (1) biotinylation and immobilization of chemically synthesized wild-type H69 to streptavidin-coated surfaces; (2) challenging the initial round of the DNA library against streptavidin-coated surfaces to eliminate DNAs with affinity for streptavidin; (3) recovery of the DNA library, excluding molecules with affinity for streptavidin, and performing subsequent rounds of *in vitro* selection against immobilized biotinylated H69; (4) PCR amplification of the DNA library in successive rounds of SELEX with a biotinylated primer and capturing of the undesired opposing single strand with streptavidin-coated magnetic beads; (5) quantification of the DNA library and determination of percentage bound to immobilized H69 in each round; (6) cloning and isolation of vectors transformed with DNA ligands with affinity for H69; (7) capillary sequencing of select

clones to identify sequences of the DNA molecules with affinity for H69; (8) characterization of secondary structures of the sequenced DNA ligands from the randomized library by searching

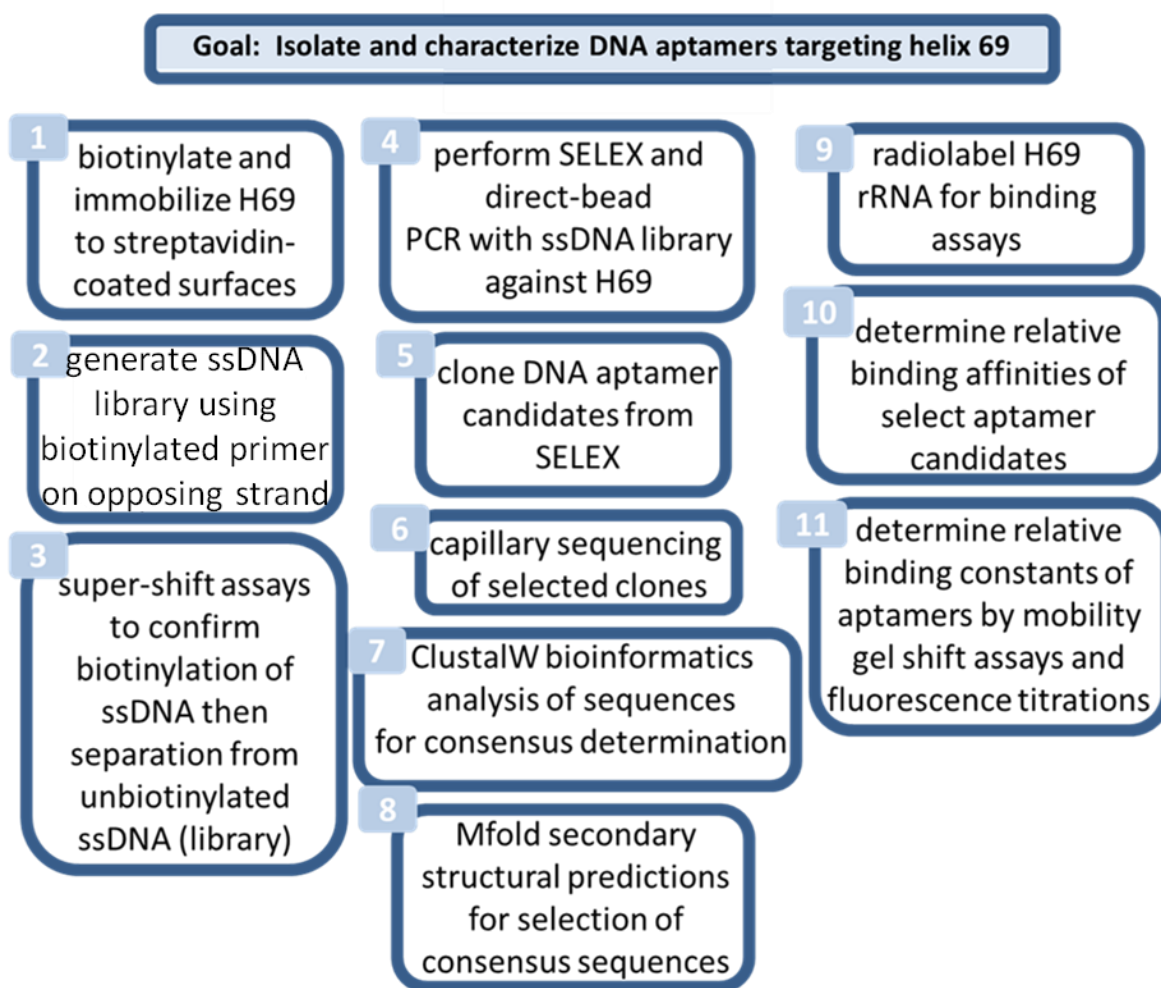


Figure 4.1. Summary of experimental approach for aptamer selection in eleven steps.

for sequence homology and consensus; (9) analysis of the sequences and structures of select DNA ligands by computational analysis with programs such as *Mfold* and Clustal W; (10)

radiolabeling of H69 with ^{32}P to perform electrophoretic mobility shift assays (EMSAs); (11) PCR amplification of select DNA aptamers using fluorescently labeled primers to generate dye-tagged sense-strand DNA aptamers against H69 for future binding and probing studies; and (12) performance of fluorescence binding assays.

In this experiment, RNAs representing H69 were biotinylated and immobilized onto streptavidin-coated surfaces. Next, SELEX was carried out with the biotin-labeled H69. Fifteen rounds of SELEX were done with an initial DNA library of 84 nucleotides containing a 40-nt random sequence region, in which the theoretically possible sequences for the initial DNA library diversity with 84 nucleotides containing a 40-nt randomized region was determined to be 1.2×10^{24} sequences using the following equation:

$$\text{Initial library diversity} = 4^N, \text{ in which } N = \text{the length of randomized sequence} \quad (\text{Eq. 4.1})$$

Data were obtained for the initial and final amount (moles) of the DNA library before and after incubation during successive rounds in which the percentage of library bound (% Bound) is calculated from n_i (initial moles of the DNA library before incubation with the target during SELEX) and n_f (the final moles of DNA) monitored by UV-VIS spectroscopy:

$$\% \text{ Bound} = ((n_i - n_f)/n_i)(100) \quad (\text{Eq. 4.2})$$

Measurement of the experimental diversity of the DNA library was determined by using the expression described by **Eq. 4.3**:

$$\text{Library diversity} = (n) (\text{Avogadro's \#}) (\% \text{ library bound}) \quad (\text{Eq. 4.3})$$

in which n = moles used in each round of SELEX.

4.3. Experimental procedures

4.3.1. Preparation of a randomized 84-nt oligonucleotide ssDNA library and DNA primers for SELEX

A synthetic ssDNA library, including a random sequence of 40 nucleotides flanked by two primers with binding sequences for PCR amplification and cloning (5'-gccggatccgggcctcatgtcgaa-N40-agctcagaagaaacgctcaa-3'), was designed, and purchased from Midland Certified Reagents (Midland, Texas). The molar extinction coefficient or molar absorptivity (ϵ) for the ssDNA library was $554,400 \text{ M}^{-1}\text{cm}^{-1}$. A forward primer (5'-gccggatccgggcctcatgtcgaa-3'), a reverse primer (5'-ttgagcggtttattctgagct-3'), and a biotinylated reverse primer (5'-biotin-ttgagcggtttattctgagct-3') were used for PCR amplification and ssDNA generation. All of the aforementioned oligonucleotides were synthesized by Midland Certified Reagent Company (Midland, Texas) and purified by 15% preparative denaturing (8 M urea) polyacrylamide gel electrophoresis (PAGE). The DNA was visualized with a handheld UV lamp when the gel was placed directly on a fluorescent TLC (thin-layer chromatography) plate.

4.3.2. Preparation of H69 and biotin-H69

N^3 -methylpseudouridine ($m^3\Psi$) and pseudouridine (Ψ) were successfully incorporated into modified H69 ($\Psi m^3\Psi\Psi$) RNA, (5'-GGCCG Ψ AAC $m^3\Psi$ A Ψ AACGGUC-3', $\epsilon = 188,869 \text{ M}^{-1}\text{cm}^{-1}$), by utilizing solid-phase RNA synthesis with phosphoramidites prepared by J. Herath using a method developed by Chui and coworkers.¹⁴¹ The synthetic RNAs were deprotected according to the Dharmacon Research, Inc. protocol and then gel purified on a 20% (8 M urea) denaturing polyacrylamide gel. This modified H69 was biotinylated at the 5' end using Pierce (Rockford, IL) E-Z-link Iodoacetyl-LC-Biotin. First, 1000 pmoles of gel purified modified H69 was denatured by boiling for 2 min and immediately placing on ice. A kinase reaction was then performed by adding 1 \times PNK (T4 polynucleotide kinase) buffer, 1 mM ATP γ S, and 30, 150 or 300 units of PNK per reaction on ice, then incubated in the dark at 37 °C for 2 h. The samples were then heated at 70 °C for 10 min to inactivate PNK. Once the kinase reaction was completed, the H69 reaction mixture was dried and prepared for coupling with NIBH (*N*-iodoacetyl-*N'*-biotinylhexylene) (**Fig. 4.2a**). The NIBH was pre-warmed in a 55 °C water bath for 1 min. At the end of the coupling step, 90 mM K_3PO_4 , (pH 8) and 2 mM of NIBH in DMF (dimethylformamide) were added to each sample for a total volume of 50 μL . The samples were incubated in the dark at 50 °C for 1 h. A fraction of each H69-biotin sample was dried and then run on 15% denaturing (8 M urea) PAGE, and visualized to determine the percent efficiency of the biotin-labeling reaction. After verification of the biotin label on H69 (**Fig. 4.2b**) by visualization on a polyacrylamide gel, the sample was desalted by using microcon YM-3 filters. Matrix Assisted Laser Desorption Ionization Mass Spectrometry (MALDI-MS) was performed to confirm biotinylation of H69.

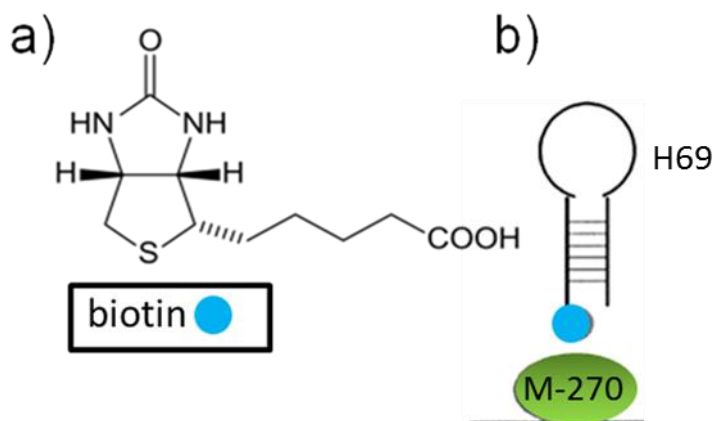


Figure 4.2. Application of a biotin tag for immobilization of H69. *N*-iodoacetyl-*N'*-biotinylohexylene), or biotin (blue circle) (a) is shown as the tag used to immobilize H69 onto streptavidin-coated magnetic Dynal beads M-270 (green oval) (b).

4.3.3. Preparation of Dynal® magnetic beads for immobilization of 5'-biotinylated $\Psi\text{m}^3\Psi\Psi$ H69 rRNA

Streptavidin-coated magnetic Dynal® M-270 beads were pre-treated according to the manufacturer's protocol. Next, 500 pmoles of 5'-biotinylated $\Psi\text{m}^3\Psi\Psi$ were mixed with 100 μL of pre-treated beads (1 mg of Dynal® M-270 beads having a binding capacity of 700 pmoles, and 10 μL of bead suspension being equal to 70 pmoles). The RNA-bead solution was gently mixed and incubated at room temperature with rotational motion at 600 RPM for 30 min, followed by a 1 minute spin down to separate the unbound from bound RNA. The supernatant was removed to determine the remaining concentration of unbound 5'-biotinylated $\Psi\text{m}^3\Psi\Psi$ by UV-VIS spectroscopy and for the calculation of percent of 5'-biotinylated $\Psi\text{m}^3\Psi\Psi$ bound to the magnetic beads.

4.3.4. Preparation of single-stranded DNA library

The initial dsDNA library was generated by PCR amplification from the randomized 84-nt DNA library pool and ssDNA was prepared using a biotinylated reverse primer and non-biotinylated forward primer. To obtain ssDNA for subsequent SELEX rounds, the resulting biotinylated dsDNA PCR product was separated into two strands (*i.e.*, ss-biotinylated antisense DNA strand separated from the sense non-biotinylated strand). First, 300 pmoles of PCR generated biotinylated dsDNA product was heated at 94 °C for 5 min and kept at room temperature for up to 15 min prior to binding to streptavidin-coated magnetic beads (**Fig. 4.2b**). Next, an aliquot of 10 µL of pre-washed magnetic beads were incubated with 300 – 1,000 pmoles of the DNA library to give a final volume of 300 µL in binding buffer D (50 mM Tris-HCl, pH 7.5, 10 mM MgCl₂, 50 mM NaCl, 1 mM dithiothreitol). This dsDNA mixture was incubated with streptavidin-coated Dynal® magnetic beads for 30 min at 20 °C to trap the ss-biotinylated DNA strand and mixed at 1050 RPM using an Eppendorf Thermomixer Mastercycler Gradient 5331. Next, a magnetic stir bar was used to aggregate the magnetic streptavidin-coated beads and allow efficient removal of the supernatant containing the desired sense strand (*i.e.*, non-biotinylated sense ssDNA). Finally, the biotin-strand capturing for separation of the sense strand was confirmed by agarose gel analysis and super-shift assays. All samples were run on a 1% agarose gel at 90 V/cm for 1 h with NEB® 100-bp ladder (New England Biolabs, USA; NEB #3231). Double-stranded biotinylated DNA PCR products allowed to bind to streptavidin-coated beads were subsequently incubated with and without streptavidin solutions. Next, samples containing double-stranded biotinylated antisense strands and non-biotinylated sense strands of the DNA library (**Fig. 4.3**) were treated with a 0.25 µM streptavidin solution (SA). Following

incubations with the streptavidin solution, biotinylated non-sense strands were captured and separated from non-biotinylated sense strand for recovery and use of non-biotinylated sense strands library samples in SELEX rounds to be challenged against the targeted biotinylated-H69.

4.3.5. Direct-bead PCR

SELEX experiments were performed with streptavidin magnetic beads, Dynal® M-270 streptavidin-coated beads (Dynal Biotech, Norway), Taq DNA polymerase (Promega Corporation, USA) was used for amplification after each selection round, and the resulting products were purified with a PCR Clean-Up System (Promega Corporation, USA) according to the manufacturer's instructions. First, a streptavidin challenge protocol for round 0 of SELEX was performed with the isolated ssDNA library. Using the recovered denatured/renatured supernatant of the ssDNA library, 300 - 1,000 pmoles were challenged against streptavidin-coated beads without H69 (to eliminate any DNA ligands with affinity for streptavidin), and incubated for 30 min at 20 °C with a rotational velocity of 1050 RPM. The percentage of bound library to streptavidin beads was determined. Rounds 1 – N were carried out with 300 pmoles of ssDNA mixed with double deionized H₂O to a final volume of 50 µL and denatured at 94 °C for 5 min, and then immediately renatured on ice for 10 min. Following renaturing, 240 µL of binding buffer B (10 mM Tris-HCl, pH 7.5, 10 mM MgCl₂, 50 mM NaCl, 1 mM dithiothreitol) and 30 µL Dynal® M-270 magnetic beads precoated with 5'-biotinylated Ψm³ΨΨ H69 at a molar ratio of 1:75 of biotin-H69:DNA library (2 pmoles of RNA to 150 pmoles of DNA) were mixed. The randomized 84-nt DNA library pool of about 10¹⁴ candidates

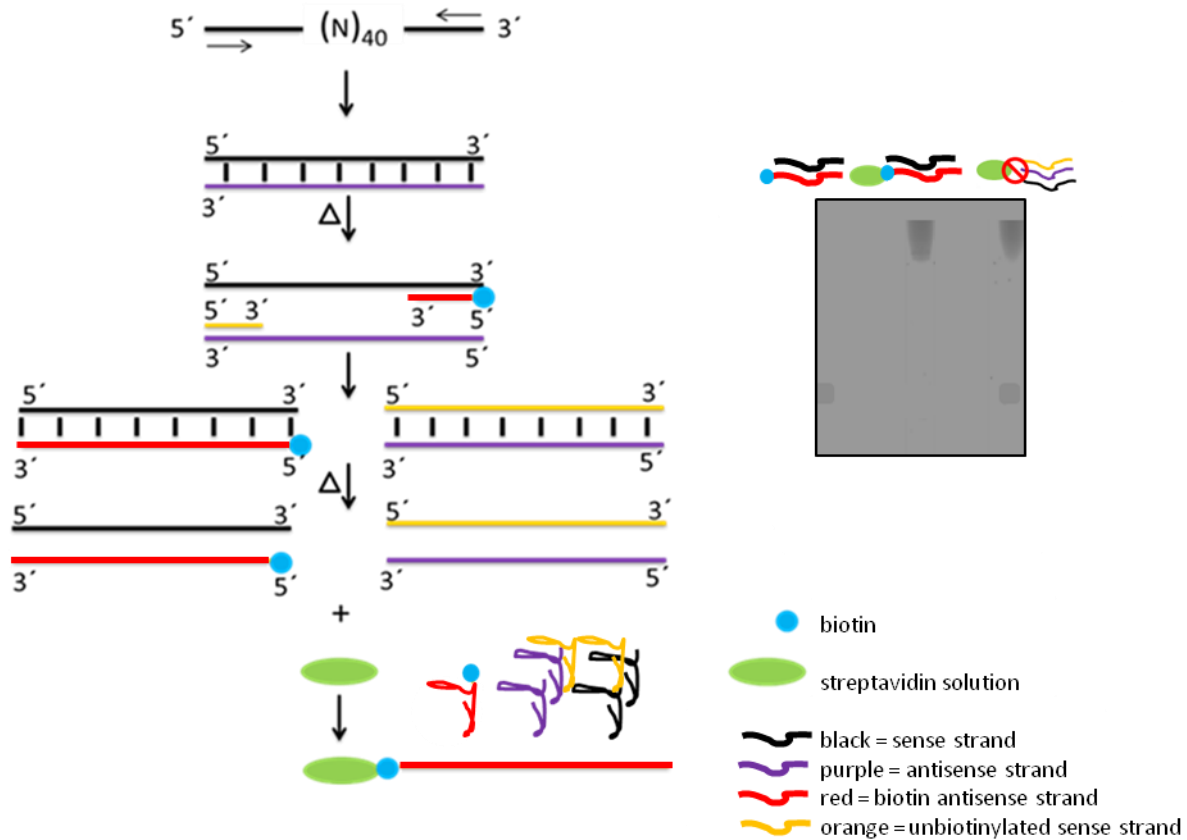


Figure 4.3. Confirmation of biotinylated DNA library by super-shift assay. DNA library strand separation was verified by using a streptavidin solution for the super-shift assay. The double-stranded DNA library is biotinylated by PCR with a reverse biotinylated primer (blue circle) and a forward non-biotinylated primer. To isolate the single-stranded DNA library, the PCR-amplified library was separated by heat treatment. This sense-strand, non-sense-strand separation was performed by incubation of biotinylated double-stranded PCR-amplified DNA library captured using a $0.25 \mu\text{M}$ streptavidin solution (green oval). Ultimately, to obtain ssDNA for subsequent SELEX rounds, the resulting biotinylated dsDNA PCR product was separated from the non-biotinylated strands by heating at $94 \text{ }^\circ\text{C}$ for 5 min and allowed to equilibrate at room temperature followed by incubation with streptavidin-coated Dynal[®] magnetic beads for 30 min at $20 \text{ }^\circ\text{C}$ to trap the ss-biotinylated DNA strand. This step was done at 1050 RPM using an Eppendorf Thermomixer Mastercycler Gradient 5331. The recovered sense strands could then be incubated with immobilized biotinylated-H69 during rounds #1-15 of SELEX.

were mixed with biotin-H69 immobilized to either streptavidin-coated 96-well plates or magnetic beads (**Fig. 4.4**). Incubations were performed at 20 °C for 30 min with a rotational velocity of 1050 RPM. Once the incubations were complete, the beads were pelleted and the supernatant was recovered to determine the percentage of 84-nt library bound to H69. Enrichment of the 84-nt library still bound to H69/streptavidin-coated beads was performed by direct-bead PCR. Direct-bead PCR was performed by amplifying a mix of the pelleted beads (containing the immobilized biotin-H69 with the DNA library from the SELEX round) and buffer (200 μ M MgCl₂, 200 μ M dNTPs, 4 μ M each of forward and reverse primers, 10 \times reaction buffer, Taq polymerase (1 unit \sim 0.5 μ L)) in a final reaction volume of 50 μ L (**Table 4.1**).

Table 4.1. Direct-bead PCR amplification of H69-bound DNA library

Steps of cycles	Temperature	Time
1. Denaturing	96 °C	20 sec
2. Annealing	56 °C	20 sec
3. Extension	60 °C	4 min
4. Repeat steps 1-3 for 30 cycles		

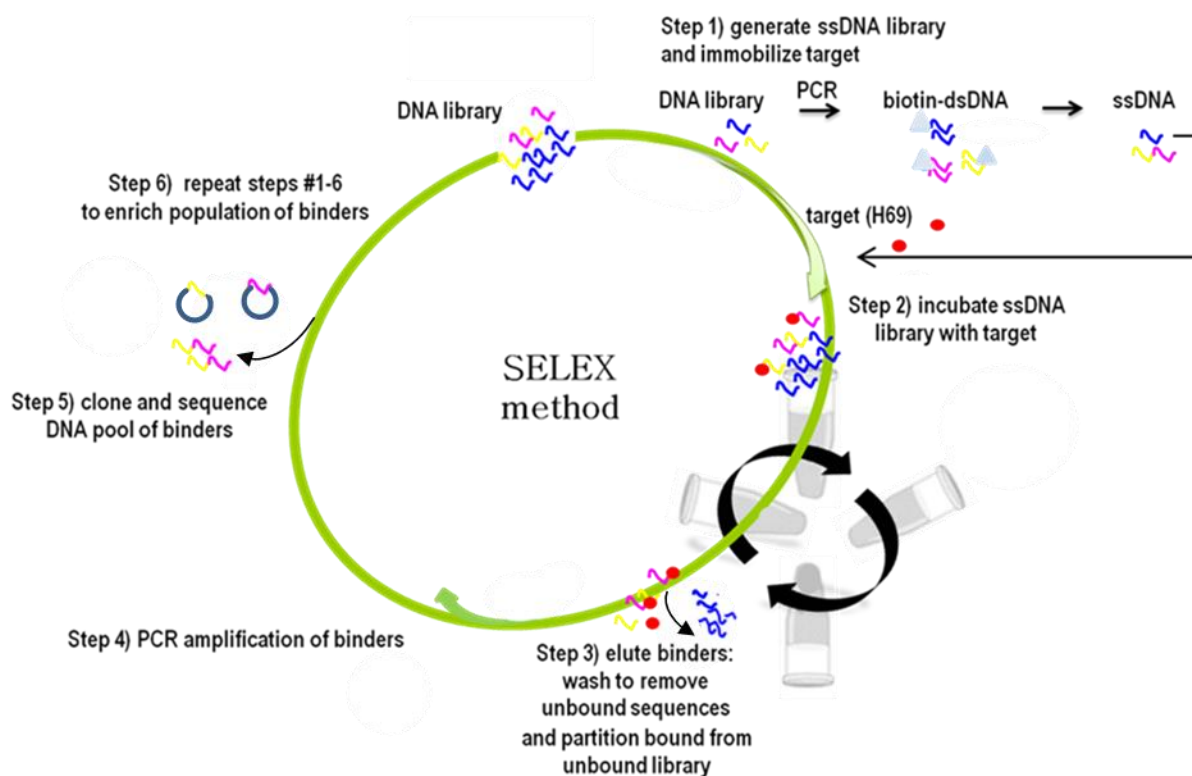


Figure 4.4. Summary of SELEX procedure. Experimental design to isolate and characterize DNA aptamers against H69. SELEX rounds involve of the repetition of successive steps of incubation of the library pool with the target, partition of the unbound from bound, and enrichment by direct-bead PCR amplification of aptamer candidates. Steps #1-5 show the generation of the ssDNA synthesized randomized DNA oligonucleotide library, incubation, partition of non-binders, and library enrichment. Step #6 represents the repetition of successive steps that consist of binding, partitioning of the library and the target molecules until the H69 binders are enriched through PCR amplification. The new enriched pool of selected ssDNA ligands are then used as the starting material for the successive rounds of selection until the diversity of the library is significantly reduced (typically 6 to 20 rounds).

4.3.6. Cloning and sequencing

Select ssDNAs were amplified by PCR using unmodified forward and reverse primers and then cloned into the pCR[®]4.1-TOPO vector. Plaques of positive DNA inserts from selected PCR products of SELEX rounds from the 3rd, 4th, 5th, 6th, 7th, 8th, and 11th (streptavidin-coated beads)

and the 9th, 13th, 14th, and 15th (streptavidin-coated plates) were cloned into pCR[®]4.1-TOPO using TOPO[®] TA Cloning[®] Kit (Carlsbad, CA) according to the manufacturer's instructions,¹⁴² and *E. coli* cells (DH5 α) were transformed via heat shock. All clones were isolated using a QIAprep[®] Miniprep Kit (Germany). The clones with inserted DNA fragments were confirmed by PCR amplification using primers complementary to the sequence of the M13 region of the plasmid. Positive clones with full-length inserts were confirmed and analyzed on agarose gels stained with ethidium bromide. Successful clones were transformed and grown on agar plates with 50 $\mu\text{g}/\text{mL}$ ampicillin at 37 °C for 10-15 h. Plasmid transformation efficiency (T_fE), reported as # of transformants/ μg DNA, was monitored and calculated according to **Eq. 4.3**, in which C = the number of colonies, V_t = the total volume of transformation mix (tmix) plated, and DF = dilution factor:

$T_fE =$

$$\left(\frac{\# \text{ of } C}{10 \text{ pg puC19} + \text{ insert}}\right) (10^6 \text{ pg}/\mu\text{g}) (300 \mu\text{L } V_t / 10\text{-}50 \mu\text{L plated tmix}) (\text{DF}) \quad \text{(Eq. 4.3)}$$

Plasmids containing individual aptamer sequences were prepared using the Qiagen Mini-Prep Kit (Valencia, CA). DNA sequencing was performed on a CEQ 8000 capillary DNA sequencer (Beckman-Coulter) following the manufacturer's recommended procedures. Base calling following the sequencing procedure was performed with the CEQ 8000 package. Overnight cultures were grown from single colonies of *E. coli* strains at 37 °C in rich liquid media 2 \times YT (16 g/L tryptone, 10 g/L yeast extract, 5 g/L NaCl) supplemented with ampicillin (100 $\mu\text{g}/\text{mL}$).

Culture densities were monitored for 12 h after induction until the cell growth density measured at OD₆₀₀ was within a range of 0.5 – 0.6.

4.3.7. Identification of sequence consensus by Clustal W and *Mfold* structure prediction

The consensus of primary sequences for cloned and sequenced DNA ligand candidates from select SELEX methods utilizing streptavidin-coated magnetic bead immobilization and streptavidin-coated plates immobilized with H69 were generated for the DNA aptamer candidates. Primary sequence homology and identification of consensus sequences between sequenced rounds were identified using the Clustal W¹⁴³ multiple sequence alignment computer program.¹⁴⁴ Secondary sequence predictions and values for theoretical standard-state free energies were performed for sequences showing homology. Both secondary structural predictions and standard-state free energies for select sequenced DNA aptamers were obtained using *Mfold*[®] algorithms with the *Mfold*[®] software package (version 2.3) by Zuker and Jaeger.

4.3.8. Radiolabeling of wild-type H69 for electrophoretic mobility shift assays (EMSAs)

For the evaluation of dissociation constants of H69-DNA aptamer complexes, EMSAs were performed for 20 sequenced DNA ligands as preliminary binding affinity studies with wild-type H69 (**Fig. 4.5**). Single-stranded sense strands of DNA aptamer candidates #1-20 were generated by direct PCR amplification from isolated clones and prepared using sense strand by capturing

(See section **4.3.4. Preparation of single-stranded DNA library**). Dissociation constant (K_d) values of H69-DNA aptamer complexes were deduced from the shift of 1 nM of [32 P] 5'-end-labeled H69 in the presence of an increasing concentration of DNA aptamer. [32 P] 5'-end-labeled H69 (1 nM) was incubated with DNA aptamers for 10 min at 23 °C in binding buffer B and resolved by EMSA with either 20 or 10% (19:1) crosslinked polyacrylamide gels with 0.5× TBE buffer at 10 mA. The gel was pre-run at 10 mA for 30 min. The gels were developed inside a cassette at -80 °C for 16-24 h and visualized for quantification of bound and unbound H69 on a Typhoon phosphorimager (Molecular Dynamics) and quantified using ImageQuant® software (Molecular Dynamics).

4.3.9. Preparation of FAM-DNA

A 5'-fluorescein-labeled DNA aptamer construct with one less guanosine at the 5' end to eliminate the phenomenon of purine-quenching effects was synthesized and purified by Integrated DNA Technologies (Coralville, Iowa) for FAM-H69DNAaptamer18:

(5'-FAM-cggatccgggcctcatgtcgaaCTCCCGGGCACTATTTCTGGGACTAGTTCTGCAGGTTTTtgagcgtttattct-gagct-3').

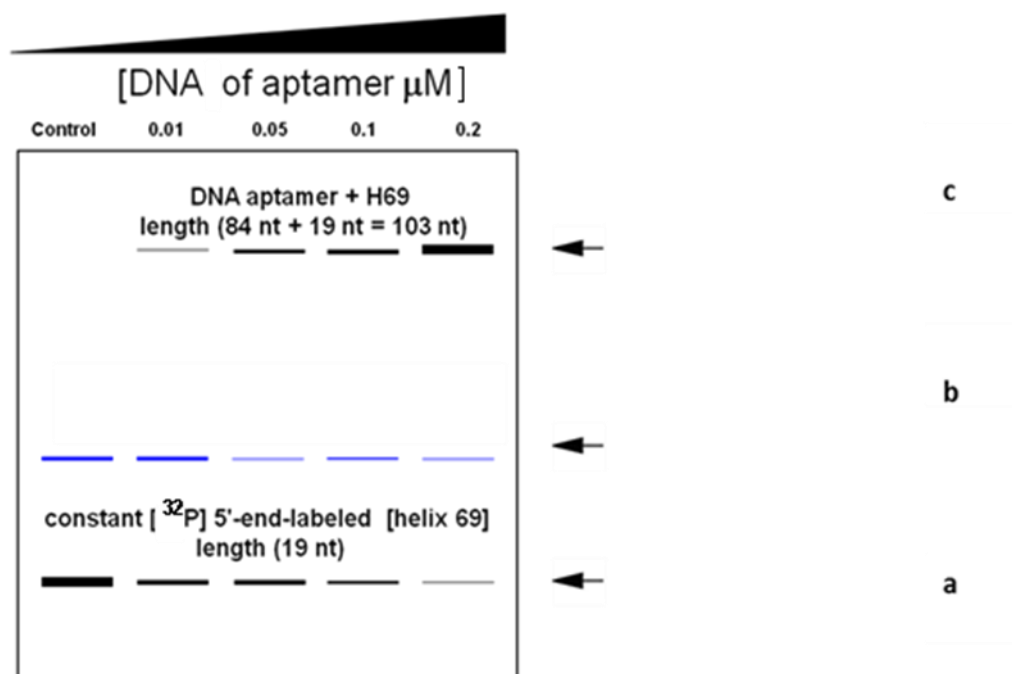


Figure 4.5. Model analysis of electrophoretic mobility-shift assays (EMSA) for DNA ligands. Assays performed with DNA ligands incubated against [^{32}P] 5'-end-labeled H69 are proposed to form complexes if the DNA ligands bind to target RNA. SELEX-generated DNA ligands incubated with varying concentrations of H69 in the ranges near to their dissociation constant (K_d) would show the concentration of DNA aptamer to be inversely proportional to the band intensity of labeled H69 (a). Observations of possible intermediate complexes and/or higher-order structures (b). Corresponding with the decrease in band intensity of [^{32}P] 5'-end-labeled H69, DNA aptamers with affinity for H69 would form bound complexes (c) and be visible by EMSA as an increase in band intensity (a).

4.3.10. Fluorescence experiments and determining dissociation constants (K_d s)

To determine dissociation constants of select SELEX-generated DNA aptamer candidates for H69 by relative fluorescence measurements, the dye-tagged H69DNAapt18 was used. Titrations were performed with increasing concentrations of wild-type H69, unmodified H69 motifs, or unrelated sequence A-site rRNA (duplicates were only performed for wild-type H69). Solutions of 300 nM FAM-H69DNAapt18 in binding buffer C (10 mM Tris-HCl, pH 7.5, 10 mM MgCl_2 , 50

mM NaCl) were titrated against a concentration range of RNA from 0 – 1,500 nM. Fluorescence emission spectra were monitored over a range of wavelengths (*i.e.*, $\lambda = 500-650$ nm) and excited at 517 nm, (*i.e.*, excitation band pass of 2.5 mm slit width and emission slit width of 10 mm). All measurements were taken at 37 °C, and samples were pipeted up and down while incubating inside a cuvette within the cuvette holder of the spectrometer for 2 min before fluorescence intensities were measured. Then, aliquots of the RNA were added sequentially, with 2 min of equilibration time before each fluorescence measurement. Fluorescence experiments were performed on a Cary Eclipse luminescence spectrometer, and Kaleidograph was used to analyze the data. Fluorescence intensities were corrected for volume changes according to the relationship of $F_{i,corr} = (F_{i,obs}) (V_i/V_0)$, in which $F_{i,corr}$ is the corrected intensity for point *i* of the titration, $F_{i,obs}$ is the measured intensity at point *i*, V_i is the volume after the *i*th addition, and V_0 is the initial volume (initial reaction volume 200 μ L). The data were fit to the expression described by **Eq. 4**, where K_d is defined as the apparent dissociation constant, [RNA] is the concentration of RNA ranging from 0 – 1,500 nM, [DNA] is the concentration of the DNA (held constant at 300 nM), and *c* is a constant that relates fluorescence intensity to concentration:

$$\text{Dissociation constant} = \left(K_d + [\text{RNA}] + [\text{DNA}] - \sqrt{((K_d + [\text{RNA}] + [\text{DNA}])^2 - 4[\text{DNA}][\text{RNA}])} \right) / 2c \quad (\text{Eq. 4.4})$$

The K_d values for simple binding were determined by plotting *Fr* (relative fluorescence) against the total RNA concentration, $[\text{RNA}]_t$, in which *Fr* represents the fraction of fluorescence intensity due to the bound species used in the following equation:

$$Fr = (F_{0,corr} - F_{i,corr}) / (F_{0,corr} - F_{F,corr}) \quad (\text{Eq. 4.5})$$

The values in **Eq. 4.5** are defined as follows: 1) sample at the initial point $F_{0,corr}$ (all free); 2) $F_{i,corr}$ is the sample at point i in the titration; and 3) $F_{F,corr}$ represents the sample at the final titration point (all bound).¹⁴⁵

CHAPTER 5 – RESULTS: CHARACTERIZATION OF DNA APTAMERS FOR H69

SELEX is an efficient and effective screening method for selecting DNA ligands (aptamers) against H69. Initial amplification of the synthesized 84-nt DNA library containing a 40-nt randomized sequence region yielded aptamers that exhibit moderate (μM) affinity for biotinylated wild-type H69. The $\Psi\text{m}^3\Psi\Psi$ H69 was immobilized to both streptavidin-coated plates and magnetic beads for *in vitro* selections (11 rounds on magnetic streptavidin-coated beads and 15 rounds on 96-well streptavidin-coated micro-titer plates). Percentages of bound DNAs in the library were monitored during SELEX by using UV-Vis spectroscopy and used for estimations of pool diversity. The best results were obtained when rotational incubation on sphere-shaped surfaces was used instead of the forward and backward rocking incubation method used on the 96-well streptavidin-coated titer plates. Once the diversity of the library was reduced to approximately 1×10^4 molecules using the SELEX method with magnetic beads, the DNA samples were pooled and cloned for further isolation and characterization by sequencing and binding assays.

5.1. Biotin-strand capturing for separation of sense strand and non-sense strands confirmed by agarose gel analysis and super-shift assays

Each SELEX round was performed using single-stranded DNA for single-stranded aptamers against H69. A biotinylated DNA primer was used in PCR to generate a tagged antisense strand. To obtain ssDNA, the resulting biotinylated dsDNA PCR product was separated into two strands by heating and cooling (*i.e.*, the antisense ss-biotinylated DNA strand was separated from the

sense non-biotinylated strand) followed by incubation with streptavidin-coated Dynal® magnetic beads and collection of the supernatant. The separation of the biotinylated antisense strand was confirmed by super-shift assays (**Fig. 5.1**). Super-shifting of the biotinylated antisense strand with streptavidin was observed by gel electrophoresis. The sense strand DNA could be verified as being single stranded, because there was an absence of super-shift upon incubation of the recovered supernatant (single-stranded non-biotinylated DNA library) with the streptavidin solution (lane #7 of **Fig. 5.1**).

5.2. SELEX generated DNA aptamers against H69 with streptavidin-coated 96-well plates and Dynal® magnetic beads

Two alternative methods of incubation were selected and compared, specifically, a rotational incubation on sphere-shaped streptavidin surfaces (beads) versus 96-well micro-titer plates using a forward and backward rocking incubation method. Twelve rounds of SELEX were performed on streptavidin-coated magnetic beads, and fifteen were performed using streptavidin-coated plates. The first binding analysis was monitored as the percent of bound DNAs in the library during SELEX by using UV-Vis spectroscopy. Evolution of the DNA library was also monitored by using UV-VIS spectroscopy until a plateau in the percent bound was reached (*i.e.*, no significant change in the percent DNA bound in each successive round of SELEX). At this point, the *in vitro* selection process was considered to be complete. SELEX performed using streptavidin-coated plates showed a fluctuating trend of increasing and decreasing percentages of bound DNA ligands between successive rounds #1 -15 (**Fig. 5.2**). An overall trend of increasing percentage of bound DNA library to H69 with each successive round was observed for SELEX performed using streptavidin-coated magnetic beads of 77% between successive

rounds #1 -11 (**Fig. 5.2**). The best results were obtained when rotational incubation on sphere-shaped surfaces was done instead of the forward and backward rocking incubation method used on the 96-well streptavidin-coated micro-titer plates. Overall, preliminary percentage of the bound DNA library results indicate that screening DNA aptamer candidates against H69 utilizing biotinylated $\Psi m^3 \Psi \Psi$ H69 immobilized on streptavidin-coated beads was more effective than using the streptavidin-coated plate method (**Fig. 5.2**).

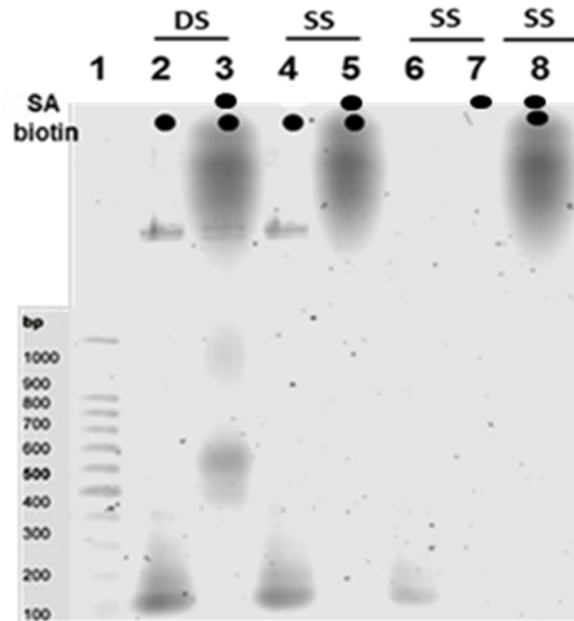
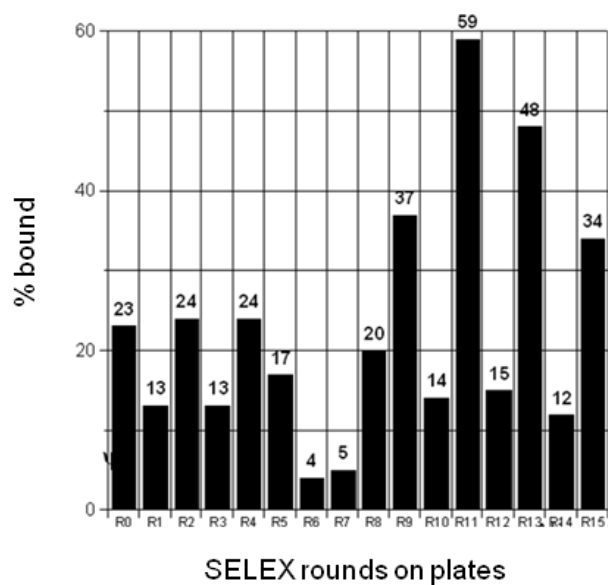


Figure 5.1. Super-shift assay for biotin-strand capture for separation of the sense and antisense-strands. Results were confirmed by agarose gel analysis and super-shift assays to generate the initial single-stranded DNA library as follows: lane #2: DS+b (biotinylated double-stranded DNA library); lane #3: (DS+b)+SA (biotinylated double-stranded DNA library incubated with streptavidin solution); lane #4: SS+b (biotinylated single-stranded DNA library); lane #5: SS+b (biotinylated single-stranded DNA); lane #6: SS (non-biotinylated single-stranded DNA library); lane #7: SS + SA (single-stranded DNA library incubated with streptavidin solution); and lane #8: (SS+b) + SA (biotinylated single-stranded DNA library incubated with streptavidin solution). All samples were run on a 1% agarose gel at 90 V for 1 h with a 100 bp ladder (lane #1).

a)



b)

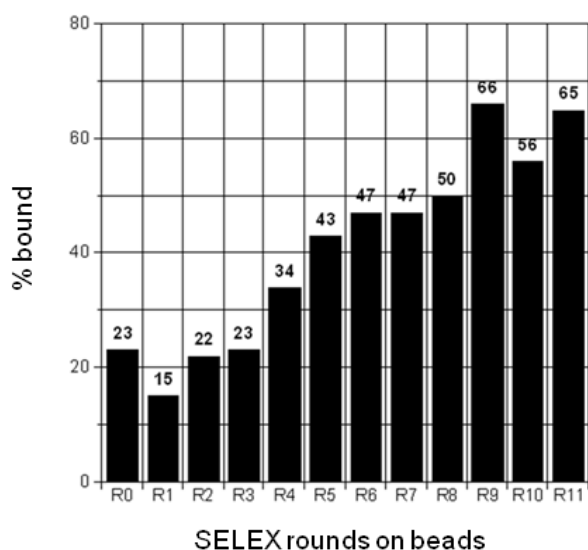


Figure 5.2. Results of binding of DNA library pools from SELEX rounds. H69 binders were generated by the SELEX process. Percent bound of DNA library was determined by UV-Vis spectroscopic monitoring of starting and ending amount (pmoles) of library recovered within the supernatant. SELEX rounds were challenged with 5'-biotinylated- $\Psi m^3 \Psi \Psi$ immobilized to streptavidin-coated 96-well micro-titer plates (a). Results from SELEX rounds challenged with 5'-biotinylated- $\Psi m^3 \Psi \Psi$ immobilized to streptavidin-coated magnetic beads (b).

5.3. Inverse proportionality of reduced diversity to increased percent DNA bound confirmed with each successive round

Evolution of the DNA library was monitored using UV-VIS spectroscopy. There was a broad range of binding affinities exhibited by the diverse pool of selected DNA ligands to H69 (**Fig. 5.2**). With each successive round, unbound DNA library ligands were washed away before the PCR amplification step. The DNA library populations having affinity for H69 were enriched during the SELEX process with each subsequent round of incubations with immobilized H69 using direct-bead PCR amplification. Ultimately, this enriched library population of binders to H69 was expected to exhibit lower sequence diversity with each subsequent round. The predicted diversity level could be determined by using the information of percent bound and UV-Vis quantification of products for each round (**Eq. 4.3**). The diversity of the library was reduced to approximately 1×10^4 molecules using the SELEX method with magnetic beads (**Table 5.1**). The final round of SELEX represented the maximum enrichment of the DNA library to be cloned and sequenced for identification of DNA aptamer candidates, and rounds #9, 13, 14 (plates) and 3, 4, 5, 6, 7, 8, and 11 (beads) were chosen for cloning and sequencing analysis and identification of the DNA aptamer candidates (**Table 5.1**).

5.4. Sequencing and cloning results

Once SELEX was complete, a total of 120 clones were isolated representing ten plasmid DNA clones each from SELEX rounds #3, 4, 5, 6, 7, 8, and 11 (streptavidin-coated magnetic-beads), ten plasmid DNA clones from SELEX rounds #9, 13, 14, and 20 clones from round #15

(streptavidin-coated plates). Positive transformants were analyzed by colony PCR using the combination of the cloning vector-specific M13 forward (5'-gaattcgcctt-3') and M13 reverse primers (5'-agggcgaattctgc-3') from the *E. coli* colonies. Plaques of 100 DNA inserts were

Table 5.1. SELEX round diversity for DNA pools challenged with 5'-biotinylated- Ψ m³ Ψ .

SELEX	Percent bound (magnetic beads)	Estimated diversity value (DNA library members)
Round 0	23	1×10^{13}
Round 1	15	10×10^{12}
Round 2	22	2×10^{12}
Round 3	23	3×10^{11}
Round 4	34	9×10^{10}
Round 5	43	7×10^9
Round 6	47	2×10^8
Round 7	47	5×10^5
Round 8	50	8×10^3
Round 9	66	5×10^3
Round 10	56	8×10^2
Round 11	65	5×10^2

selected for capillary gel electrophoresis sequencing and 58% of the sequenced clones were positive and unambiguously identified to contain full-length 84-nt DNA insert with both flanking primer regions of the cloning vector (*i.e.*, M13 forward and reverse primers) and the complete

forward and reverse PCR flanking primer sequencings of the 40-nt randomized region of the 84-nt DNA library (Fig. 5.3).

Aptamer # (5'→3')	Forward Primer	40-nt Randomized Region	Reverse Primer
Aptamer 1	gccggatccgggcctcatgtcgaa	CGGGACCTAACACACACCTCCCCAACCCACCCCA	agctcagaagaacgctcaa
Aptamer 2	gccggatccgggcctcatgtcgaa	ACGCGGACCTAACACACACCTCCCCAACCCACCCCA	agctcagaagaacgctcaa
Aptamer 3	gccggatccgggcctcatgtcgaa	CTCGGCCCTTTGACCAAAGAGAGAACAAAAATAAA	agctcagaagaacgctcaa
Aptamer 4	gccggatccgggcctcatgtcgaa	ACGGACCTAACACACACCTCCCCAACCCACCCCA	agctcagaagaacgctcaa
Aptamer 5	gccggatccgggcctcatgtcgaa	CGACGGACCTAACATCAACCTGCCCAACCCACCTCA	agctcagaagaacgctcaa
Aptamer 6	gccggatccgggcctcatgtcgaa	TTTATCCCTCACATGGGAACTTCCGTACGCCTATGAGTT	agctcagaagaacgctcaa
Aptamer 7	gccggatccgggcctcatgtcgaa	ACGCGGACCTAACACACACCTCCCCAACCCACCCCA	agctcagaagaacgctcaa
Aptamer 8	gccggatccgggcctcatgtcgaa	CTAAGGGACTATTCTGCAGTTTAAACGAATTCGACCCT	agctcagaagaacgctcaa
Aptamer 9	gccggatccgggcctcatgtcgaa	ACGCGGACCTAACACACACCTCCCCAACCCACCCCA	agctcagaagaacgctcaa
Aptamer 10	gccggatccgggcctcatgtcgaa	AACGACGGAACTAACCAACAACCTACCCCAACCCAC	agctcagaagaacgctcaa
Aptamer 11	gccggatccgggcctcatgtcgaa	ACGCGGACCTAACACACACCTCCCCAACCCACCCCA	agctcagaagaacgctcaa
Aptamer 12	gccggatccgggcctcatgtcgaa	GCCCTGCCCGCATACCTCACTTCTTTCTAGACCCACACT	agctcagaagaacgctcaa
Aptamer 13	gccggatccgggcctcatgtcgaa	CAGGTCGCTTACGCCGCTGCCCACTCAACCAACCCCT	agctcagaagaacgctcaa
Aptamer 14	gccggatccgggcctcatgtcgaa	ACGCGGACCTAACACACACCTCCCCAACCCACCCCA	agctcagaagaacgctcaa
Aptamer 15	gccggatccgggcctcatgtcgaa	TACCTAGATCCCCTCTCCAACCTTGCTAACCTACCCCA	agctcagaagaacgctcaa
Aptamer 16	gccggatccgggcctcatgtcgaa	ACGCGGACCTAACACACACCTCCCCAACCCACCCCA	agctcagaagaacgctcaa
Aptamer 17	gccggatccgggcctcatgtcgaa	TGCAAGTTTCAACAAGCAATTCAGCACACATTTGCAGCA	agctcagaagaacgctcaa
Aptamer 18	gccggatccgggcctcatgtcgaa	CTCCCCGGGCACTATTTCTGGGACTAGTTCTGCAGGTTT	agctcagaagaacgctcaa
Aptamer 19	gccggatccgggcctcatgtcgaa	GGGACTATTTCTGCAGGTTTGGGACTAGTTCTGCAGGTTT	agctcagaagaacgctcaa
Aptamer 20	gccggatccgggcctcatgtcgaa	CGGGACCTAACACACACCTCCCCAACCCACCCCA	agctcagaagaacgctcaa

Figure 5.3. Sequence results for DNA library. Aptamers sequenced represent rounds #3, 4, 5, 6, 7, 8, and 11 (streptavidin-coated magnetic beads) and rounds #9, 13, 14, and 15 (streptavidin-coated plates). The randomized 40-nt region (red) is flanked by both forward and reverse primers (blue).

5.6. Clustal W sequence analysis identified consensus sequences

The web-based sequence alignment computer program, Clustal W, (<http://www.ebi.ac.uk/Tools/msa/clustalw2/>) was used to further analyze these positively sequenced clones. Clustal W identified 20 sequences showing significant sequence homology within the 40-nt randomized region (Fig. 5.4). They were then assigned to the following groups according a consensus of their primary sequences: group 1 (*i.e.*, aptamers #1, 2, 4, 5, 7, 9, 10,

11, 14, 15, 16, and 20); group 2 (*i.e.*, aptamers #8, 18, and 19; and group 3 (*i.e.*, aptamers # 3, 6, 12, 13, and 17). Group 1 was the largest and has a consensus sequence of 5'-ACGCGGACCTAACACACACCTCCCCCAACCACCCACCC-3' and group 2 has a consensus sequence of 5'-GGGACTATTTCTGCACGTT-3' (Fig. 5.4). Finally, sequences from group 3 represented an “orphan” group, as they did not exhibit any sequence homology aptamers from groups 1 or 2. Despite this, all groups were included for further analysis by *Mfold* to identify secondary structural homology and possible shared common motifs.

```

CLUSTAL W (1.81) multiple sequence alignment (5'→3')
3Aptamer      ----CTCGGCCCCCTTTGACCAAAGAGA-GAACAAAAAATAAA-----
13Aptamer     -----CAGGTCGCTTACGCCCGCTGCC-CACTCAACCAACCACCT---
7Aptamer      --ACGCGGACCT-----AACACACACCT-CCCCCAACCACCCACCC--
9Aptamer      --ACGCGGACCT-----AACACACACCT-CCCCCAACCACCCACCC--
16Aptamer     --ACGCGGACCT-----AACACACACCT-CCCCCAACCACCCACCC--
14Aptamer     --ACGCGGACCT-----AACACACACCT-CCCCCAACCACCCACCC--
11Aptamer     --ACGCGGACCT-----AACACACACCT-CCCCCAACCACCCACCC--
2Aptamer      --ACGCGGACCT-----AACACACACCT-CCCCCAACCACCCACCC--
1Aptamer      ---CGCGGACCT-----AACACACACCT-CCCCCAACCACCCACCCCA
4Aptamer      ----ACGGACCT-----AACACACACCT-CCCCCAACCACCCACCC--
20Aptamer     --CGACGGACCT-----AACACAACCTC-ACCCCAACCACCCACCC--
5Aptamer      --CGACGGACCT-----AACATCAACCTGCCCAACCACCCTCAC---
10Aptamer     AACGACGGAACCTAAACAACAACAACCTACCCCAACCAC-----
15Aptamer     -TACCTAGATCCC---CCTCTCCAACCTTCGCTAACCTACCC-----
12Aptamer     ---GCCCTGCCCGCA--TACCTCACTTCTTTCTAGACCCACACTC----
8Aptamer      --CTAAAGGGACTATT-CCTGCACGTTTAAA---CGAATTCGACCT--
19Aptamer     -----GGGACTATTTCTGCACGTTTAGGATCTGAATTCGACCC---
18Aptamer     CTCCCCGGGACTATTTCTG-GGACTAGTTCTGCAGGTTT-----
17Aptamer     --TGCAAGGTTTCA---ACAAGCAATTCAGCACACATTTGCAGCA----
6Aptamer      -----TTTATCCCTCACATGGGAAACTT-CCGTACGCCTATGAGTT---

```

Figure 5.4. Clustal W multiple sequence alignment data consensus sequences of DNA library. Alignment results from Clustal W data analysis of SELEX products of rounds challenged against biotin-labeled H69 immobilized to streptavidin-coated magnetic beads. Groups of consensus sequences were found for the 40-nt randomized regions and include group 1 (shaded grey), group 2 (outlined in black), and group 3 (no box or shading).

5.7. *Mfold* analyses predicted diverse secondary structures for consensus sequences

The *Mfold*[®] package (version 2.3)¹³⁵ uses free energy rules to determine optimal and suboptimal secondary structures of single-stranded DNA molecules, and was used to obtain secondary structural predictions for select sequenced DNA aptamer candidates as well as their theoretical standard-state free energies. The *Mfold* results were used to identify secondary structural motif regions for classification of the 20 DNA aptamers into families. Each aptamer that was analyzed for both untruncated (84-nt) and truncated (40-nt) sequences showed at least one secondary structural motif (*i.e.*, hairpin, bulge, etc.), and many exhibited more unique and diverse secondary structures while simultaneously exhibiting conserved motifs with other aptamers of the library. Also, *Mfold* analysis of aptamers #8 and 18 revealed hairpin loops of similar size (20-nt) and sequence to their target, H69 (19-nt). As expected, a full-length 80-nt (untruncated) aptamer *Mfold* standard-state free energies (ΔG° in kcal/mol) were greater (thermodynamic stabilities) compared to the corresponding 40-nt (truncated) (**Table 5.2**). The *Mfold* secondary structural predictions represent possible folding with minimized energy levels for the aptamer candidates, and only approximations of their ΔG° values can be determined from the prediction methods.

Overall, our results from secondary structures predicted by *Mfold* for untruncated full-length aptamers #1-20 reveal both primary sequence homology motifs (*i.e.*, hairpin loops, bulges, etc.) and were assigned to five families. Family I includes aptamers #8 and #18. Next, family II consists of aptamers #3, 6, and 12 (blue) (**Fig. 5.5**). Family III consist of aptamers #3, 13 and 19 (red) (**Fig. 5.5**). Family IV consists of aptamers #1, 7, 9, 11, 14 and 16 (green) (**Fig. 5.5**).

Table 5.2. Thermodynamic analysis of cloned and sequenced H69-aptamers.

Aptamer #	Sequenced randomized region of DNA aptamers	ΔG° [a]	ΔG° [b]
		kcal/mol	kcal/mol
1	CGCGGACCTAACACACACCTCCCCAACCACCCACCCCA	+0.61	-3.35
2	ACGCGGACCTAACACACACCTCCCCAACCACCCACCCC	+0.61	-17.31
3	CTCGGCCCTTTGACCAAAGAGAGAACAAAAAATAAA	-2.22	-6.03
4	ACGGACCTAACACACACCTCCCCAACCACCCACCCC--	+0.61	-3.51
5	CGACGGACCTAACATCAACCTGCCCCAACCACCTCAC	+0.80	-3.91
6	TTTATCCCTCACATGGGAACTTCCGTACGCCTATGAGTT	-1.57	-6.17
7	ACGCGGACCTAACACACACCTCCCCAACCACCCACCC	+0.61	-3.04
8	CTAAAGGGACTATTCTGCACGTTTAAACGAATTCGACCC <u>T</u>	-4.09	-9.13
9	ACGCGGACCTAACACACACCTCCCCAACCACCCACCCC-	+0.61	-3.64
10	AACGACGGAACCTAAACAACAACAACCTACCCCCAACCC	+1.20	-4.58
11	ACGCGGACCTAACACACACCTCCCCAACCACCCACCCC	+0.61	-3.64
12	GCCCTGCCCGCATACCTCACTTCTTTCTAGACCCACACTC	+0.42	-6.15
13	CAGGTCGCTTACGCCCGCTGCCCCACTCAACCAACCACCT	-0.64	-6.08
14	ACGCGGACCTAACACACACCTCCCCAACCACCCACCCC	+0.61	-3.64
15	TACCTAGATCCCCCTCTCCAACCTTCGCTAACCTACCCC	+0.27	-3.95
16	ACGCGGACCTAACACACACCTCCCCAACCACCCACCCC	+0.61	-3.64
17	TGCAAGGTTTCAACAAGCAATTCAGCACACATTTGCAGCA	-1.65	-6.13
18	CTCCCCGGGCACTATTTCTGGGACTAGTTCTGCAGGTTT	-4.15	-8.13
19	GGGACTATTTCTGCACGTTTAGGATCTGAATTCGACCC-	-0.87	-7.84
20	CGACGGACCTAACACAACCTCACCCCAACCACCCACCCC	+0.70	-3.91

The identification of 20 clones with the consensus sequence in the randomized region: Standard-state free energy of reactions (ΔG° in kcal/mol) of both 40-nt^[a] length (truncated) and 80-nt^[b] length (untruncated) are reported for sequenced clones of SELEX DNA library.

Family V includes aptamers #4, 5, 10 and 20 (orange) (**Fig. 5.5**). Aptamers lacking sequence or structural consensus matching any of the aforementioned families were not assigned a color (*i.e.*, aptamers #2, 15 and 17) (**Fig. 5.5**). Conserved secondary structural motifs of H69DNAaptamers were identified that correspond with the target's 19-nt hairpin loop (**Fig. 5.6**). Interestingly, one of the selected DNA ligands (H69DNAapt18) contained a conserved 20-nt hairpin-loop motif with complementarity to the loop region of the targeted *E. coli* wild-type H69. This 20-nt hairpin motif of H69DNAapt18 retained its conserved 20-nt motif within the truncated 40-nt *Mfold* structural prediction representing only the randomized region of the 84-nt DNA library (**Table 5.3**). Thermodynamic analysis of cloned and sequenced H69-aptamers were performed and among the 120 clones, 100 individual sequences were identified, 20 of which were found to have a consensus sequence by Clustal W software analysis, and their secondary structures were investigated using the *Mfold* program.¹⁴⁹

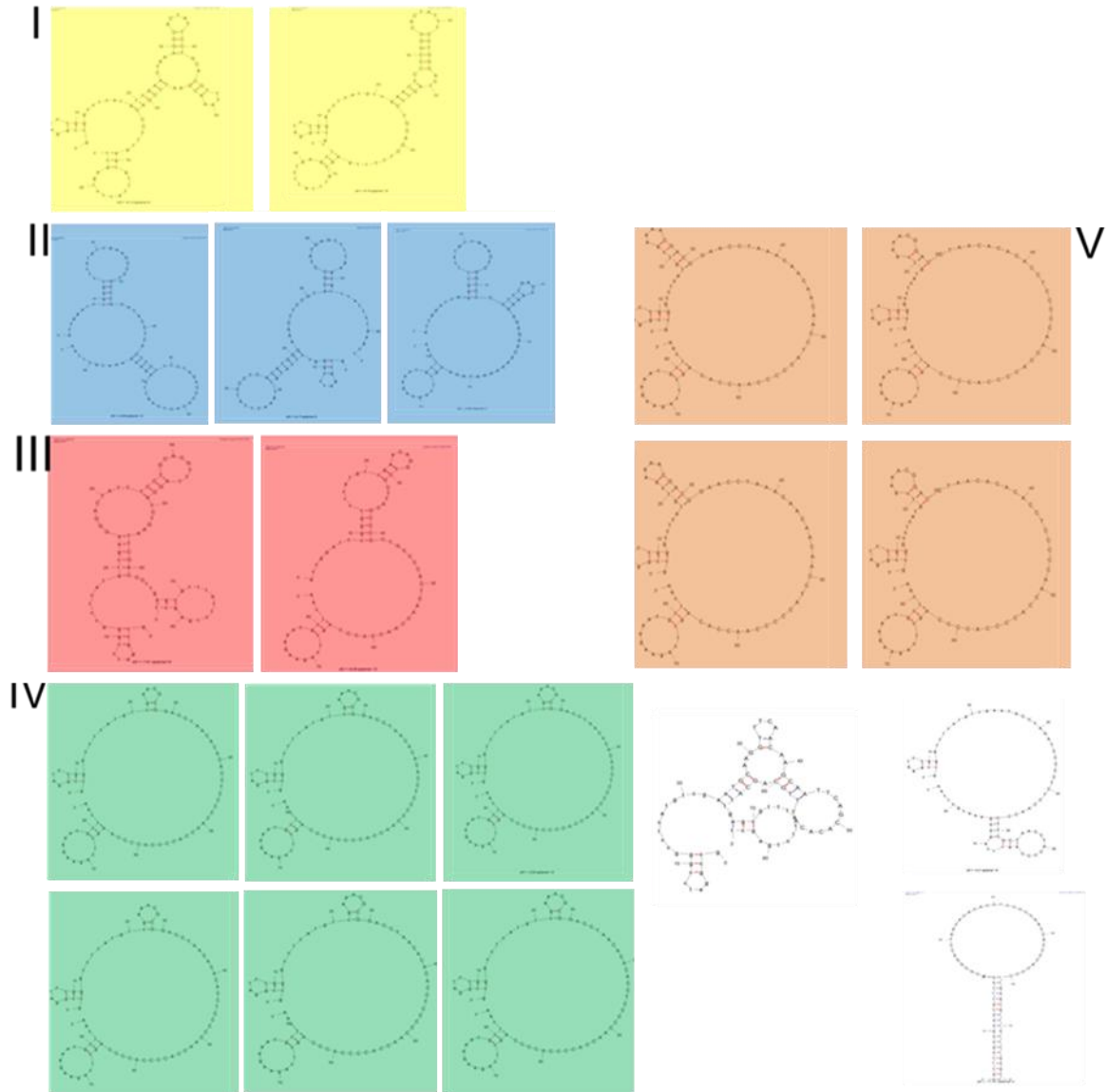


Figure 5.5. *Mfold* family grouping results from SELEX with magnetic beads for aptamers #1-20. Predicted structures include both the flanking and randomized regions of the full-length 84-nt aptamers. These 20 sequences were divided into five families containing the following aptamers: family I (#8, #18 shown in yellow), II (#3, #6, #12 shown in blue), III (#13, #19 shown in red), IV (#1, #7, #9, #11, #14, #16 shown in green), and V (#4, #5, #10, #20 shown in orange). Aptamers without a family are not highlighted.

Table 5.3. Conserved hairpin motifs of aptamers #8 and 18.

Aptamer	Length (nt)	Sequence (5'→3')	DNA loop regions (5'→3')
apt #18	84	gcggatccgggcctcatgtcgaaCTCCCGG GCCTATTTC CTGGGA CTAGTTCTGCAGGTTTtcgagtcctcttgcgagtt (untruncated H69DNAapt18)	GCCTATTTC
apt #18	40	CTCCCGG GCCTATTTC CTGGGACTAGTTCTGCAGGTTT (truncated H69DNAapt18)	GCCTATTTC
apt #8	84	gcggatccgggcctcatgtcgaaCTAAAGG GACTATTC CTGCA CGTTTAAACGA AATTCGACCCTtcgagtcctcttgcgagtt (untruncated)	GACTAT TTTAA
apt #8	40	CTAAAGG GACTATTC CTGCAC CGTTTAAACGA AATTCGACCCT (truncated)	GACTAT TTTAA

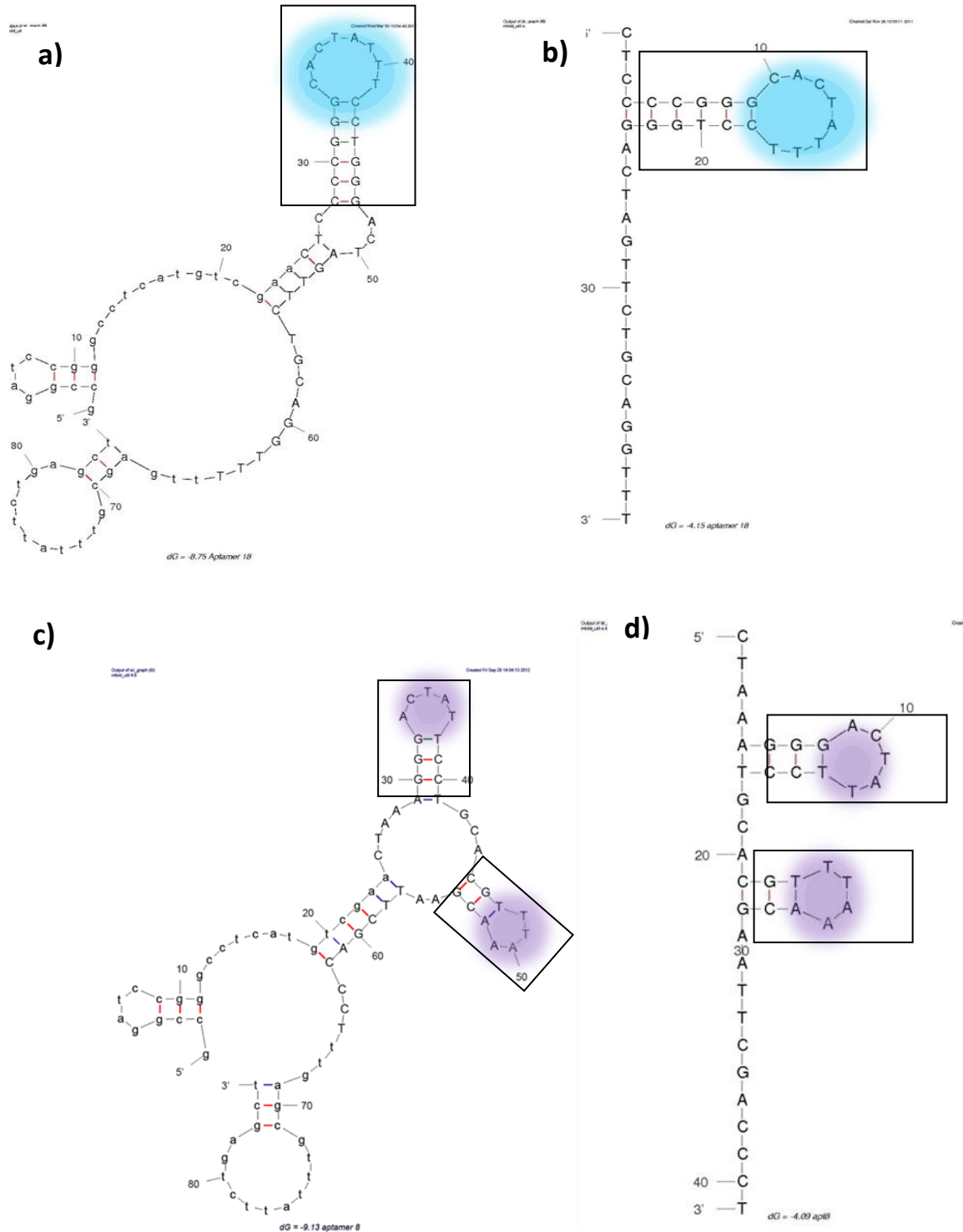


Figure 5.6. Conserved hairpin motifs of aptamers #8 and 18. Untruncated 84-nt aptamer#18 (a) versus truncated 40-nt length aptamer #18 (b) has a conserved sequence and hairpin apex loop region (blue). Untruncated 84-nt aptamer#8 (c) versus truncated 40-nt length aptamer #8 (d) has a conserved sequence and hairpin apex loop region (purple).

5.8. Diversity of DNA structures

Primary sequence and secondary structural information on the DNA aptamer candidates were obtained to identify a consensus and level of diversity. Complete predicted *Mfold* structures of full-length (84-nt) and truncated (40-nt) aptamer # 18 are shown in **Figures 5.7 and 5.8** and (see **Appendix Figures A1-A37** for full structures of untruncated and truncated aptamers #1-7, and #9-17, and #19-20).

Figure 5.7. *Mfold* structural analysis of untruncated aptamer #18.

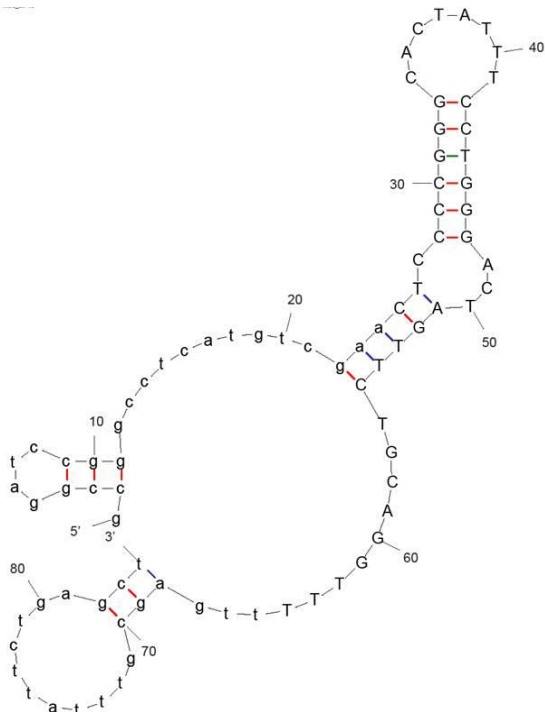
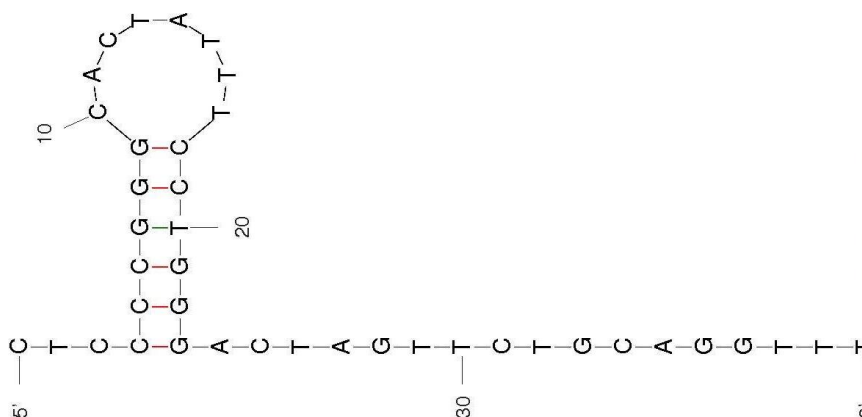
<i>Mfold</i> Structural Analysis		Aptamer #18
Length:		84-nt (untruncated)
Sequence:	5'-gccgatccgggcctcatgtcgaaCTCCCCGGGCACTATTTTCCT GGGACTAGTTCTGCAGGTTTtgagcgttattctgagct-3'	
2° structural motifs:		hairpin loops: L1, L2 and L3 internal loop: IL1
Family:		

Figure 5.8. Mfold structural analysis of truncated aptamer #18.

Mfold Structural Analysis	Aptamer #18
Length:	84-nt (truncated)
Sequence:	5'-CTCCCCGGGCACTATTTCTGGGACTAGTTCTGCAGGTTT-3'
2° structural motifs:	hairpin loop: L1
Family:	I



5.9. Dissociation constants for H69DNAapt18: binding to wild-type H69 observed by EMSA and fluorescence titration experiments

Aptamers presumed to have affinity for wild-type H69 based on primary sequence and secondary structural analysis were selected to be further characterized by EMSA experiments.

Electrophoretic mobility shift assays (EMSAs) of DNA/RNA complexes were used to determine apparent binding constants for aptamers #1-20. Preliminary binding results from EMSA gel analysis were crude and show moderate binding affinity (nM range) for H69 (**Table 5.4.**). Although EMSAs of DNA/RNA complexes were not clearly detected for all 20 selected aptamers, preliminary binding experiments with aptamers against radiolabeled H69 revealed formation of complexes with aptamers #16, 17, and 18 in the mid nM range (**Figs. 5.9, 5.10, and 5.11**). All other EMSA results for aptamers #1-15 and aptamers #19-20 are shown in **Appendix Figures A38 - 58**. These experiments were not repeated due to the large amount of material required and limitations of the chemically synthesized target H69 as well as the individual aptamers.

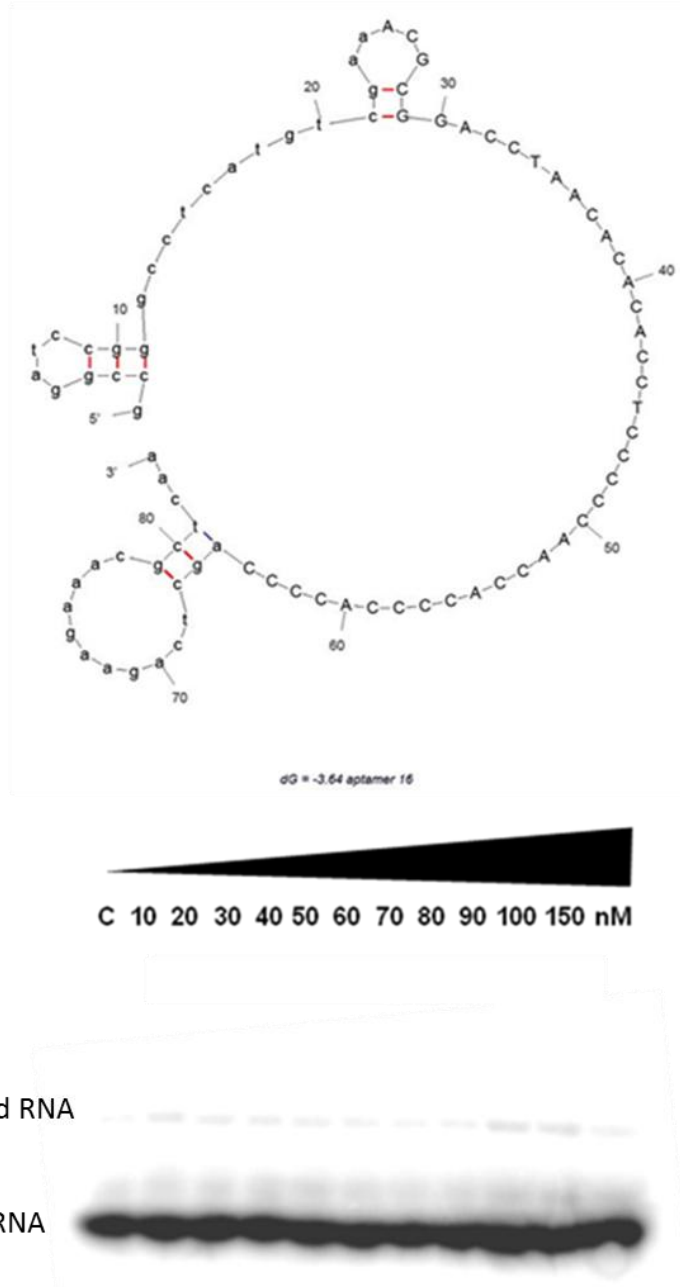


Figure 5.9. Preliminary EMSA binding results for DNA aptamer #16. EMSA gel was performed on a 10% non-denaturing polyacrylamide gel with $0.5\times$ TBE running buffer and run for 1 h at 15 mA. H69 was denatured at $94\text{ }^{\circ}\text{C}$ for 1 min and cooled to refold for 2 h at $37\text{ }^{\circ}\text{C}$. $[^{32}\text{P}]$ 5'-end-labeled wild-type H69 (1 nM) was pre-incubated at $37\text{ }^{\circ}\text{C}$ for 15 min in buffer containing 50 mM Tris-HCl pH 7.5, 10 mM MgCl_2 , 50 mM NaCl. DNA aptamer #16 has an increasing concentration (0 – 150 nM) incubated with 1 nM of H69. A dark arrow indicates evidence of $[^{32}\text{P}]$ -H69 forming complexes with DNA aptamers ($\geq 10\text{ nM}$). The complex was difficult to visualize; however, a decrease in the amount of uncomplexed material is evidence for a binding event.

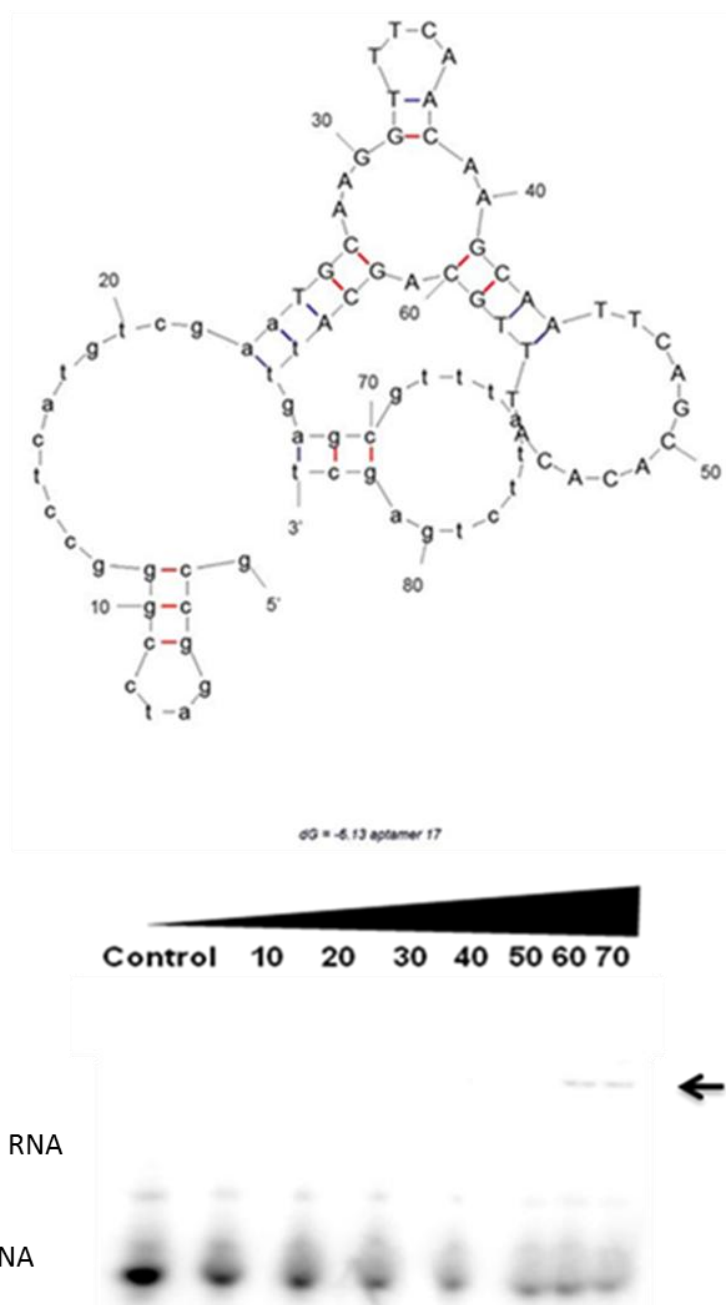


Figure 5.10. Preliminary EMSA binding results for DNA aptamer #17. Reaction conditions are the same as in EMSA experiment from Fig. 5.9. Secondary *Mfold* structure prediction of aptamer #17 is pictured above EMSA gel analysis for aptamer #17 of increasing concentration (0 – 70 nM) incubated with 1 nM of H69. A dark arrow indicates evidence of [³²P]-H69 forming complexes with DNA aptamer #17 (≥ 60 nM).

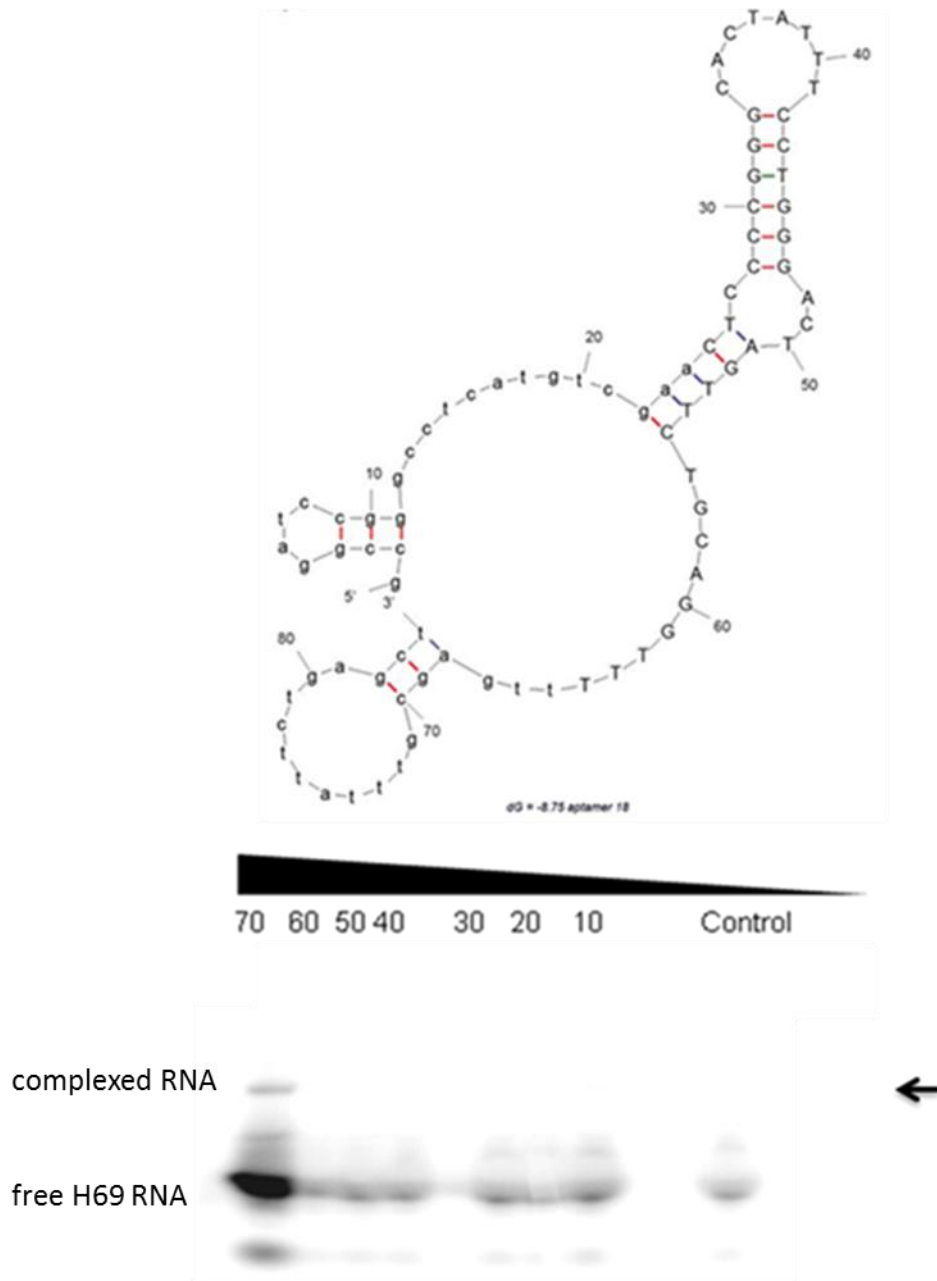


Figure 5.11. Preliminary EMSA binding results for DNA aptamer #18. Reaction conditions are the same as in EMSA experiment from **Fig. 5.9**. Secondary *Mfold* structure prediction of aptamer #18 is pictured above EMSA gel analysis for aptamer #18 of increasing concentration (0 – 70 nM) incubated with 1 nM of H69. A dark arrow indicates evidence of [³²P]-H69 forming complexes with DNA aptamer #18 (≥ 60 nM).

Table 5.4. Summary of apparent dissociation constants (K_d s) from EMSA binding experiments.

APTAMER #	K_d (nM)
8	80
9	60
10	90
11	90
16	100
17	70
18	70

All K_d values are reported in (nM) range. No binding was observed for aptamers #1-7, 12-15, and 19-20.

5.10. Fluorescence titration comparison binding studies: DNA aptamer #18 binding results

DNA/RNA complexes were further characterized by fluorescence titration assays to confirm the previous binding assays (*i.e.*, monitoring of percent bound in SELEX rounds and EMSAs). Based on the combined results from the monitoring of the percent bound of DNA library to H69 during SELEX rounds and analysis of the aforementioned complexes observed from EMSA assays, DNA aptamer #18 was chosen to be synthesized with a fluorescein tag for further binding characterization to H69 and related constructs. Binding of the isolated, sequenced, and characterized DNA aptamer #18 to H69 constructs and A-site rRNA were monitored by a decrease in the fluorescence emission intensity of the attached fluorescein dye. Fluorescence quenching upon binding of fluorescently labeled ligand (300 nM) was observed in the range of 0 – 1,000 nM for modified and unmodified H69 constructs (*i.e.*, $\Psi\Psi\Psi$ and UUU), and unrelated A-

site rRNA during titrations. Fluorescence data were collected until saturation was reached and data were fitted to a binding curve using for relative fluorescence (F_r) free RNA.

Interestingly, the conserved motif of DNA aptamer #18 also exhibits sequence complementarity to the wild-type H69 loop region that may be partially responsible for selectivity and high affinity binding by fluorescence titrations with wild-type H69. Fluorescence titration comparison binding studies show that DNA aptamer #18 has greater affinity for wild-type H69 ($\Psi m^3 \Psi \Psi$) over unmodified H69s (UUU) and more than 100-fold greater affinity over the unrelated A-site rRNA. The truncated FAM-H69DNAaptamer18 was not synthesized and the dissociation constants for wild-type H69 were not measured and compared. Fluorescence titrations of modified or unmodified H69 constructs with FAM-H69DNAapt18 provided spectra used for determining dissociation constants for DNA aptamer #18. Fluorescence titration experiments did not exhibit large differences in aptamer #18 dissociation constants. All had modest affinity in the low μM range. The trend in the relative affinities for binding to fluorescently labeled DNA aptamer #18 was found to decrease in the order: $\Psi m^3 \Psi \Psi > \Psi \Psi \Psi > UUU > A\text{-site}$ (**Figs. 5.12 – 5.15**).

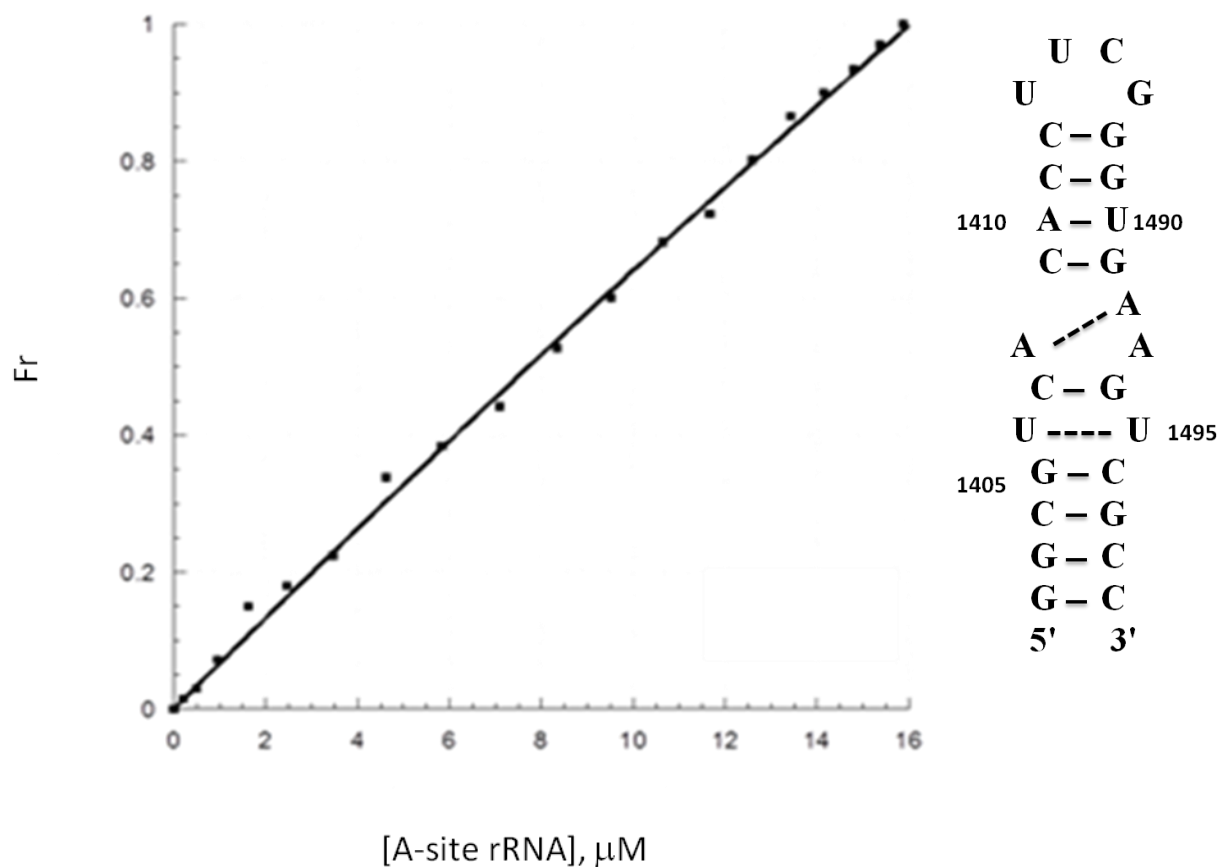


Figure 5.12. Relative binding affinities of fluorescently labeled DNA aptamer #18 to A-site rRNA. The dissociation constant of the fraction of A-site bound to F-H69DNAapt18 aptamer obtained by fitting data to quadratic **Equation 4.4** is $>100 \mu\text{M}$ ($R^2=0.99$). An estimated K_d from visual analysis of the half-maximal binding of rRNA could not be determined from the range of A-site rRNA concentrations tested.

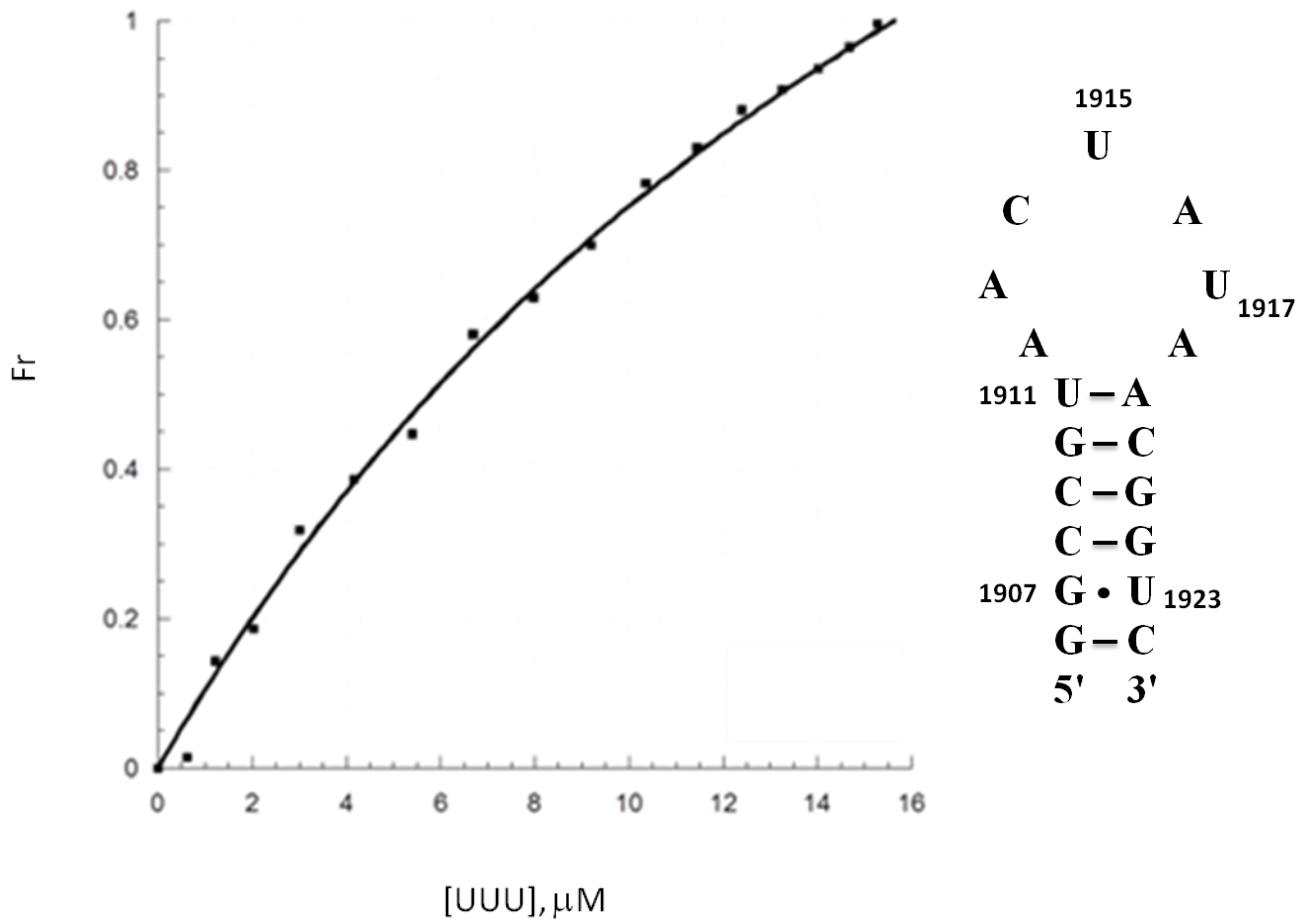


Figure 5.13. Relative binding affinities of fluorescently labeled DNA aptamer #18 for UUU. The dissociation constant of the fraction of UUU bound to F-H69DNAapt18 aptamer obtained by fitting data to quadratic **Equation 4.4** is $22 \mu\text{M}$ ($R^2=0.99$). The estimated K_d obtained from visual analysis of the half-maximal binding of UUU to F- H69DNAapt18 is $\sim 6 \mu\text{M}$.

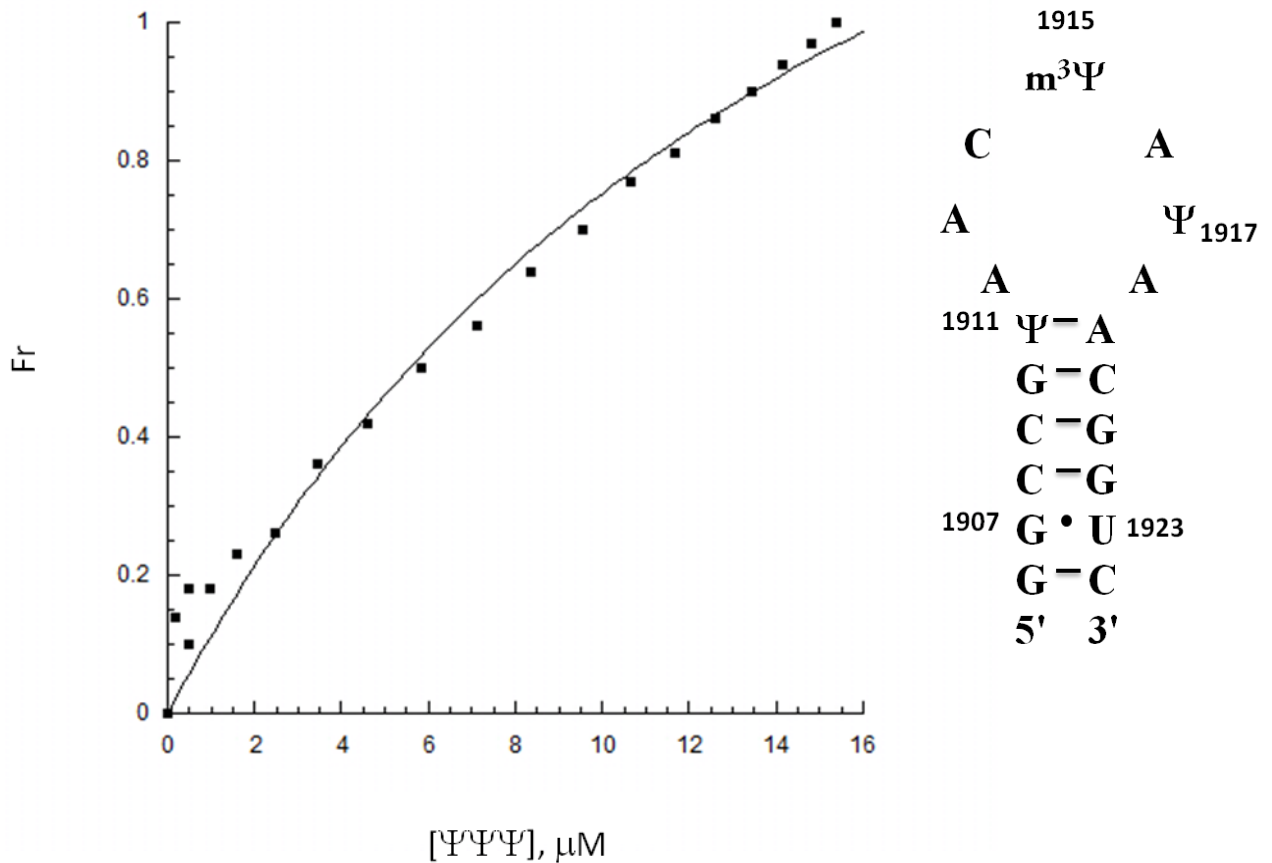


Figure 5.14. Relative binding affinities of fluorescently labeled DNA aptamer #18 for ΨΨΨ.

The dissociation constant of the fraction of ΨΨΨ bound to F-H69DNAapt18 aptamer determined by fitting to **Equation 4.4** is 14 μM ($R^2=0.96$). The estimated K_d obtained from visual analysis of the half-maximal binding of ΨΨΨ to F-H69DNAapt18 is ~4 μM.

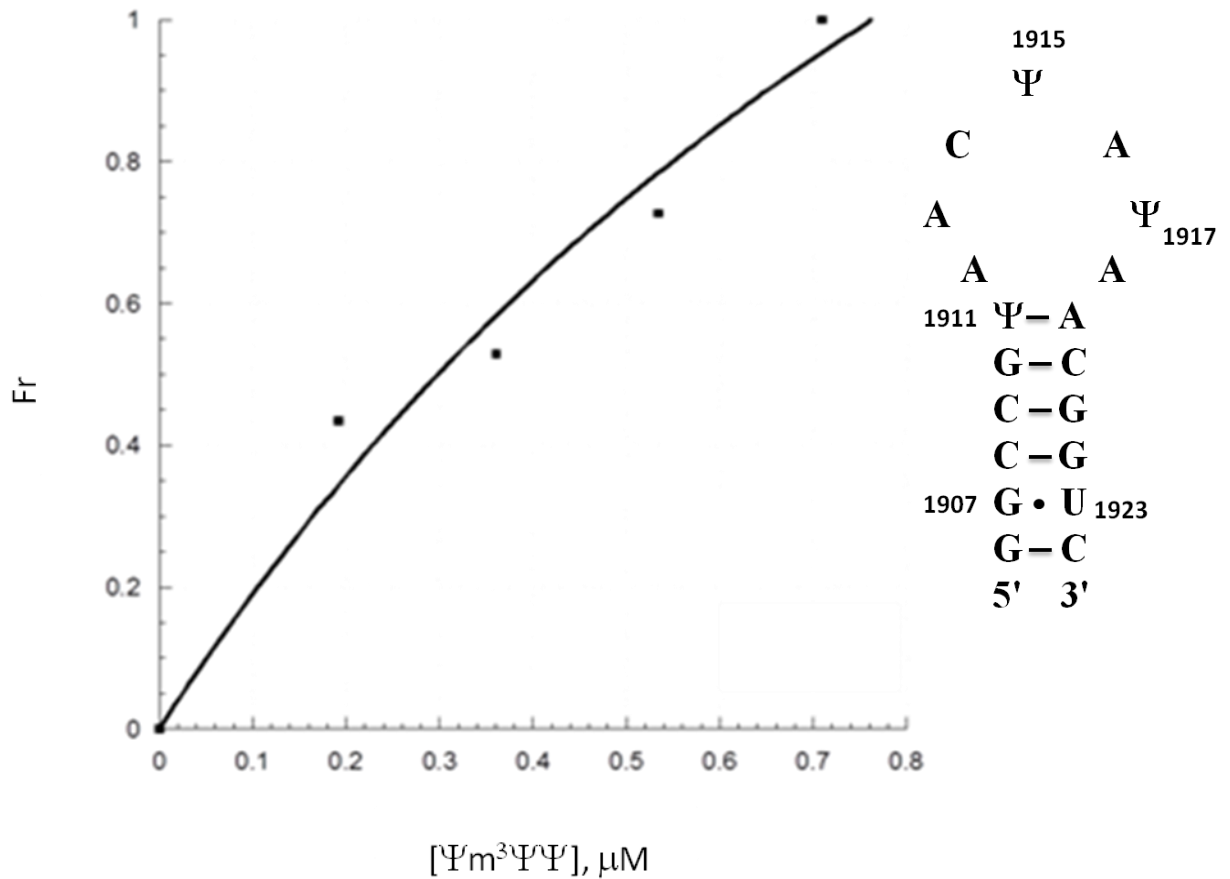


Figure 5.15. Relative binding affinities of fluorescently labeled DNA aptamer #18 for Ψm³ΨΨ. The dissociation constant of the fraction of Ψm³ΨΨ bound to F-H69DNAapt18 aptamer calculated by fitting to **Equation 4.4** is 1 μM ($R^2=0.96$). The estimated K_d obtained from visual analysis of the half-maximal binding of ΨΨΨ to F-H69DNAapt18 is ~300 nM.

CHAPTER 6 – DISCUSSION: DNA APTAMERS SELECTIVE FOR WILD-TYPE H69

Our research goals were to identify DNA ligands from a randomized library that could be generated with moderate (low μM) affinity and selectivity for wild-type H69, a highly conserved motif participating in the inter-subunit bridge B2a of ribosomes.⁸⁰ This 19-nt hairpin-loop structure contains three conserved pseudouridine (Ψ) modifications at positions 1911, 1915, and 1917, in which Ψ 1915 is further modified to 3-methylpseudouridine ($m^3\Psi$).⁸¹ Helix 69 plays important roles in protein synthesis, and the development of novel therapeutics based on DNA aptamers targeting H69 would be helpful to counter emergent bacterial resistance.

6.1. SELEX optimization and DNA aptamer consensus sequences

DNA library pools were selected within 11 rounds of SELEX, and the products were confirmed by agarose gel super-shift assays between each SELEX step. After the repetition of successive steps of incubation, partitioning, and amplification, the unbound oligonucleotides were removed and binders with affinity for H69 were enriched through PCR amplification. The initial 84-nt DNA library with an initial diversity of 1×10^{13} , was incubated with wild-type biotin-H69 using two methods of immobilization (*i.e.*, 96-well plates and streptavidin-coated magnetic beads). The newly enriched pool of selected ssDNA ligands served as the starting library for successive rounds of selection until the final diversity of the library was reduced to approximately 1×10^4 , representing an enriched pool of H69-specific aptamer candidates. This refined library was obtained after the 11th round of SELEX performed without the need to

increase the selection stringency between subsequent rounds (incubation times, buffer conditions, etc.). Specifically, successive rounds of SELEX showed an overall increase in affinity of the DNA library for wild-type H69. Our best percent of the bound library was achieved using rotational incubation with H69 bound to streptavidin-coated magnetic beads coupled with direct bead PCR rather than the initial experimental method (*i.e.*, rocking incubation with H69 bound to streptavidin-coated 96-well plates). The more uniform incubation achieved with the rotational incubation method and H69-bound beads versus plates, presumably maximized the surface area for the DNA library to bind, thus explaining the observed increase in percent bound of DNA library with subsequent rounds of SELEX.

Analyses of H69-binding DNA aptamers using Clustal W and *Mfold* (see **Section 6.3** for discussion of *Mfold* results) combined allowed for groupings based on homology of either primary or secondary structure. DNA aptamers were assigned to three groups based on *Mfold* folding results as follows: group 1 (*i.e.*, aptamers #1, 2, 4, 5, 7, 9, 10, 11, 14, 15, 16, and 20); group 2 (*i.e.*, aptamers #8, 18, and 19; and group 3 (*i.e.*, aptamers # 3, 6, 12, 13, and 17). Group 1 consensus sequence = 5'-ACGCGGACCTAACACACACCTCCCCCAACCACCCCACCC-3') followed by group 2 consensus sequence = 5'-GGGACTATTTCTGCACGTT-3'). Group 3 did not show a consensus sequence and thus represented an “orphan” group.

6.2. Determination of selectivity and affinity of DNA aptamers for wild-type H69

The affinity and selectivity of H69DNAapt18 and H69DNAapt8 for wild-type H69 were determined by EMSAs and fluorescence titrations. The dissociation constants of the aptamers,

i.e., H69DNAapt18 and H69DNAapt8, and wild-type H69 were determined by EMSAs to be within the range of 70-80 nM. The error could not be determined due to a low amount of synthetically modified RNA and inability to repeat the experiments. Fluorescence titrations were employed to characterize the specificity of aptamer H69DNAapt18 for wild-type H69 by direct comparisons of the dissociation constants between the aptamer and related RNA constructs related (wild-type, $\Psi\Psi\Psi$, and UUU) as well as an unrelated RNA (A site). Plots of fluorescence titrations of F-H69DNAapt18 bound to wild-type H69 and related RNA constructs ($\Psi\Psi\Psi$ and UUU) as well as unrelated A-site rRNA did not reach saturation within the ranges tested. Therefore, both extrapolated K_d values from calculations using **Equation 4.4 (Figures 5.12 – 5.15)**. The apparent dissociation constants (K_{dS}) of aptamer H69DNAapt18 were determined by fluorescence intensity measurements of a 5'-fluorescein-tagged variant in the presence of increasing concentrations of H69 constructs or the unrelated A-site RNA. The K_{dS} are as follows: [$\Psi m^3\Psi\Psi$ (wild-type H69)] = $1 \pm 0.95 \mu\text{M}$; [$\Psi\Psi\Psi$] = $12 \mu\text{M}$; [UUU] = $22 \mu\text{M}$; and [A-site] $>100 \mu\text{M}$). As shown in **Table 6.1**, the strongest binding (*i.e.*, $K_d = 1 \pm 0.95 \mu\text{M}$) was observed between H69DNAapt18 and wild-type H69. The dissociation constant was increased to $12 \mu\text{M}$ for H69DNAapt18 and $\Psi\Psi\Psi$ when *N3*-methylation at $\Psi 1915$ was not present in the RNA. A further increase in K_d (decreased affinity) was observed between H69DNAapt18 and UUU ($22 \mu\text{M}$), the unmodified H69 without pseudouridylations or *N3*-methylation. The binding between H69DNAapt18 and A-site RNA was the weakest ($K_d >100 \mu\text{M}$). Although, the extrapolated K_d values of H69DNAapt18 for $\Psi m^3\Psi\Psi$, $\Psi\Psi\Psi$, and UUU are approximately 3-fold greater than the visually estimated values (**Table 6.1**), the overall trend of decreasing order of

binding affinities of H69DNAapt18 for wild-type H69 versus variants remained conserved for both methods used to obtain K_d s (i.e., $\Psi m^3\Psi\Psi > \Psi\Psi\Psi > UUU > A$ -site).

Table 6.1. Comparison of K_d values of aptamer #18 binding to wild-type H69 and various rRNA motifs.

DNA Aptamer Targets/rRNA Constructs Structures:			
1915 $m^3\Psi$ C A A Ψ_{1917} A A 1911 $\Psi - A$ G - C C - G C - G 1907 G • U 1923 G - C 5' 3' <i>E. coli</i> wild-type H69 $\Psi m^3\Psi\Psi$	1915 Ψ C A A Ψ_{1917} A A 1911 $\Psi - A$ G - C C - G C - G 1907 G • U 1923 G - C 5' 3' <i>E. coli</i> H69 $\Psi\Psi\Psi$	1915 U C A A U 1917 A A 1911 U - A G - C C - G C - G 1907 G • U 1923 G - C 5' 3' <i>E. coli</i> H69 UUU	1410 U C U G C - G C - G A - U 1490 C - G A A A A C - G U - - - - U 1495 1405 G - C C - G G - C G - C 5' 3' <i>E. coli</i> 16S A-site
RNA type	K_d [μ M] ^[a]	K_d ^[c]	
$\Psi m^3\Psi\Psi$ (wild-type H69)	1 ± 0.95 ^[b]	~300 nM	
$\Psi\Psi\Psi$ (unmethylated H69)	14	~4 μ M	
UUU (unmodified H69)	22	~6 μ M	
A-site (16S rRNA)	>100	N.D.	

Experimental conditions for all fluorescence titrations were performed in 20 mM Tris-HCl (pH 7), 140 mM NaCl, 5 mM MgCl₂ with 2 min incubation times between each sample reading. ^[a] K_d estimates were obtained using **Equation 4.4** and K_d s were averaged from spectral values measured at $\lambda = 510$ nm and 520 nm. ^[b]The K_d values and standard deviation were measured and calculated from the average of two independent $\Psi m^3\Psi\Psi$ fluorescence titration experiments. ^[c]These values represent an estimate of K_d by visual inspection of the binding curve at the half-maximal binding of rRNA to F-DNAH69apt18.

These results demonstrate that H69DNAapt18 can recognize wild-type H69 sequence specifically, and suggest that the binding affinity could be subjected to subtle variations in structure or capabilities to form different intermolecular interactions of the H69 variants at different modification states. Furthermore, this is the first time that a DNA aptamer generated through SELEX is shown to recognize specific RNA modifications, and H69DNAapt18 exhibits greater binding affinity compared to a peptide or aminoglycoside binder of H69 (Table 6.2).^{146,147} Aminoglycosides naturally target RNA with high affinity and have been shown to bind to H69 with μM affinity (Table 6.2).¹⁴⁷

Table 6.2. Comparison of dissociation constant K_d values of aptamer #18 binding to wild-type H69 and various rRNA motifs to H69 binding phage display generated heptapeptide, NQVANHQ-NH₂ and aminoglycoside, neomycin.

RNA Target	K_d at pH 7.0 (μM) (RNA+ H69DNAapt18) by fluorescence	K_d at pH 7.0 (μM) (RNA + NQVANHQ- NH ₂) by ESI-MS	K_d at pH 7.0 (μM) (RNA + neomycin) by ESI-MS
$\Psi\text{m}^3\Psi\Psi$	1 ± 0.95	11 ± 1	3.0 ± 0.6
UUU	22	19 ± 2	1.4 ± 0.6
A-site	> 200	49 ± 10	-
$\Psi\Psi\Psi$	14	4.6 ± 1.7	1.2 ± 0.4
Human H69	N.D.	50 ± 8	N.D.

6.3. *Mfold* structural analysis of DNA aptamers and potential kissing-kissing loop interactions between H69DNAapt18 and H69

Our experimental approach was designed to generate H69-DNA aptamer candidates with diversity in both their primary sequences and secondary structures. *Mfold* analysis was carried out on 20 of the selected DNA aptamers, both the untruncated (84-nt) and truncated (40-nt) forms. *Mfold* structures revealed similarities within the number and types of motifs present

within predicted secondary structures of the potential H69-DNA aptamers, and thus were divided into five families (**Figure 5.4**) containing the following aptamers: family I (#8, #18), II (#3, #6, #12), III (#13, #19), IV (#1, #7, #9, #11, #14, #16), and V (#4, #5, #10, #20). Aptamers #2, 15, and 17 did not exhibit significant structural similarity with any of the aforementioned families and therefore were excluded from a family assignment.

Aptamers H69DNAapt18 and H69DNAapt8, were both assigned to group 2 (Clustal W) as well as family 1 (*Mfold*), and exhibited features in their secondary structures that are ideal for binding to H69. A 20mer stem-loop structure in H69DNAapt18 was identified by *Mfold* predictions, in both the truncated and untruncated constructs (**Fig. 6.1a**). In H69DNAapt8, two hairpin structural motifs were observed in the *Mfold* predicted secondary structure (**Fig. 6.1b**). As shown in **Fig. 6.2**, the 20mer hairpin motif in H69DNAapt18, from residues 28 to 47, shows sequence complementarity to H69 (from 1906 to 1924, *E. coli* numbering). The loop region of this 20mer motif is proposed to potentially form initial interactions with the loop region of H69 by multiple base-pairing possibilities (**Table 6.3**). Similarities in sequences in secondary structures were also observed between the 20mer hairpin in H69DNAapt18 and the 13mer hairpin in H69DNAapt8, which exhibited sequence complementarity to H69 in the loop regions (**Table 6.3**). The 10mer hairpin in H69DNAapt8 also shows certain sequence complementarity to H69, as shown in **Table 6.3**, however the sequence context is very limited for base-pair formation. These results suggest that the hairpin motifs in DNA aptamers H69DNAapt18 and H69DNAapt8 may form extensive DNA/RNA duplexes with H69, initiated by the so called “kissing” loop-loop interactions within the loop regions.¹²⁴ Furthermore, these kissing loop residues within the proposed H69/aptamer duplexes are conserved, specifically A1913, Ψ1915,

A1916, and Ψ1917 (wild-type H69)⁸² are conserved within all phylogeny, and H69DNAapt18 residues T37, A38, T40 and T41 appear in both the untruncated and truncated forms as well as exhibit significant conservation with H69DNAapt8 residues T35, A36, T37, and T38. The aforementioned observed conservations for H69 and the DNA aptamers suggests that these residues may be essential for H69/aptamer binding and possible kissing loop formation.

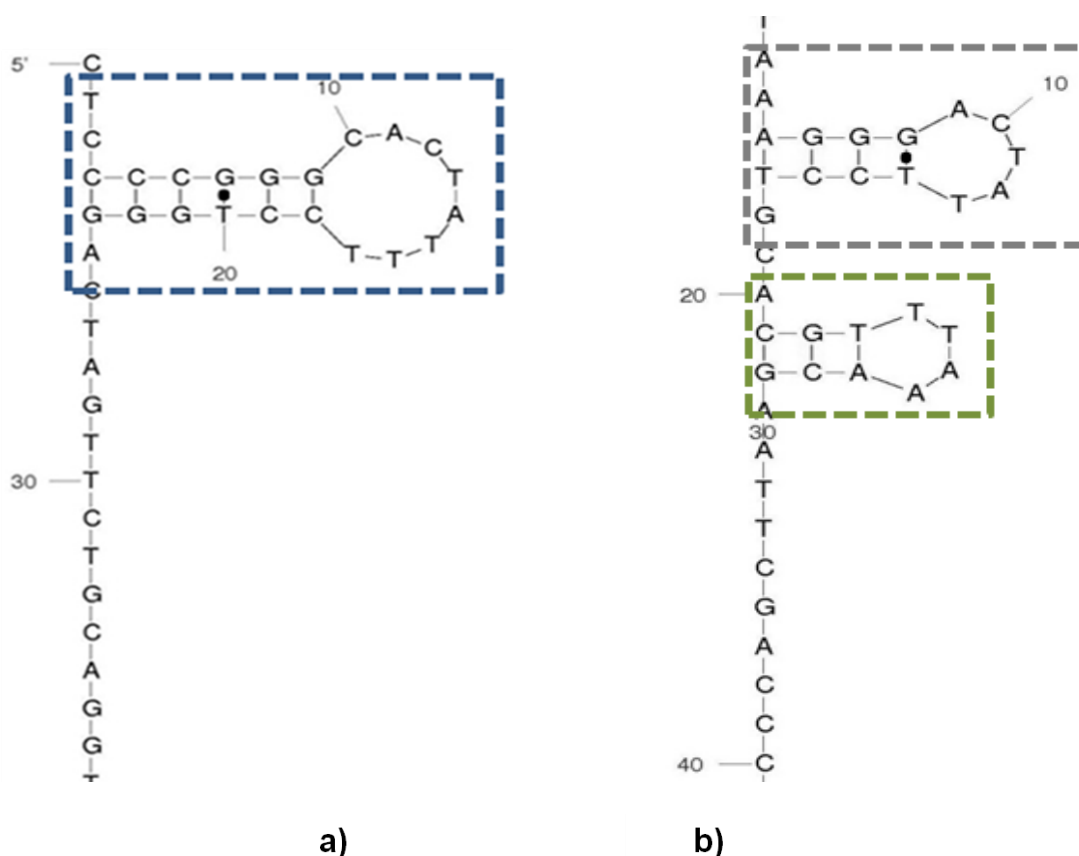


Figure 6.1. Conserved hairpin motifs and proposed interactions of H69 and truncated H69DNAapt18 and truncated H69DNAapt8. (a) Truncated H69DNAapt18 is shown with one conserved motif boxed in dotted rectangles matching the conserved motif of the corresponding full-length untruncated H69DNAapt18. (b) H69DNAapt8 is shown to have two conserved motifs boxed in grey and green dotted rectangles matching the conserved motifs of the corresponding untruncated H69DNAapt8. Furthermore, these conserved apex loop regions of H69DNAapt18 and H69DNAapt8 share the common sequence 5'-ACTATT-3'.

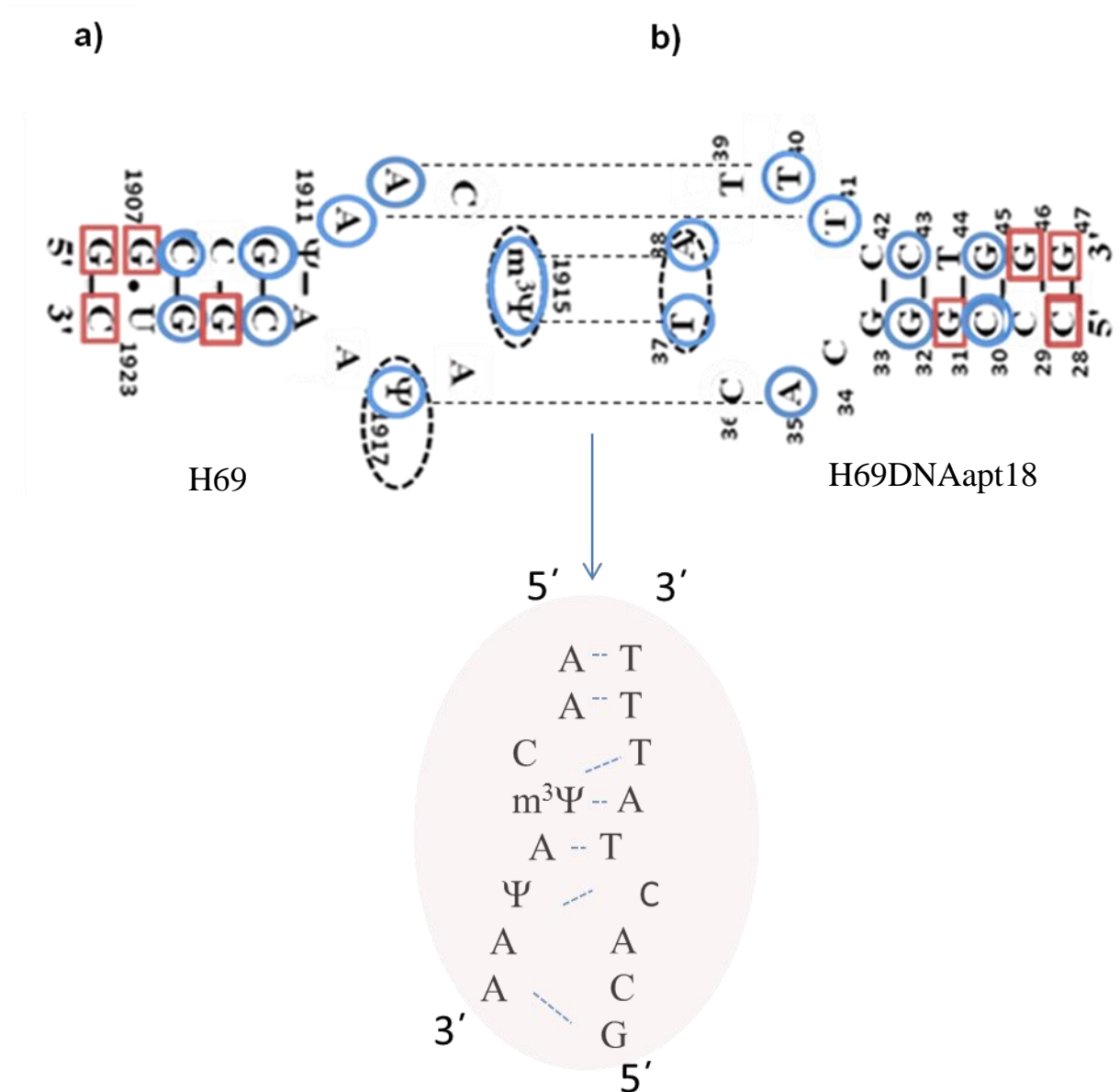


Figure 6.2. Hairpin motifs of aptamer versus target with kissing loop structure. H69DNAapt18 exhibits complementarity to the wild-type H69 loop region. The 19-nt hairpin loop structure of H69 of *E. coli* 23S ribosomal RNA (a) has conserved regions and complementarity to 20-nt hairpin H69DNAapt18 (b). The 3-methylpseudouridine of wild-type H69 at the apex of its hairpin loop, dotted oval (black), designated as residue 1915 (*E. coli* numbering) with base-pair complementarity to the apex region of positions 37 and 38 dotted oval (black), of H69DNAapt18 (b). Conserved nucleotide bases are boxed (red), and complementary bases are circled (blue). Pseudouridine position 1917 of wild-type H69 (a) highlighted within a dotted oval (black) also shows base-pair complementarity to position 40 in a dotted oval (black) of H69DNAapt18 (b).

Table 6.3. Proposed base pairing of hairpin apex region of DNA aptamers duplexed with H69.
All proposed bonding interactions within the duplex sequence are in bold letters.

hairpin	H69/aptamer duplex sequence	m ³ Ψ-A	m ³ Ψ-T	Ψ-A	Ψ-T	A-T
H69	5' A A C m³Ψ A Ψ A 3' <small>1912 1913 1914 1915 1916 1917 1918</small>	1	1	1	-	2
H69DNAapt18	3' T T T A T C A C 5' <small>41 40 39 38 37 36 35 34</small>					
H69	5' A A C m³Ψ A Ψ A 3' <small>1912 1913 1914 1915 1916 1917 1918</small>	1	1	-	1	1
H69DNAapt8	3' T T A T C A - 5' <small>38 37 36 35 34 33</small>					
H69	5' A A C m³Ψ A Ψ A 3' <small>1912 1913 1914 1915 1916 1917 1918</small>	1	-	1	1	1
H69DNAapt8 (truncated)	3' - - - A A T T 5' <small>34 33 32 31</small>					

In conclusion, H69-binding DNA aptamers with diversities in sequences and structures were generated by SELEX experiments, which employed streptavidin-coated magnetic beads. Aptamers H69DNAapt18 and H69DNAapt8 were shown to bind wild-type H69 with dissociation constants of 70-80 nM by EMSA. H69DNAapt18 also exhibited differential specificities towards H69 of different modification states. *Mfold* analysis on DNA aptamers H69DNAapt18 and H69DNAapt8 suggests that a DNA/RNA hybrid duplex may form between the hairpin motifs in the DNA aptamers and H69, resulting from potential “kissing” loop-loop interactions.

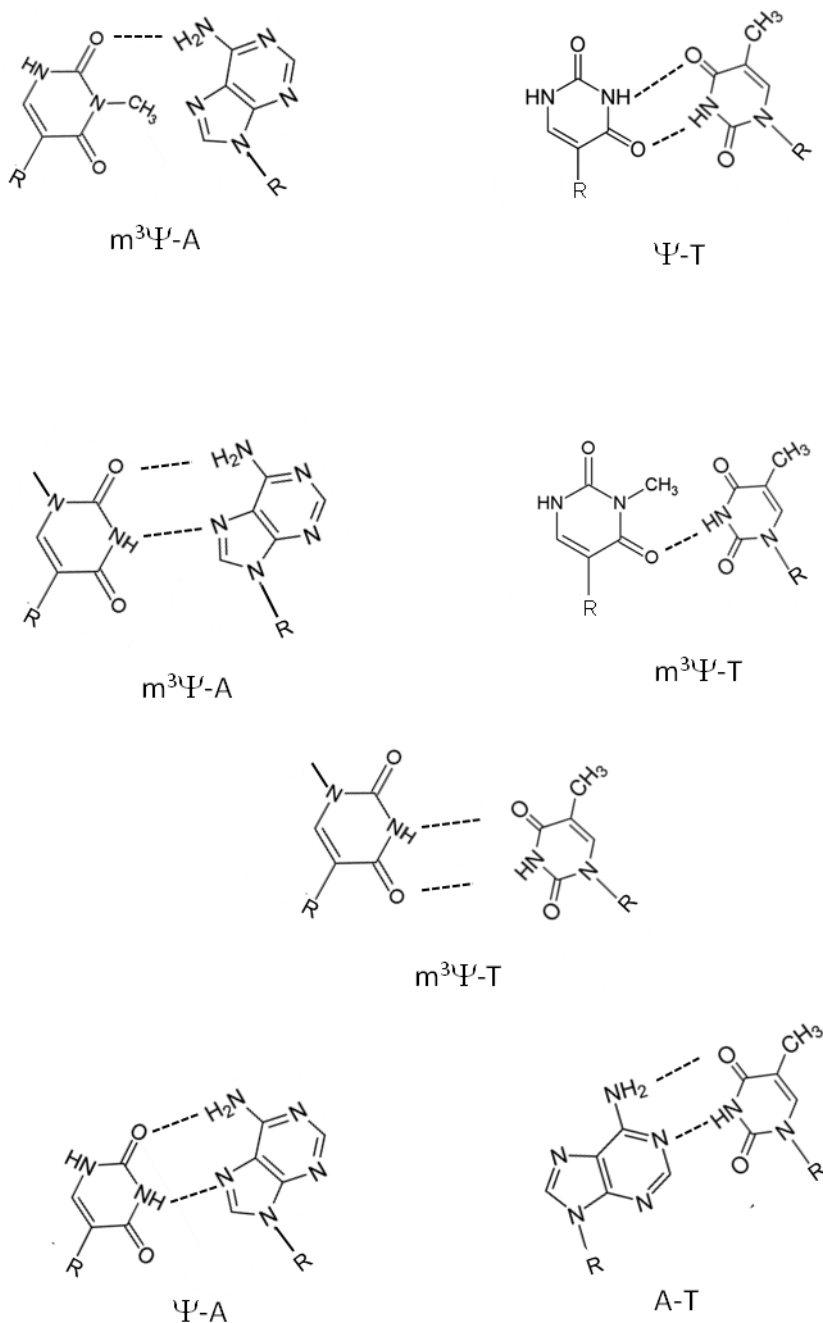


Figure 6.3. Possible complementary base pairs of the proposed kissing-kissing loop-loop RNA/DNA duplexes of aptamers #8 and #18 bound to the apex region of H69. Proposed Watson-Crick (*i.e.*, Ψ -T; A-T¹⁴⁸; and Ψ -A¹⁴⁹) and non Watson-Crick base pairing (*i.e.*, $m^3\Psi$ -A; $m^3\Psi$ -T) are illustrated as from the hairpin loop regions of the aptamer/H69 complexes.

CHAPTER 7 - FUTURE DIRECTIONS

7.1. Future directions: H69-DNA aptamer drug development

The DNA aptamers selected for binding to H69 provide interesting tools for further studies of the ribosome. We have obtained one DNA aptamer that can bind selectively to wild-type H69. Further work to enhance affinity and selectivity *in vivo* could then lead to assays and inhibition of protein synthesis within infectious microbes. To ascertain the ability of H69DNAapt18 to bind to *E. coli* wild-type H69 during the assembly of the 50S and 30S subunits for protein synthesis, we propose whole ribosome binding studies to monitor the effect of aptamers on ribosome assembly and/or protein synthesis. The H69-DNA aptamers developed in this study may be optimized, and at the same time, 70S ribosome formation assays should be developed to further evaluate the potential of aptamers as novel therapeutics.

In this work, we employed *in vitro* binding assays, namely EMSA and fluorescence titrations with a labeled aptamer. Our approach should be extendable to further study of the interactions of all of the DNA aptamers that were selected and exhibited formation of complexes with H69 (*i.e.*, aptamers #1-7, 9-17, and 19-20). The identity of the specific nucleotides and base pairs involved in the proposed DNA/RNA complexes remain unknown; therefore the design of experiments that can identify which residues of the stem and loop regions of H69DNAapt18 are involved in key contacts with H69 (*i.e.*, chemical footprinting and mutation analysis) are desired. Additional binding studies (*i.e.*, surface plasmon resonance and electrospray ionization mass spectrometry) would be ideal to evaluate the binding affinities of the conserved truncated

motifs versus the untruncated forms of promising DNA aptamers identified as high-affinity binders by fluorescence titration assays.

Our results suggest that H69DNAapt18 has the ability to specifically recognize modified nucleotides and methylated sites of RNA motifs. The observed modest discriminating binding selectivity of H69DNAapt18 for $\Psi\text{m}^3\Psi\Psi$ over $\Psi\Psi\Psi$ and UUU suggests that H69DNAapt18 may be able to recognize variations in modified versus unmodified bases. It would be interesting to expand this research and explore the potential of H69DNAapt18 as a probe for pseudouridine and methyl-pseudouridine within wild-type H69 and its unmodified constructs. This binding affinity and specificity needs to be confirmed by additional experiments to provide greater insight into whether H69DNAapt18 has varying binding affinity for modified versus unmodified RNA nucleotides (*i.e.*, uridine, pseudouridine and methylpseudourine) in different sequence contexts. Additional characterization of the properties of H69DNAapt18 would clarify its potential use *in vitro* and/or *in vivo* as an “RNA modification probe” and provide insight into the structural and functional roles of natural modified nucleotides. Importantly, designing a higher affinity DNA aptamer as a probe could potentially help explore additional biological roles of pseudouridine present in the ribosome as well as shed more light on the significance of methylation in natural RNA motifs that are rich in modified nucleotides.

Ideally, our original DNA library generated by SELEX may have greater binding affinity for H69 by changing the stringency conditions between successive rounds. Essentially, increased stringency may affect the percentage of DNA library bound s for the earlier rounds of selection (*i.e.*, lower percent bound in initial rounds). We propose that SELEX experiments could be

repeated for the initial DNA library by including changes in the stringency (*i.e.*, binding time, number of washes, buffer salt conditions) to further enhance the overall selectivity and diversity of the DNA library with successive rounds. Specifically, the SELEX binding time could be modified to include incremental decreases in times of incubation for every 3 - 5 rounds (30 min - 15 min) and washing cycle times may be increased (*i.e.*, 2 - 5 washes after every 3 rounds of SELEX).

Furthermore, our reported fluorescence binding assays are incomplete and therefore can be enhanced to include more statistical analysis, internal fluorescence tagging, and anisotropy. Enhancements to the quality and sensitivity of detection of binding interaction between H69DNAapt18 and H69 may be achieved by employing the following changes in the fluorescence binding assay methodologies: (1) perform additional fluorescence binding experiments with target and DNA aptamers in duplicates (*i.e.*, report of statistical analysis and error bars for relative fluorescence) and report data of relative fluorescence vs. increasing concentration of target RNA constructs (UUU, $\Psi\Psi\Psi$, $\Psi m^3\Psi\Psi$, and A-site rRNA); (2) repeat fluorescence titration experiments utilizing an internal fluorophore tag on the 5' end of the stem-hairpin motif; and (3) perform fluorescence anisotropy with fluorescently tagged DNA aptamers against increasing concentrations of H69 and target RNA constructs. Ideally, larger RNA constructs and full-length ribosomal RNA would also be tested for binding.

H69/DNA aptamer site-targeting assays to evaluate binding specificities for the stem versus loop regions can be designed to further characterize the affinity of H69DNAapt18 for wild-type H69. Truncated (40 nt) length H69DNAapt18 representing the 5' and 3' ends of the stem and loop regions can also be employed within EMSA and fluorescence binding assays to monitor evidence of DNA/RNA complex formation for the individual stem regions of H69DNAapt18 to radiolabeled or fluorescently labeled H69 vs. the complete stem-hairpin of H69DNAapt18. Evidence of stem vs. complete stem-hairpin DNA/RNA complex formation could be monitored using a broader range of DNA concentrations (0-20 μM) and buffer conditions ideal for fully assembled ribosomes (*i.e.*, 100-150 mM KCl or NH_4Cl). If results show K_d constants for the fully assembled stem-hairpin H69DNAapt18 as lower or equivalent to the binding affinity to the stem region of the DNA aptamer, this could further support a hypothesis that H69DNAapt18 preferentially binds to the loop region of H69. Furthermore, complete stem-loop H69DNAapt18 incubated with increasing concentrations of point mutation variants of fluorescently labeled or radiolabeled H69, may be challenged against increasing concentrations of H69DNAapt18. Modified analogs of H69, where the loop region has point mutations of the wild-type sequence, can be employed in inhibition assays to further characterize which residues of the H69 loop are key for complex formation with H69DNAapt18.

Additionally, the identity specific residues proposed in kissing-kissing hairpin motifs of the observed DNA/RNA complexes need to be further characterized. More sensitive binding analyses can be performed with electrospray ionization mass spectrometry (ESI-MS) and nuclear magnetic resonance spectroscopy (NMR) to elucidate the specific residues of H69 that are proposed to interact with H69DNAapt18 in solution. Footprinting binding assays may be

employed using aniline-induced cleavage to gain more reliable information about the binding sites of the aptamer to H69 and specific residues proposed to contact H69DNAapt18 observed through DNA/RNA complex formations. Specifically, the proposed non-Watson-Crick base pairs (*i.e.*, $m^3\Psi$ and Ψ binding with T and A) within the loop regions of the loop-loop kissing hairpin motif model of both the conserved truncated and untruncated loop regions of H69DNAapt18 and H69DNAapt8 need to be further characterized.

Finally, to evaluate the effectiveness of H69DNAapt18 as a potential drug, ribosome assembly inhibition assays can be employed. Whole ribosomal RNA binding assays for *E. coli* can be designed to analyze H69DNAapt18's ability to affect proper rRNA assembly and provide greater insight into its potential to disrupt protein translation. Absence of the whole 70S ribosome in the presence of DNA aptamer would suggest H69DNAapt18 would have the ability to inhibit ribosomal assembly. A ribosomal assembly inhibition assay would allow for comparison of complexes formed between individual ribosomal subunits (*i.e.*, 30S and 50S) and formation of 70S rRNA in the presence and absence of FAM-H69DNAapt18, by way of monitoring changes of fluorescence as a result of binding of FAM-H69DNAapt18 to H69 during 70S ribosome formation.

7.2. Applications of selected DNAs as probes

The development and application of a probe for modified nucleotides such as pseudouridine in other sequence or structural contexts may provide a greater understanding of their biological significance in rRNA or other natural RNAs. Such a tool might prove useful for

studies exploring the roles of pseudouridine *in vivo*. Exploring the application of H69DNAapt18 as an *in vivo* probe of H69 would support its potential role in disruption of ribosomal assembly and protein synthesis. Other studies have linked increased levels of oxidized urinary Ψ with neurodegenerative conditions such as Alzheimer's and Parkinson's diseases.¹⁵⁰ Therefore, a Ψ probe may be useful for both *in vitro* and *in vivo* studies to further characterize these systems and to further explore biologically significant roles of Ψ and link to microbes and diseases.

7.3. Counter-selection aptamers: SELEX against human H69 analog with DNA aptamers

Overall, this study provides a reference point for the development of DNA aptamers that identify modified nucleotides and/or methylation sites in bacterial RNA, or could possibly function as novel therapeutics to help combat antibiotic resistance. Our work demonstrates how selection-based approaches may be used in the discovery of potential RNA-binding therapeutics, and provides a framework for selecting other DNA-binding molecules with the desired properties of RNA targeting. However, these results also show the need to evaluate the potential of DNA aptamers to bind selectively to the target RNA. Therefore, counter-selection experiments should be carried out, such as employing the human analogue to remove DNAs lacking selectivity for the bacterial RNA. Those aptamers would then be evaluated for their potential as selective therapeutics targeting only bacteria (**Fig. 7.1**). Differences in the sequence of bacterial versus human H69 are present in both the stem and loop regions of the hairpin, which are important to exploit during the development of effective and highly selective aptamers. Specifically, human H69 is void of $m^3\Psi$ within the apex region corresponding to

position 1915 of *E. coli*. Presently, our data indicate that the observed selectivity of the H69DNAapt18 aptamer for wild-type H69 may be attributed to varying binding affinities contingent upon the presence or absence of modified bases (*i.e.*, Ψ or $m^3\Psi$). Therefore, counter-selections with unmodified H69 variants would be useful. Finally, experiments that provide greater structural characterization of H69DNAapt18 binding to H69 would enhance our knowledge of the binding mechanism and formation of the observed DNA/RNA complexes, and potentially provide greater insight into the structural roles of Ψ and $m^3\Psi$ in within H69.

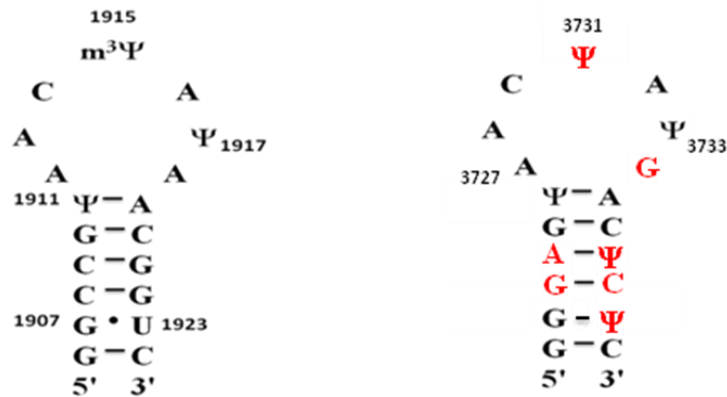
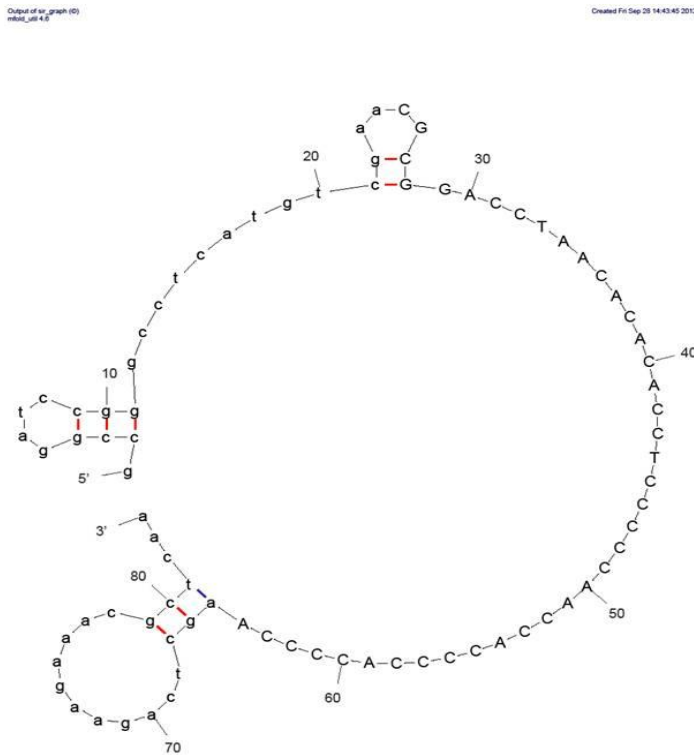


Figure 7.1. Structural comparison of bacterial versus human H69. The *E. coli* domain IV of 23S rRNA (left) is structurally distinct (red) when compared to eukaryotic of 28S rRNA ($\Psi\Psi\Psi\Psi\Psi$; Ψ 5; or human H69)¹⁵¹ (right).

APPENDIX

Figure A1. *Mfold* structural analysis of untruncated aptamer #1.

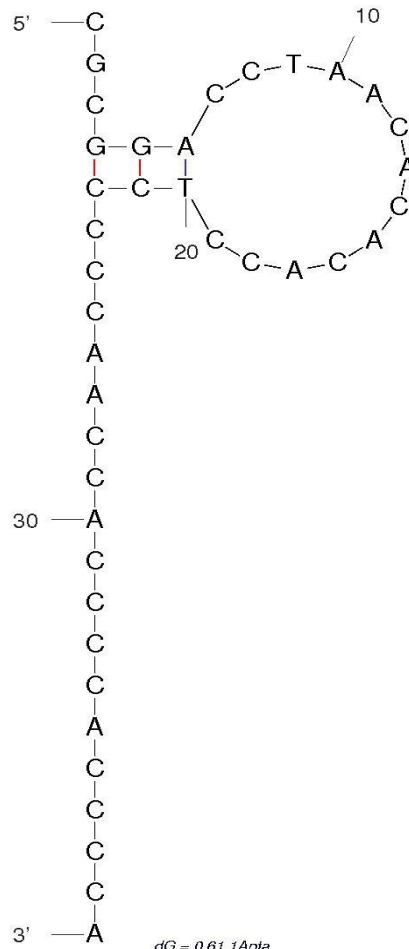
<i>Mfold</i> Structural Analysis	Aptamer #1
Length:	84-nt (untruncated)
Sequence:	
	5' - gccggatccgggcctcatgtcgaaCGCGGACCTAACACACACCTCCCCAACACCCCACCCCAgctcagaagaacgctcaa - 3'
2° structural motifs:	hairpin loops: L1, L2 and L3
Family:	IV



dG = -3.53 Aptamer 1

Figure A2. *Mfold* structural analysis of truncated aptamer #1.

<i>Mfold</i> Structural Analysis	Aptamer #1
Length:	40-nt (truncated)
Sequence:	5' - <u>CGCGGACCTAACACACACCTCCCCAACCACCCCACCCCA</u> - 3'
2° structural motifs:	hairpin loop: L1

Output of mfold graph (9)
mfold_v4.0

Created Sat Nov 26 19:02:16 2011

Figure A3. *Mfold* structural analysis of untruncated aptamer #2.

<i>Mfold</i> Structural Analysis	Aptamer #2
Length:	84-nt (untruncated)
Sequence:	5'- agctcagaagaacgctcaaACGCGGACCTAACACACACCTCCCCAACCACCCCACCCctgagcgttttctgagct -3'
2° structural motifs:	hairpin loop: L1

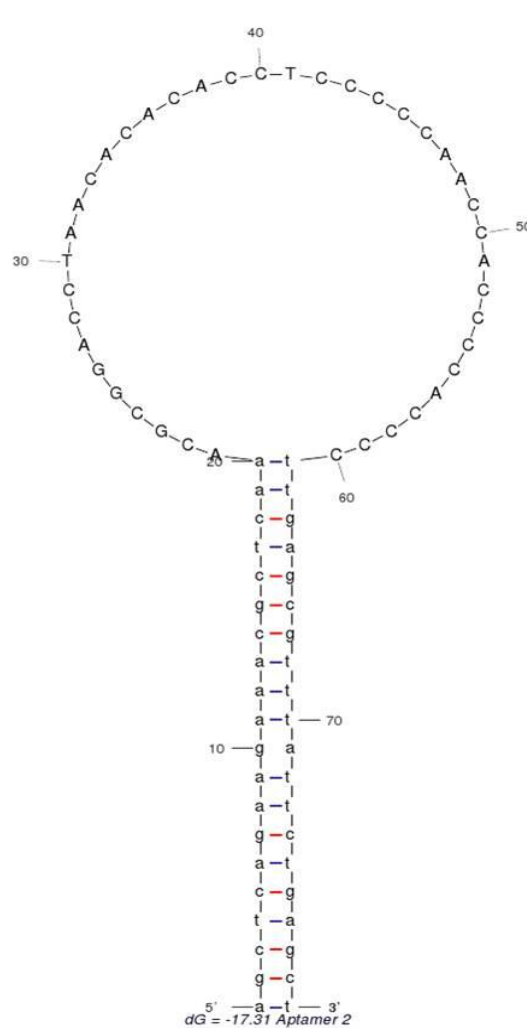


Figure A4. *Mfold* structural analysis of truncated aptamer #2.

<i>Mfold</i> Structural Analysis		Aptamer #2
Length:		40-nt (truncated)
Sequence:	5' -ACGCGGACCTAACACACACCTCCCCCAACCACCCACCCC-3'	
2° structural motifs:		hairpin loop: L1

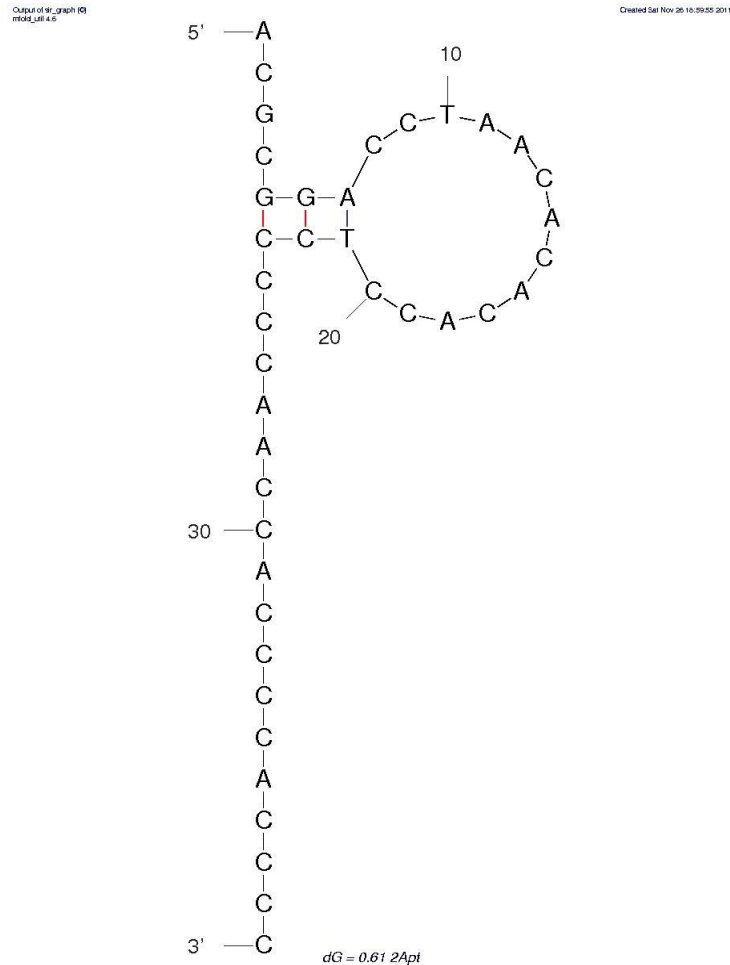


Figure A5. *Mfold* structural analysis of untruncated aptamer #3.

<i>Mfold</i> Structural Analysis	Aptamer #3
Length:	84-nt (untruncated)
Sequence:	
	5'- gccggatccgggcctcatgtcgaaCTCGGCCCCCTTTGACCAAAGAGAGAACAAAAAATAAAagctcagaagaacgctcaa -3'
2° structural motifs:	hairpin loop: L1, L2 and L3
Family:	II

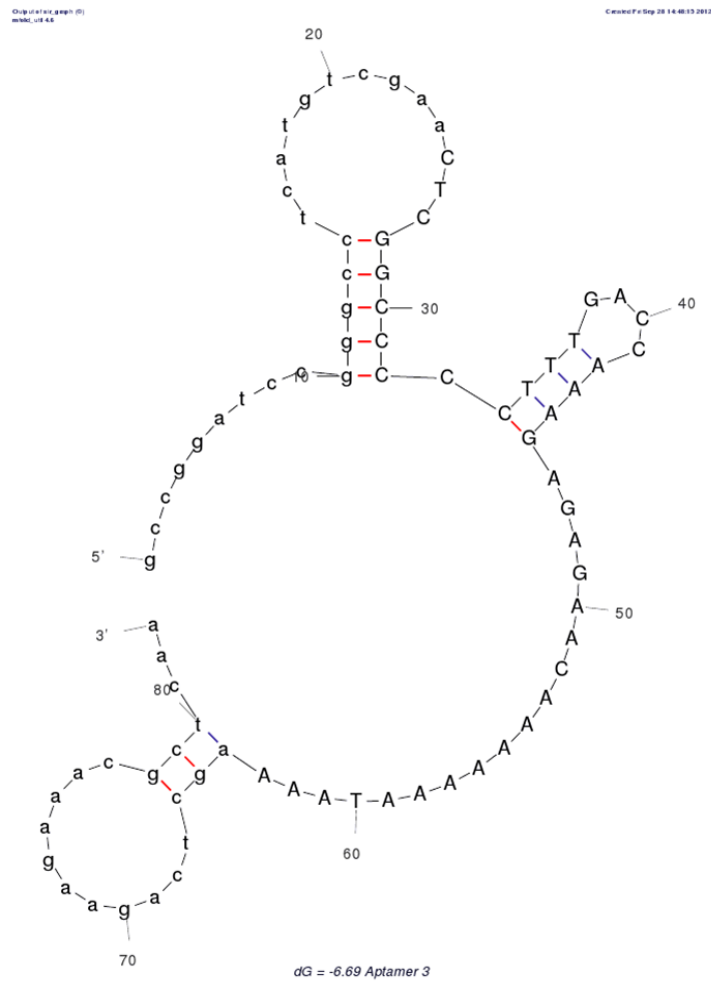


Figure A7. Mfold structural analysis of untruncated aptamer #4.

Mfold Structural Analysis	Aptamer #4
Length:	84-nt (untruncated)
Sequence:	
	5'- ccggatccgggctcatgtcgaaACGGACCTAACACACACCTCCCCAACCACCCCACCCAgctcagaagaacgctcaa-3'
2° structural motifs:	hairpin loop: L1, L2 and L3
Family:	V

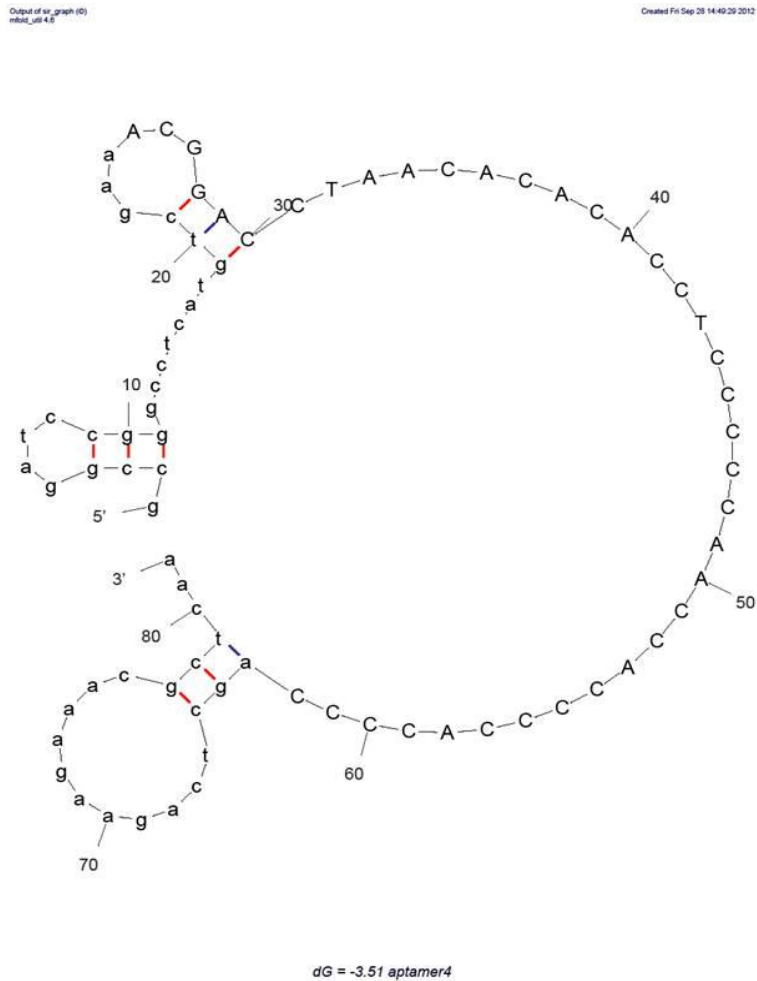
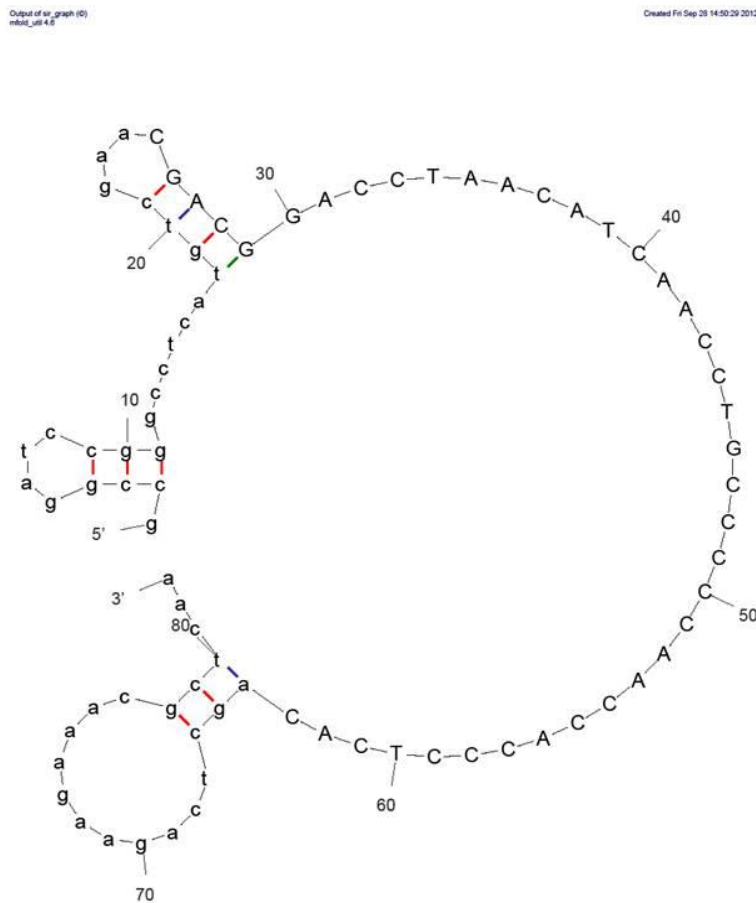


Figure A9. Mfold structural analysis of untruncated aptamer #5.

Mfold Structural Analysis	Aptamer #5
Length:	84-nt (untruncated)
Sequence:	
5'- gccggatccgggctcatgtcgaaCGACGGACCTAACATCAACCTGCCCCAACCACCTCACagctcagaagaacgctcaa-3'	
2° structural motifs:	hairpin loop: L1, L2 and L3
Family:	V



dG = -3.91 aptamer 5

Figure A10. *Mfold* structural analysis of truncated aptamer #5.

<i>Mfold</i> Structural Analysis		Aptamer #5
Length:		40-nt (truncated)
Sequence:	5'- <u>CGACGGACCTAACATCAACCTGCCCCCAACCACCCTCAC</u> -3'	
2° structural motifs:		hairpin loop: L1

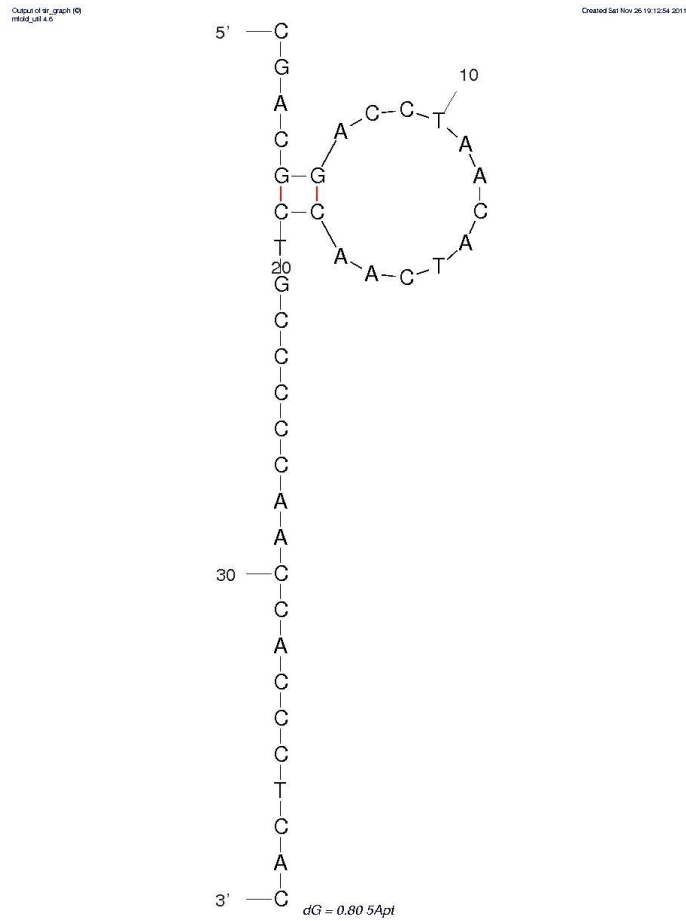


Figure A11. Mfold structural analysis of untruncated aptamer #6.

Mfold Structural Analysis	Aptamer #6
Length:	84-nt (untruncated)
Sequence:	5'- gccggatccgggcctcatgtcgaaTTTATCCCTCACATGGGAAACTTCCGTACGCCTATGAGTTtgagcgtttattctgagct -3'
2° structural motifs:	hairpin loop: L1, L2 and L3
Family:	II

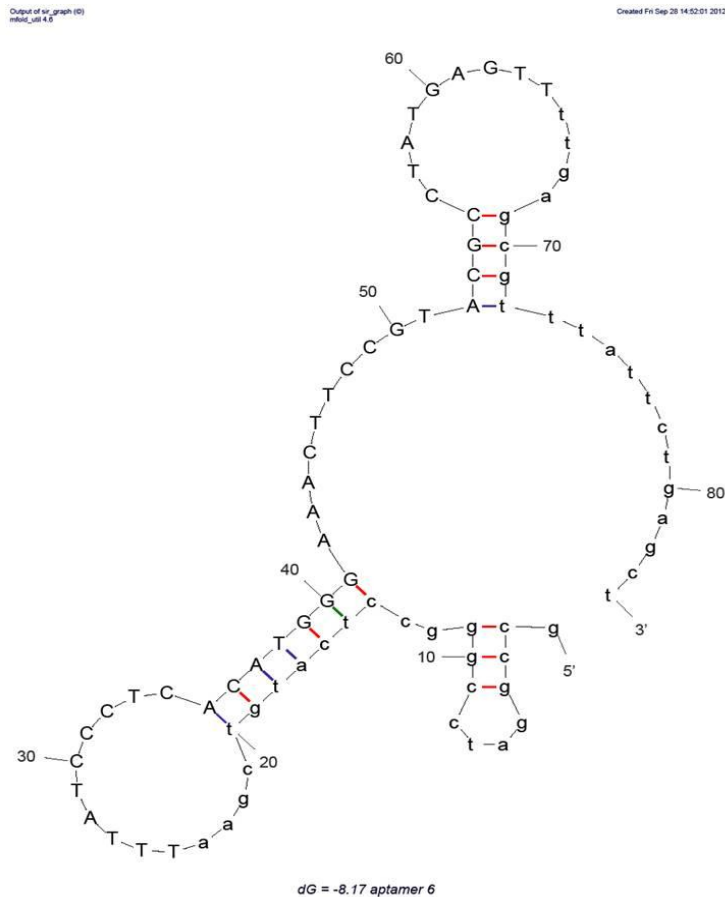


Figure A12. Mfold structural analysis of truncated aptamer #6.

Mfold Structural Analysis		Aptamer #6
Length:		40-nt (truncated)
Sequence:	5'- <u>TTTATCCCTCACATGGGAACTTCCGTACGCCTATGAGTT</u> -3'	
2° structural motifs:		hairpin loops: L1 and L2

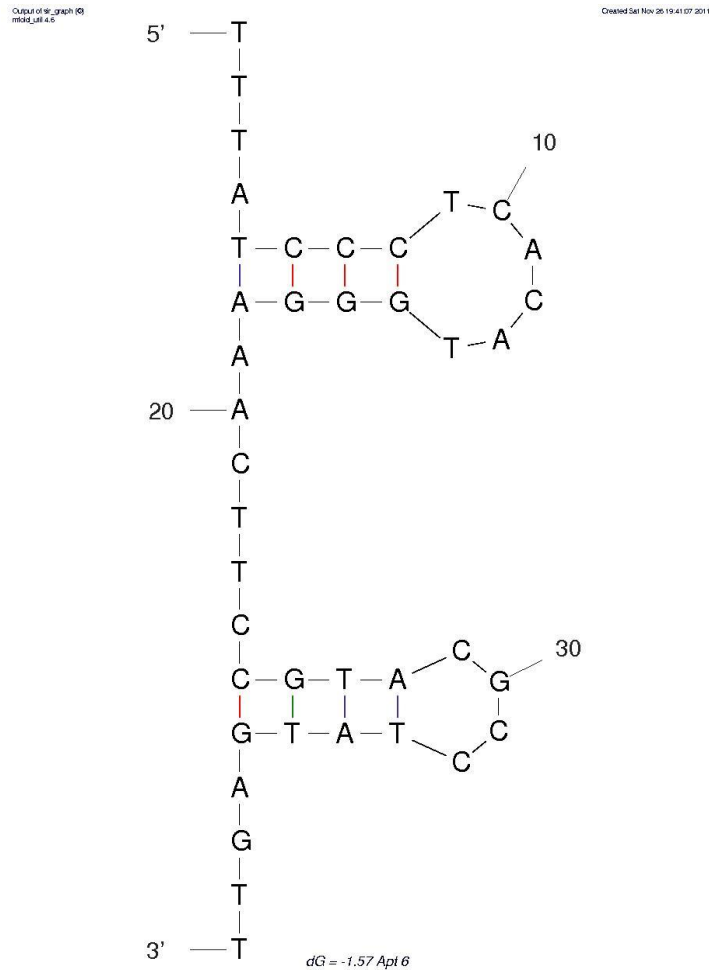


Figure A13. *Mfold* structural analysis of untruncated aptamer #7.

<i>Mfold</i> Structural Analysis	Aptamer #7
Length:	84-nt (untruncated)
Sequence:	
	5'- gccggatccgggcctcatgtcgaaACGCGGACCTAACACACACCTCCCCAACCACCCCACCCagctcagaagaaacgctcaa -3'
2° structural motifs:	hairpin loop: L1, L2 and L3
Family:	IV

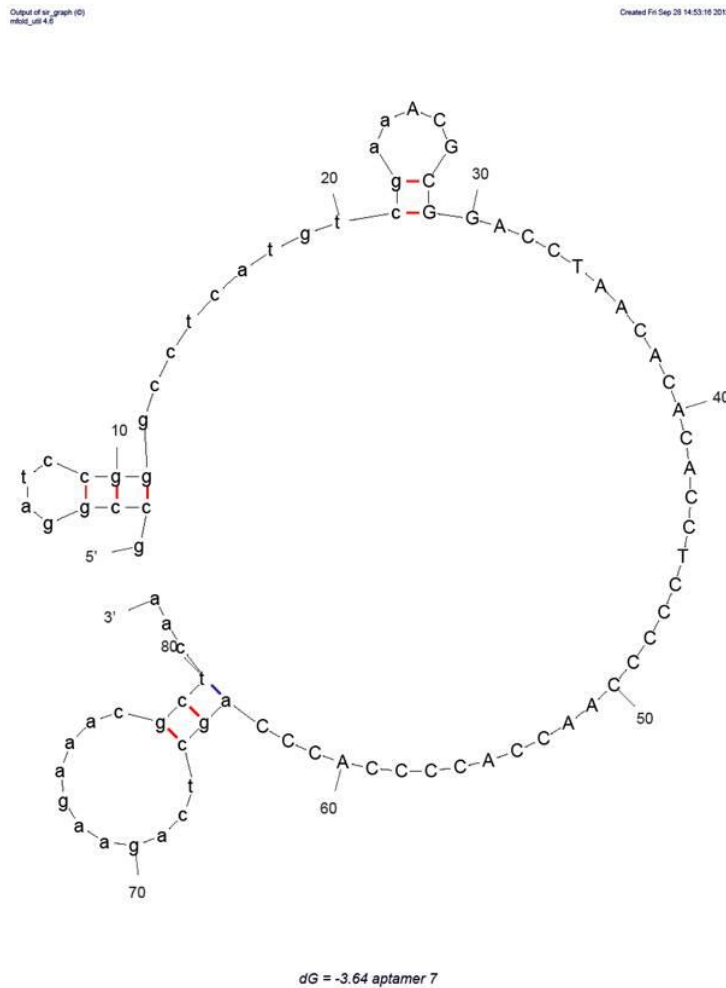


Figure A14. *Mfold* structural analysis of truncated aptamer #7.

<i>Mfold</i> Structural Analysis		Aptamer #7
Length:	40-nt	(truncated)
Sequence:	5'- <u>ACGCGGACCTAACACACACCTCCCCCAACCACCCACCC</u> -3'	
2° structural motifs:	hairpin loop:	L1

Output of mfold graph (9)
mfold_v4.6

Created Sat Nov 26 16:27:21 2011

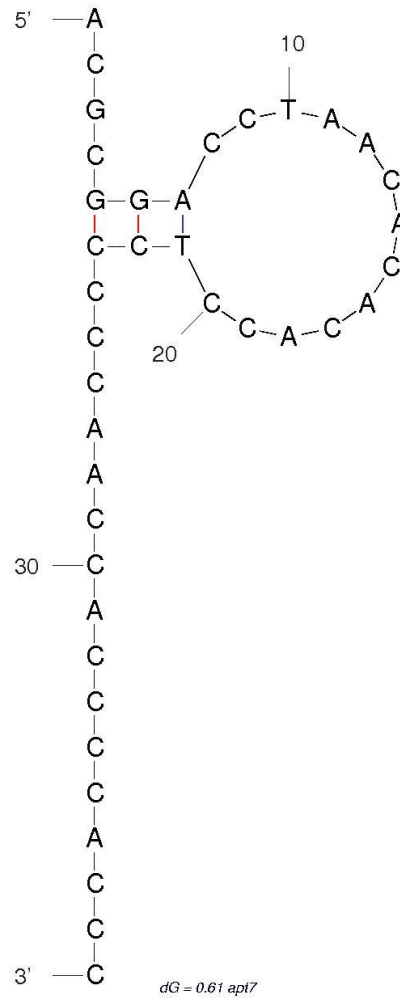


Figure A15. Mfold structural analysis of untruncated aptamer #8.

Mfold Structural Analysis	Aptamer #8
Length:	84-nt (untruncated)
Sequence: 5'- gccgatccgggctcatgtcgaaCTAAAGGGACTATTCTGCACGTTTAAACGAATTCGACCCTtgagcgtttattctgagct -3'	
2° structural motifs:	hairpin loops: L1, L2, L3 and L4 Internal loop: IL1
Family:	I

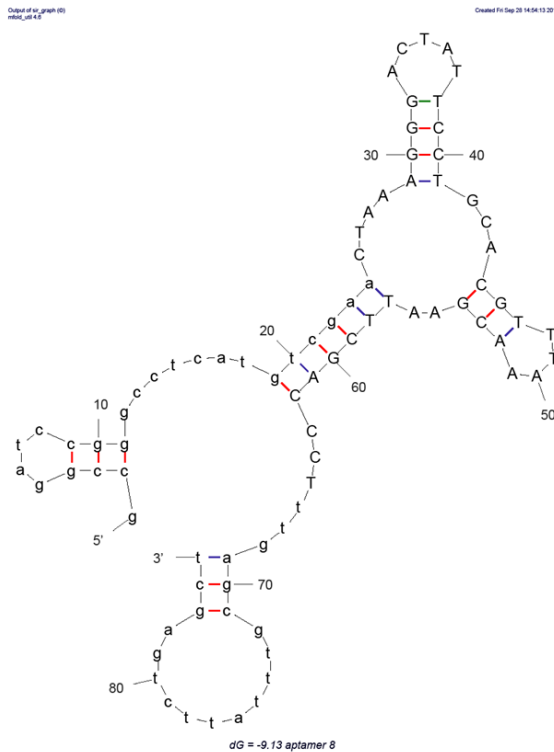


Figure A16. *Mfold* structural analysis of truncated aptamer #8.

<i>Mfold</i> Structural Analysis	Aptamer #8
Length:	40-nt (truncated)
Sequence:	
	5'- <u>CTAAAGGGACTATTCCTGCACGTTTAAACGAATTCGACCCT</u> -3'
2° structural motifs:	hairpin loops: L1 and L2

Output of mfold (K)
msig_08_02

Created Sat Nov 26 19:28:25 2011

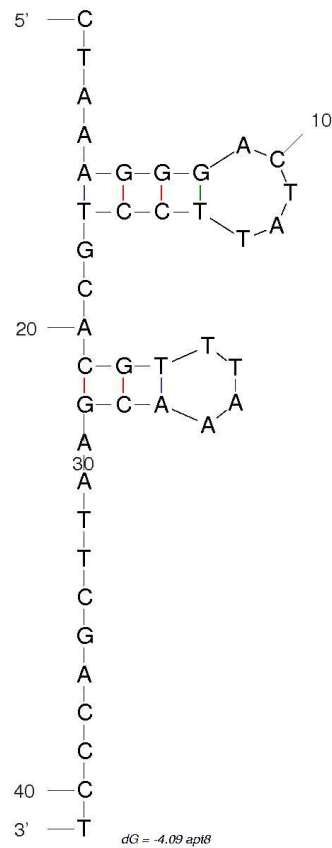


Figure A17. Mfold structural analysis of untruncated aptamer #9.

Mfold Structural Analysis		Aptamer #9
Length:		84-nt (untruncated)
Sequence:	5'- gccggatccgggcctcatgtcgaaACGCGGACCTAACACACACCTCCCCAACACCCCACCCagctcagaagaacgctcaa-3'	
2° structural motifs:		hairpin loops: L1, L2, L3 and
Family:		IV

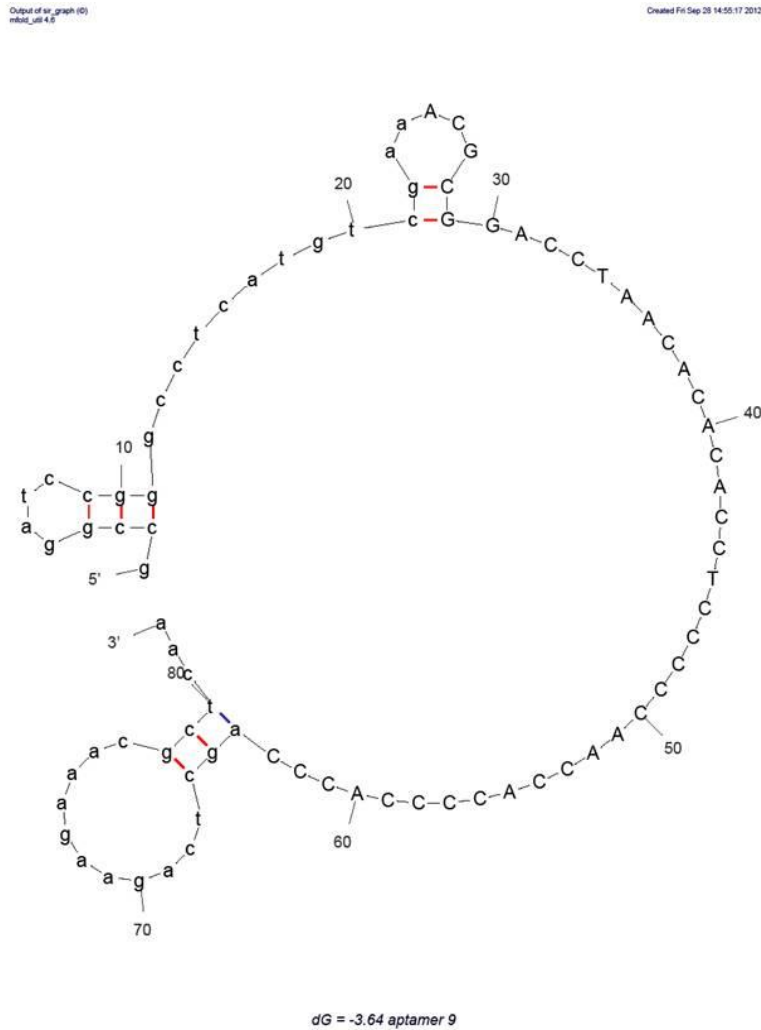


Figure A19. Mfold structural analysis of untruncated aptamer #10.

Mfold Structural Analysis		Aptamer #10
Length:	84-nt	(untruncated)
Sequence:	5'- gccggatccgggcctcatgtcgaaAACGACGGAACCTAAACAACAACCTACCCCAACCACagctcagaagaacgctcaa-3'	
2° structural motifs:	hairpin loops: L1, L2, and L3	
Family:	V	

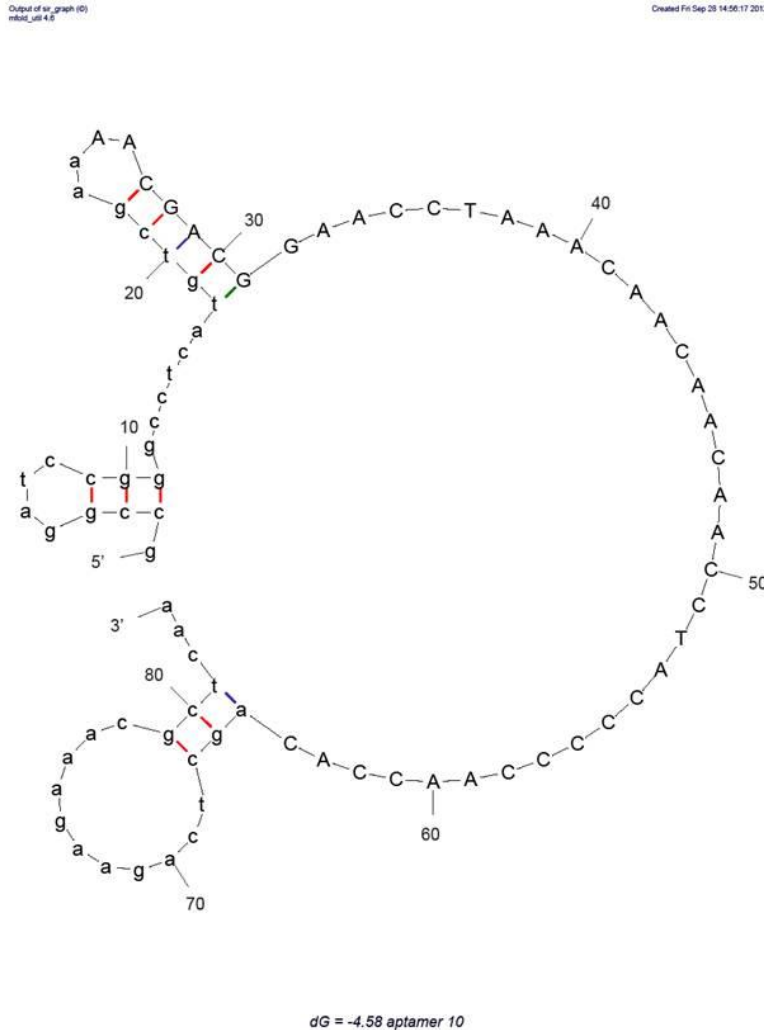


Figure A20. *Mfold* structural analysis of truncated aptamer #10.

<i>Mfold</i> Structural Analysis		Aptamer #10
Length:	40-nt (truncated)	
Sequence:	5'- <u>AACGACGGAACCTAAACAACAACAACCTACCCCAACCAC</u> -3'	
2° structural motifs:	hairpin loop: L1	

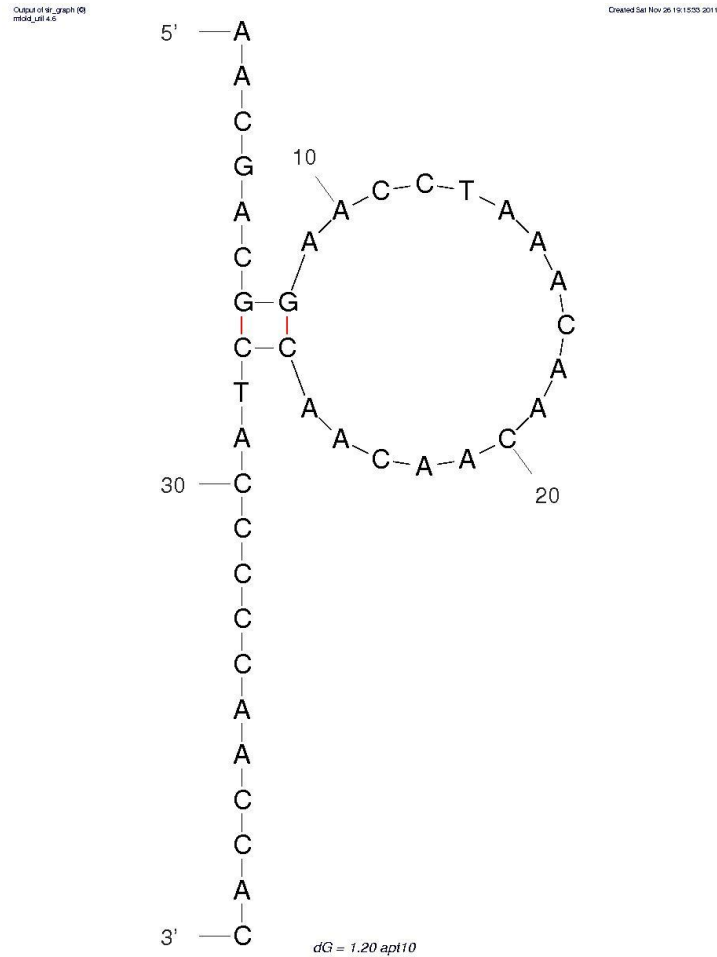


Figure A21. Mfold structural analysis of untruncated aptamer #11.

Mfold Structural Analysis		Aptamer #11
Length:		84-nt (untruncated)
Sequence:	5'- gccggatccgggctcatgtcgaacACGCGGACCTAACACACACCTCCCCCAACCACCCCACCCCagctcagaagaacgctcaa-3'	
2° structural motifs:		hairpin loops: L1, L2, L3
Family:		IV

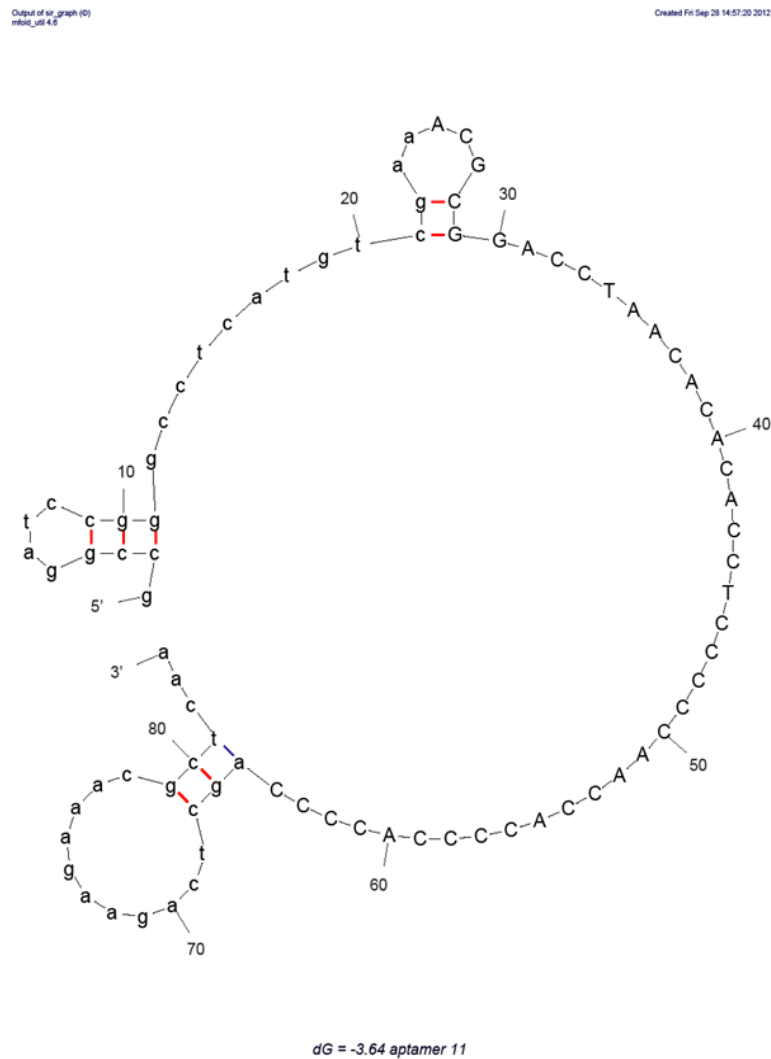


Figure A22. Mfold structural analysis of truncated aptamer #11.

Mfold Structural Analysis	Aptamer #11
Length:	40-nt (truncated)
Sequence:	
2° structural motifs:	hairpin loop: L1

5' - ACGCGGACCTAACACACACCTCCCCCAACCACCCACCCC - 3'

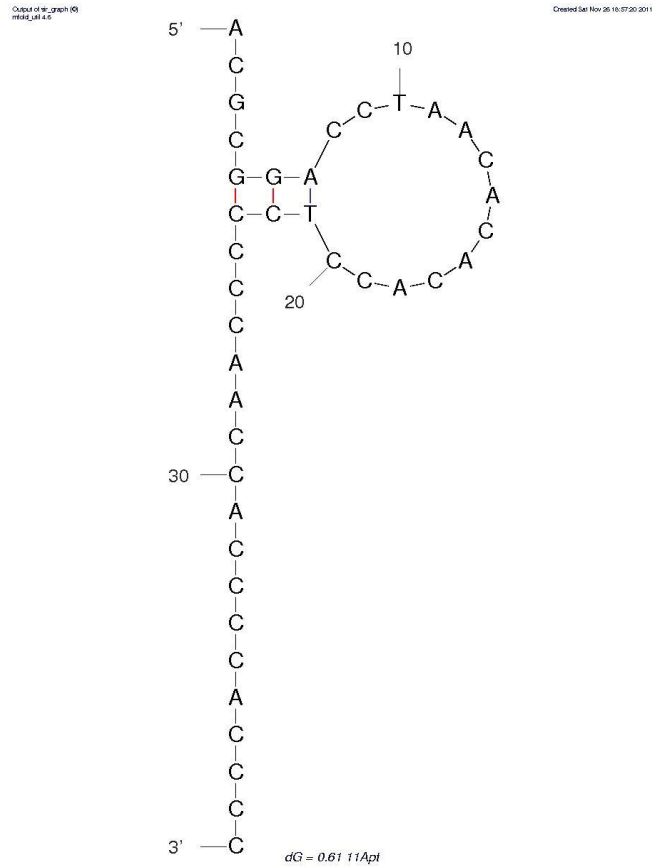


Figure A23. Mfold structural analysis of untruncated aptamer #12.

Mfold Structural Analysis	Aptamer #12
Length:	84-nt (untruncated)
Sequence:	
5' - gccggatccgggctcatgtcgaaGCCCTGCCGCATACCTCACTTCTTTCTAGACCCACACTCagctcagaagaacgctcaa-3'	
2° structural motifs:	hairpin loops: L1 and L2
Family:	II

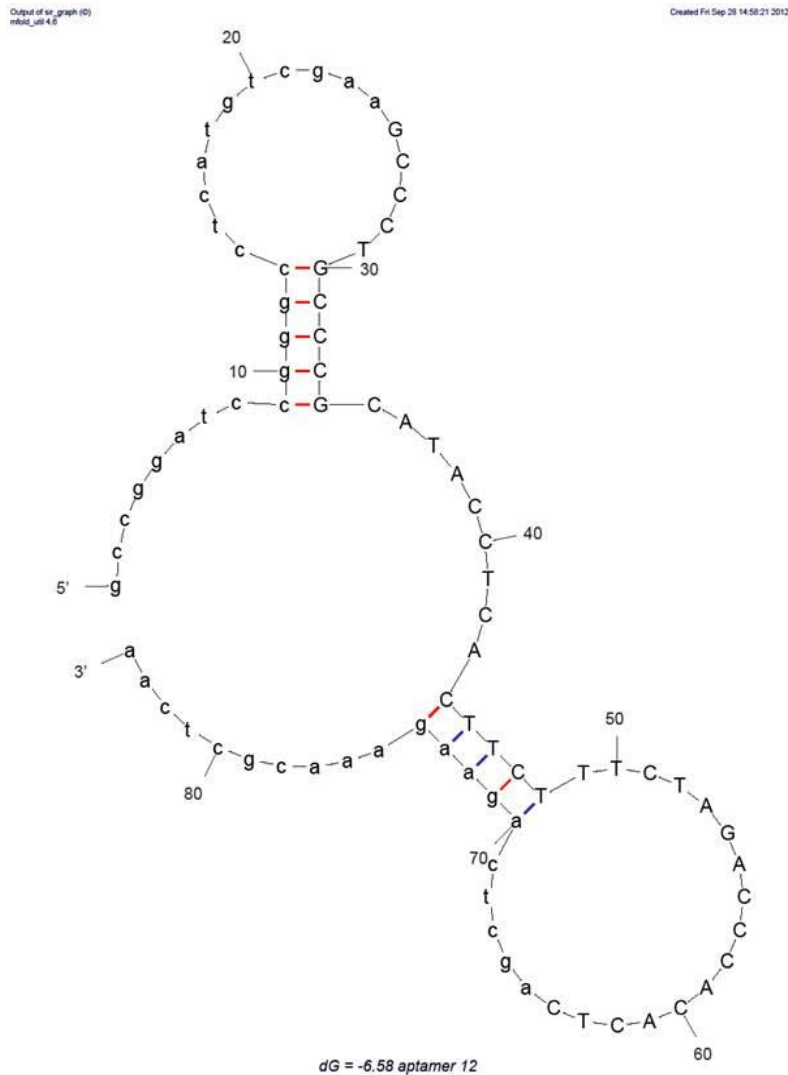


Figure A24. *Mfold* structural analysis of truncated aptamer #12.

<i>Mfold</i> Structural Analysis		Aptamer #12
Length:	40-nt	(truncated)
Sequence:	5' - <u>GCCCTGCCCGCATACTCACTTCTTTCTAGACCCACACTC</u> - 3'	
2° structural motifs:	hairpin loop:	L1

Output of the graph (9)
mfold_v3.6.6

Created Sat Nov 26 19:25:44 2011

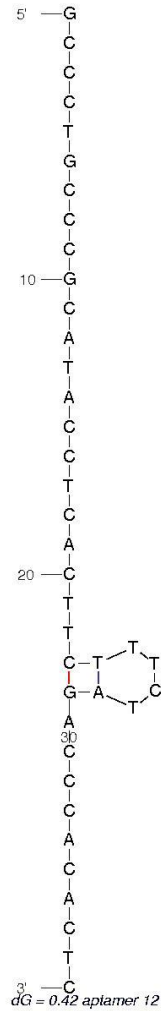


Figure A25. *Mfold* structural analysis of untruncated aptamer #13.

<i>Mfold</i> Structural Analysis		Aptamer #13
Length:	84-nt	(untruncated)
Sequence:	5'- gccggatccgggcctcatgtcgaacAGGTCGCTTACGCCCGCTGCCCCACTCAACCAACCACCTagctcagaagaacgctcaa-3'	
2° structural motifs:	hairpin loops:	L1 and L2
	internal loop:	IL1
Family:		III

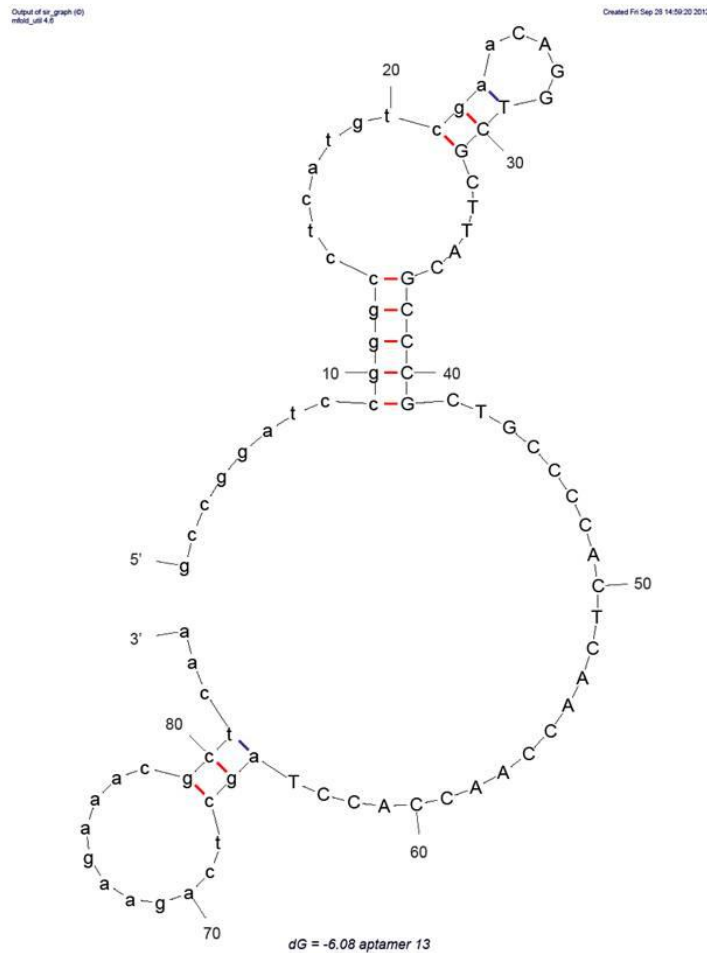


Figure A26. Mfold structural analysis of untruncated aptamer #13.

Mfold Structural Analysis		Aptamer #13
Length:		40-nt (untruncated)
Sequence:	5'- <u>CAGGTCGCTTACGCCCGCTGCCCCACTCAACCAACCACCT</u> -3'	
2° structural motifs:		hairpin loop: L1 bulge: B1

Output of mfold_graph (9)
mfold_Lut1.4.5

Created Sat Nov 26 17:43:25 2011

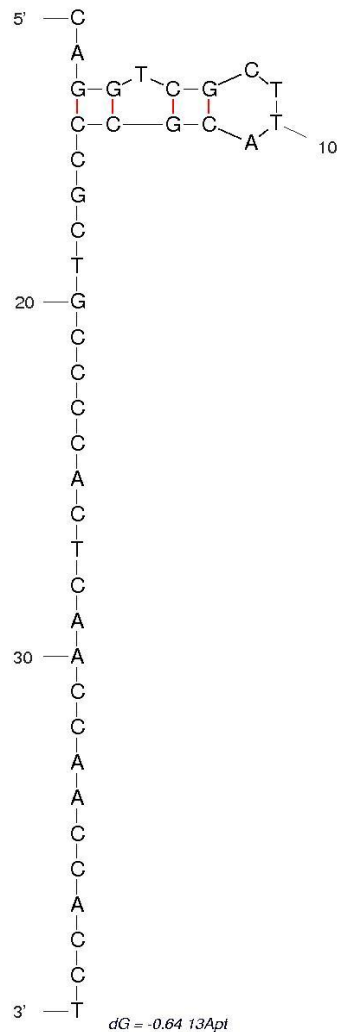


Figure A27. *Mfold* structural analysis of untruncated aptamer #14.

<i>Mfold</i> Structural Analysis		Aptamer #14
Length:	84-nt	(untruncated)
Sequence:	5'- gccggatccgggcctcatgtcgaAACGCGGACCTAACACACACCTCCCCAACACCCCACCCAgctcagaagaacgctcaa-3'	
2° structural motifs:	hairpin loops: L1, L2 and L3	
Family:	IV	

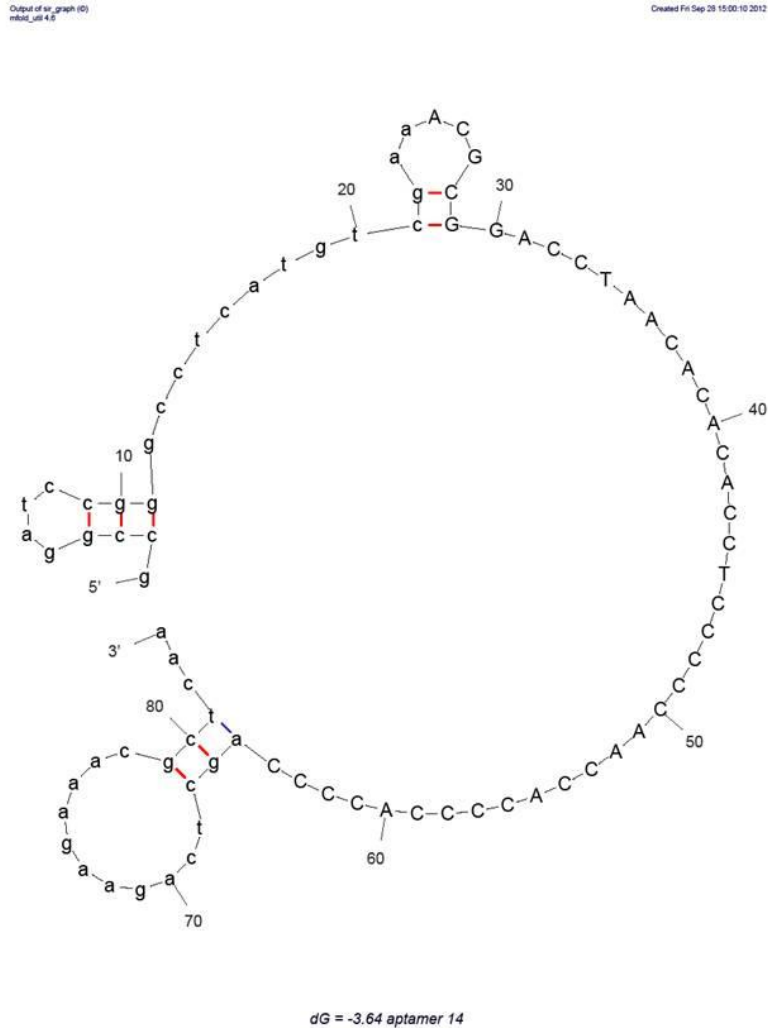


Figure A28. *Mfold* structural analysis of truncated aptamer #14.

<i>Mfold</i> Structural Analysis		Aptamer #14
Length:	40-nt (truncated)	
Sequence:	5'- <u>ACGCGGACCTAACACACACCTCCCCCAACCACCCACCCC</u> -3'	
2° structural motifs:	hairpin loops: L1	

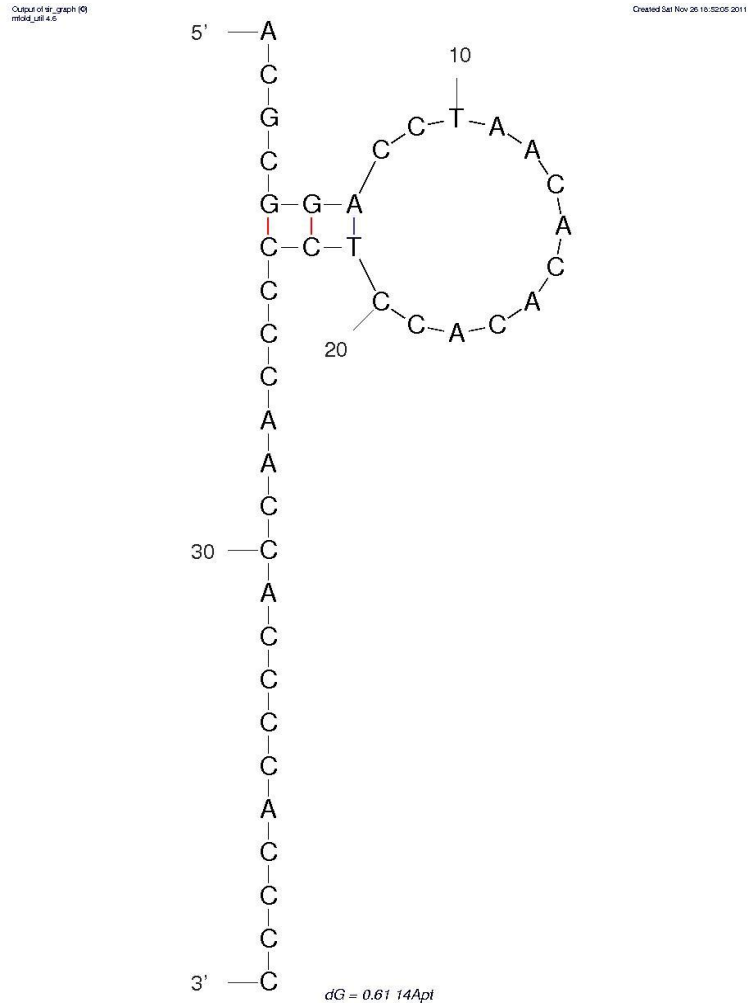


Figure A29. Mfold structural analysis of untruncated aptamer #15.

Mfold Structural Analysis		Aptamer #15
Length:	84-nt	(untruncated)
Sequence:	5'- gccggatccgggcctcatgtcgaaTACCTAGATCCCCCTCTCCAACCTTCGCTAACCTACCCAgctcagaagaaacgctcaa-3'	
2° structural motifs:	hairpin loops:	L1 and L2
	internal loop:	IL1
Family:	-	

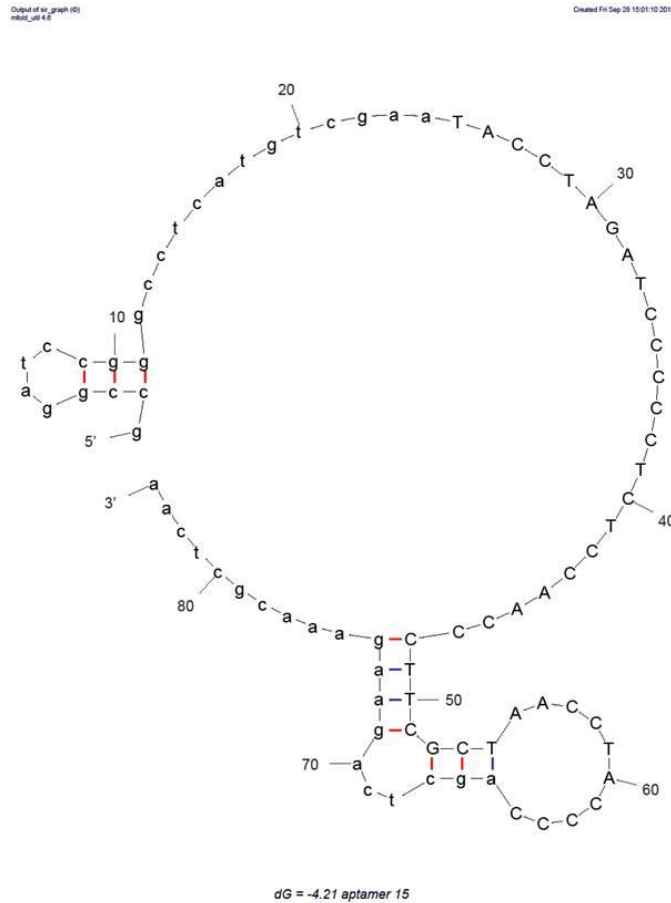
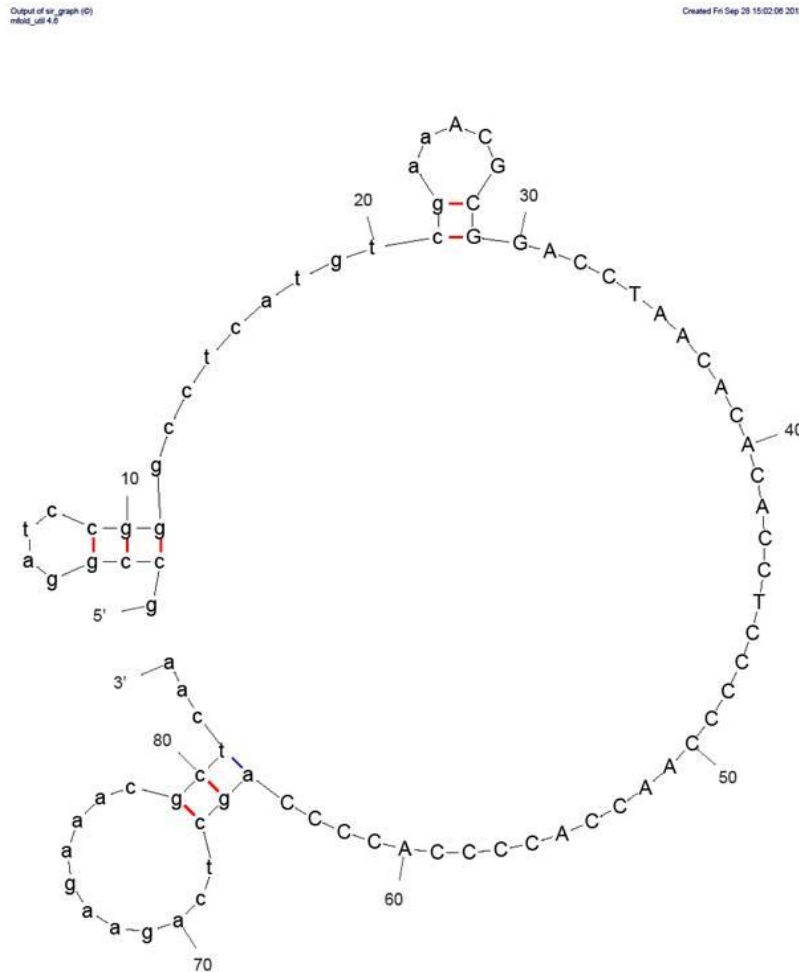


Figure A30. *Mfold* structural analysis of untruncated aptamer #16.

<i>Mfold</i> Structural Analysis		Aptamer #16
Length:		84-nt (untruncated)
Sequence:	5'- gccggatccgggctcatgtcgaaTACCTAGATCCCCCTCTCCAACCCTTCGCTAACCTACCCAgctcagaagaacgctcaa-3'	
2° structural motifs:		hairpin loops: L1, L2
Family:		IV



dG = -3.64 aptamer 16

Figure A32. Mfold structural analysis of untruncated aptamer #17.

Mfold Structural Analysis	Aptamer #17
Length:	84-nt (untruncated)
Sequence:	
5' - gccggatccgggctcatgtcgaatGCAAGGTTTCAACAAGCAATTCAGCACACATTTGCAGCAttgagcgtttattctgagct-3'	
2° structural motifs:	hairpin loops: L1, L2, L3 and L4 internal loop: IL1
Family:	-

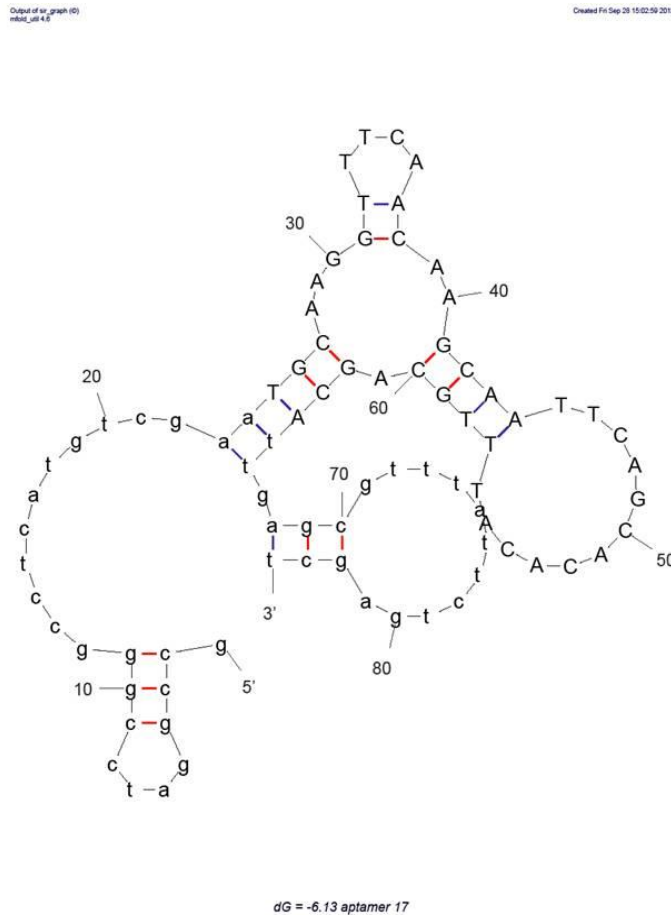


Figure A33. Mfold structural analysis of untruncated aptamer #19.

Mfold Structural Analysis	Aptamer #19
Length:	84-nt (untruncated)
Sequence: 5'- agctcagaagaacgctcaaGGGACTATTTCTGCACGTTTAGGATCTGAATTCGACCCttgagcgtttattctgagct-3'	2° structural motifs: hairpin loops: L1, L2 and L3 internal loop: IL1 Family: III

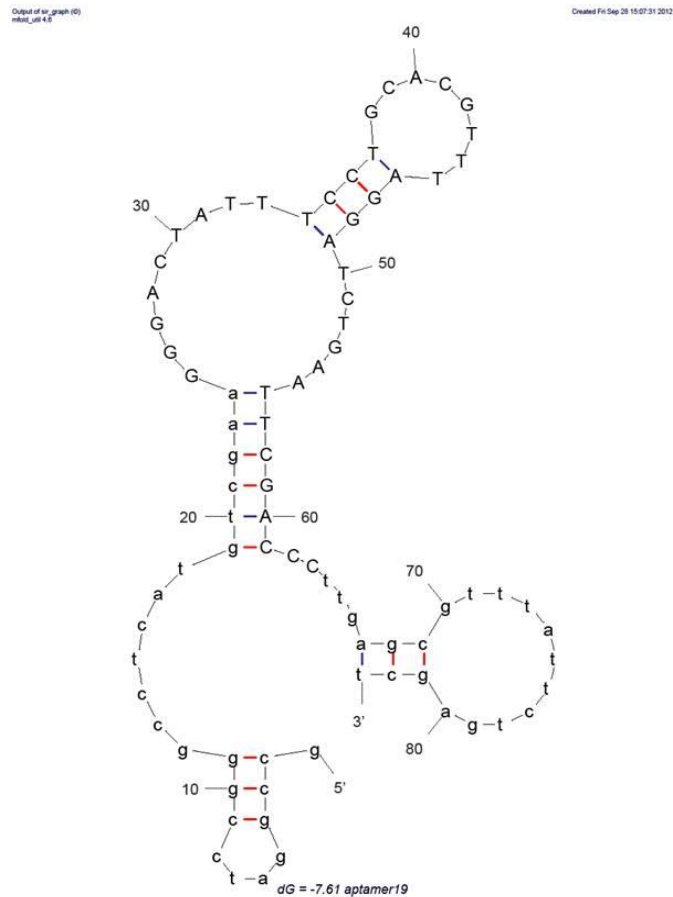


Figure A35. *Mfold* structural analysis of truncated aptamer #19.

<i>Mfold</i> Structural Analysis		Aptamer #19
Length:		40-nt (untruncated)
Sequence:	5'-GGGACTATTTCTGCACGTTTAGGATCTGAATTCGACCC-3'	
2° structural motifs:		hairpin loop: L1 and L2 internal loop: IL1

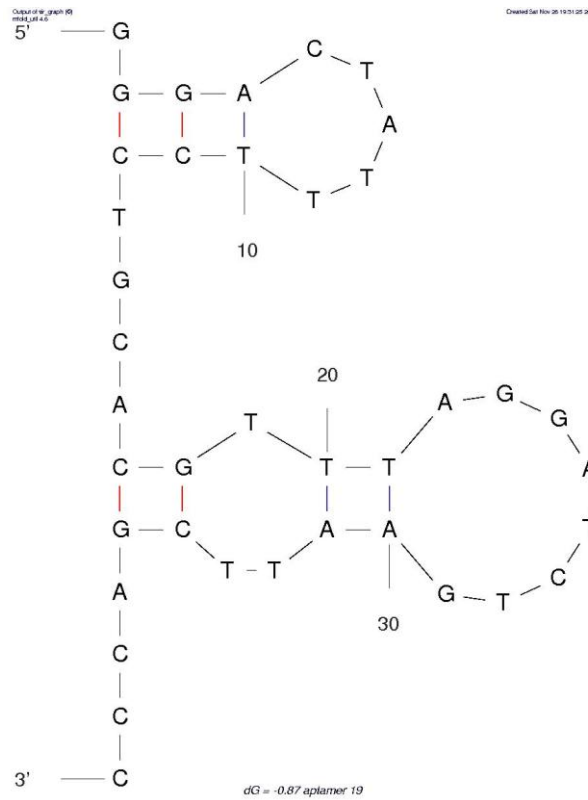
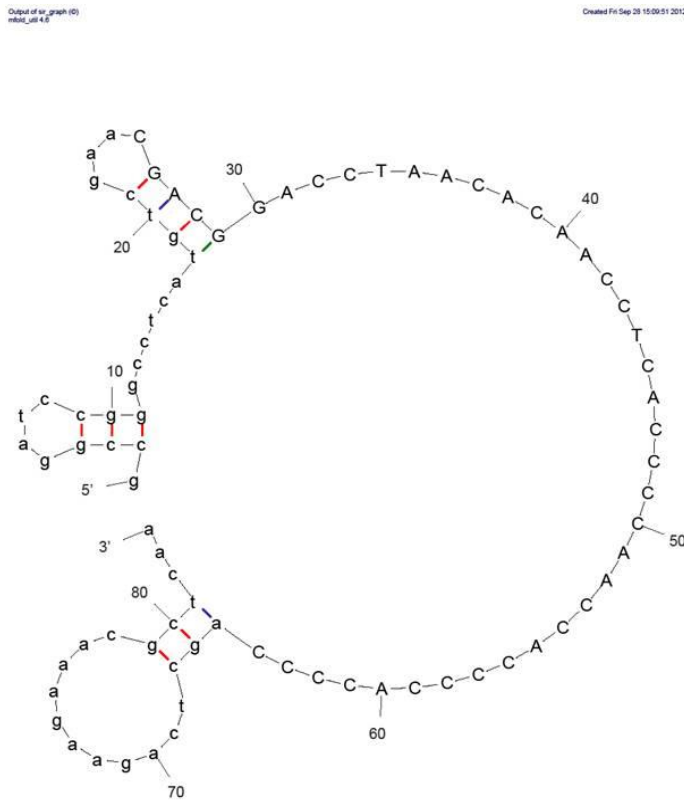


Figure A36. *Mfold* structural analysis of untruncated aptamer #20.

<i>Mfold</i> Structural Analysis		Aptamer #20
Length:	40-nt	(untruncated)
Sequence:	5' - gccggatccgggcctcatgtcgaaCGACGGACCTAACACAACCTCACCCCAACCACCCACCCAgctcagaagaaacgctcaa-3'	
2° structural motifs:	hairpin loop:	L1, L2 and L3
Family:		V



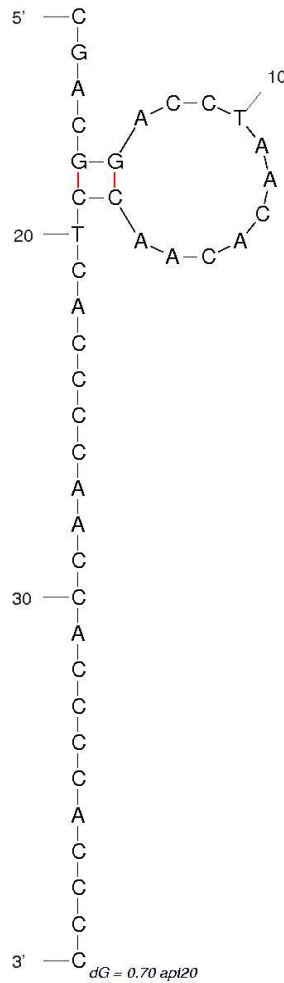
dG = -3.91 aptamer 20

Figure A37. *Mfold* structural analysis of truncated aptamer #20.

<i>Mfold</i> Structural Analysis		Aptamer #20
Length:		40-nt (truncated)
Sequence:	5' - <u>CGACGGACCTAACACAACCTCACCCCAACCACCCACCCC</u> - 3'	
2° structural motifs:		hairpin loop: L1

Output of 9f_graph (G)
mfold_v1.4.6

Created Sat Nov 26 19:09:40 2011



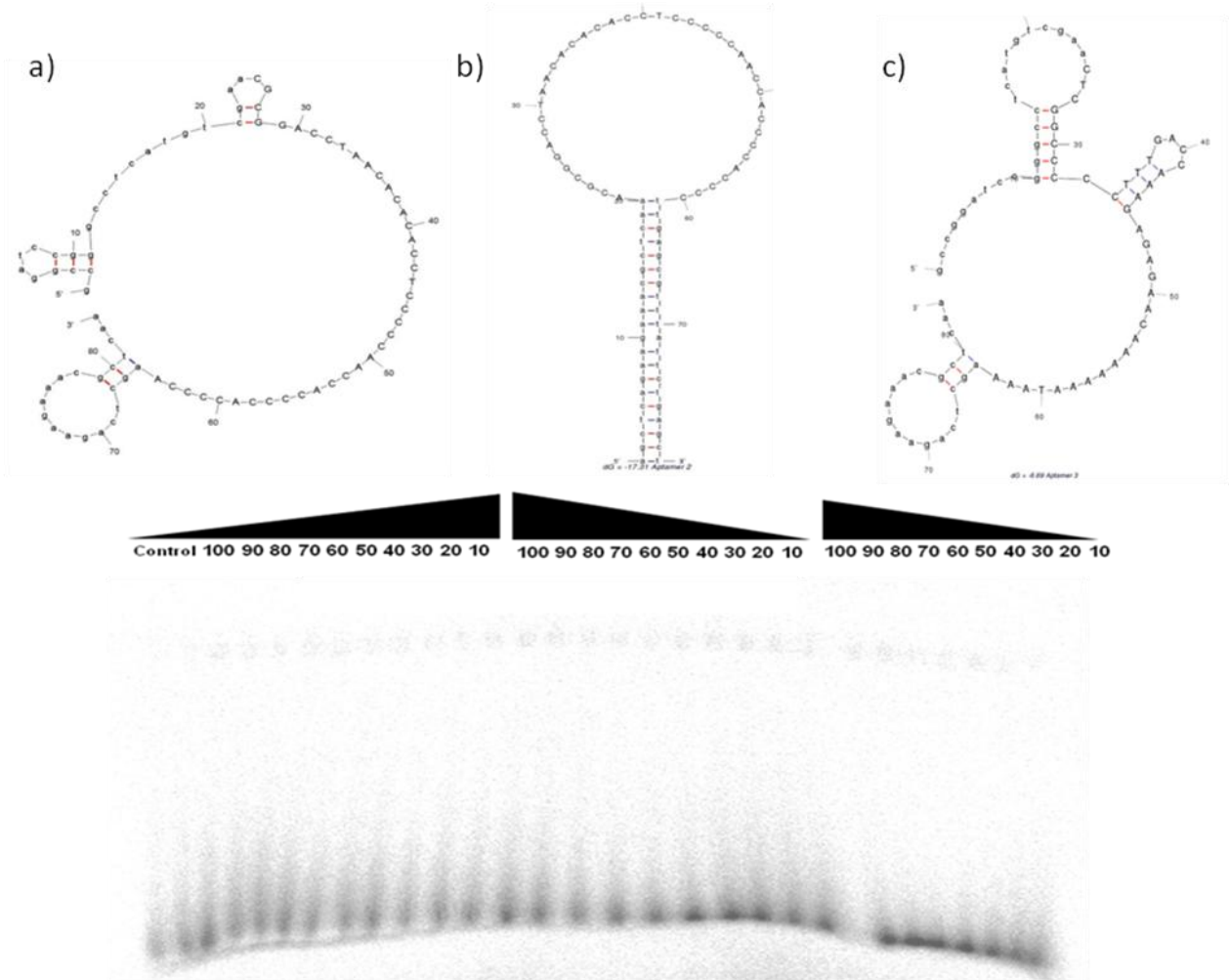


Figure A38. Preliminary DNA/H69 binding EMSA results for aptamers #1, 2 and 3. *Mfold* structural predictions for aptamer #1 (a), with aptamer #2 (b) and with aptamer #3 (c) are shown above the EMSA native gels from select cloned and sequenced SELEX rounds. All EMSA experiments were performed on a 20% non-denaturing polyacrylamide gel with 0.5× TBE running buffer and run for 3 h at 15 mA. H69 was denatured at 94 °C for 15 min and cooled to room temperature to refold for 2 h at 37 °C. [³²P] 5'-end-labeled wild-type H69 (1 nM) was preincubated at 37 °C for 15 min in buffer containing 50 mM Tris-HCl pH 7.5, 10 mM MgCl₂, 50 mM NaCl in the presence of increasing concentration of DNA aptamer (ranges 0-100 nM) against 1 nM of H69.

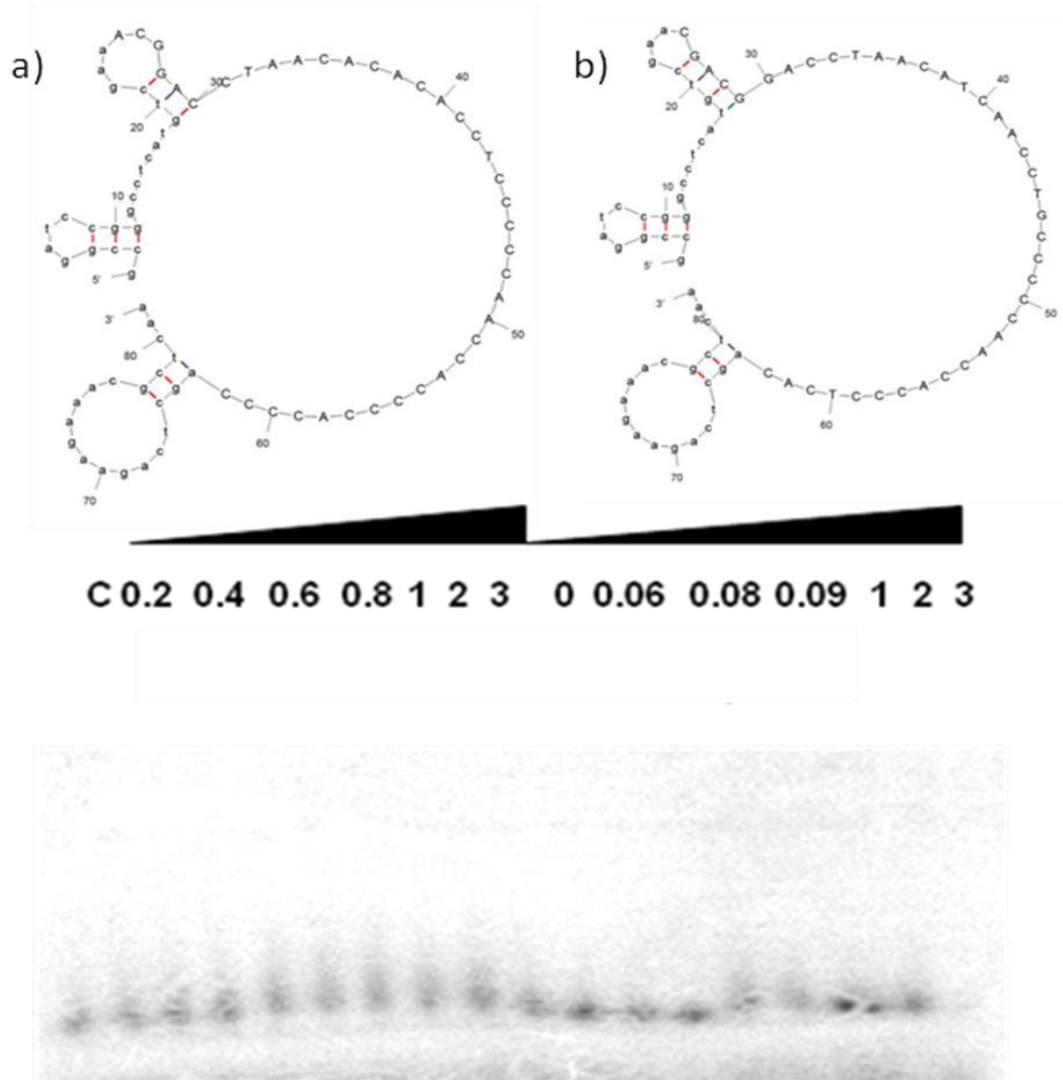


Figure A39. Preliminary DNA/H69 binding EMSA results for aptamers #4 and 5. DNA aptamers #4 (a) and 5 (b) were analyzed by EMSA on native gels and experimental conditions were the same as for aptamers in Fig. 5.8. Secondary *Mfold* structure prediction of aptamer #4 is shown above the EMSA gel analysis for aptamer #4 with increasing concentration (200 nM - 3 μM) and incubated with 1 nM of H69. Secondary *Mfold* structural prediction for aptamer #5 is also shown above the EMSA gel showing increasing aptamer concentration (0 nM – 3 μM) incubated with 1 nM of H69.

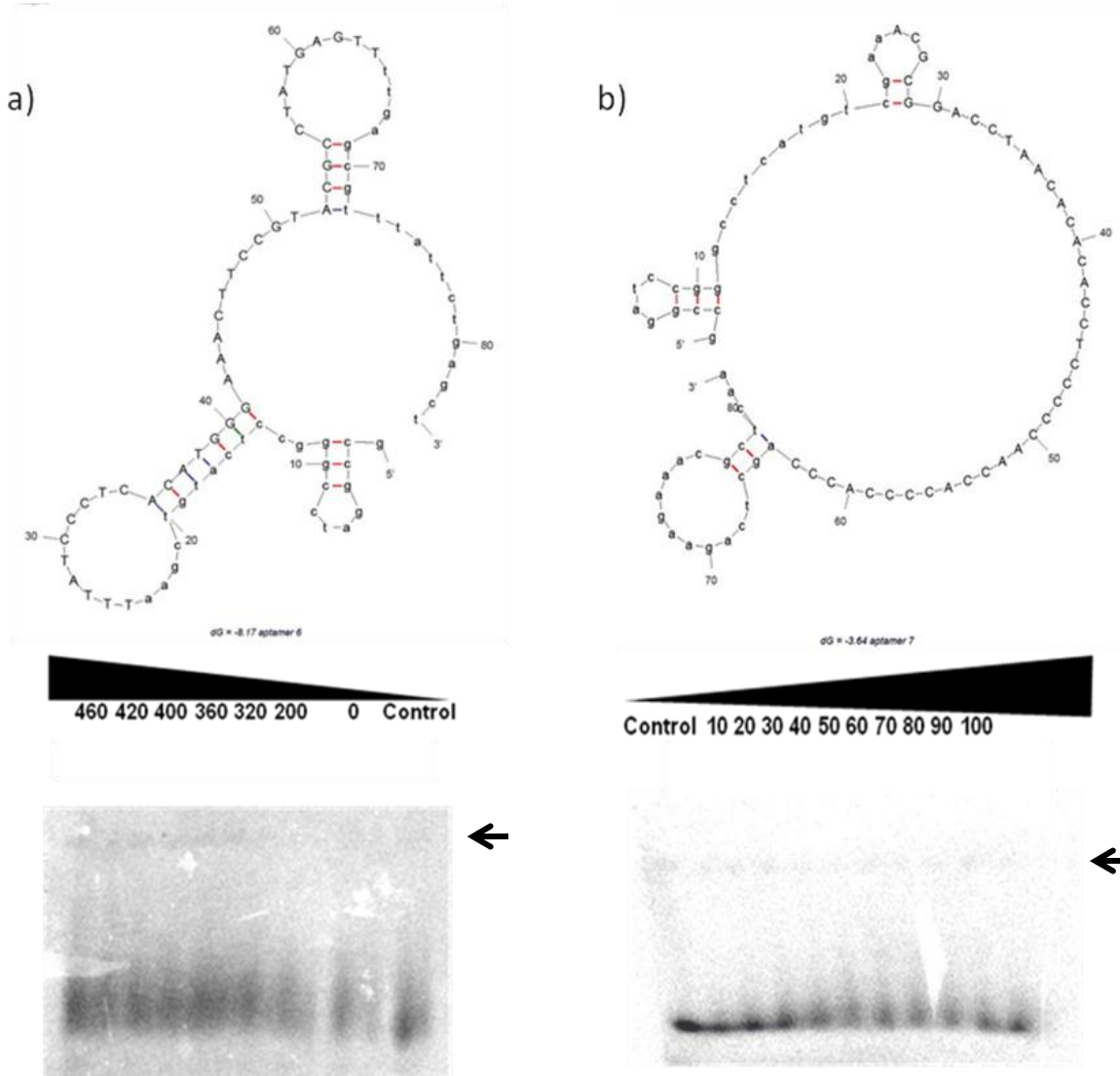


Figure A40. Preliminary DNA/H69 binding EMSA results for aptamers #6 and 7. DNA aptamers #6 (a) and 7 (b) were analyzed by EMSA on native gels using the same reaction conditions as stated in Fig. 5.8. Secondary *Mfold* structure prediction of aptamer #6 pictured above EMSA gel analysis for aptamer #7 of increasing concentration (0 - 460 nM) incubated with 1 nM of H69. Secondary *Mfold* structural prediction for aptamer #7 of increasing concentration (0 nM – 100 nM) was incubated with 1 nM of H69. Arrows are placed to indicate observed $[^{32}\text{P}]$ -H69 forming complexes with DNA aptamers #6 and 7 (≥ 320 nM for aptamer #6 and ≥ 10 nM for aptamer #7).

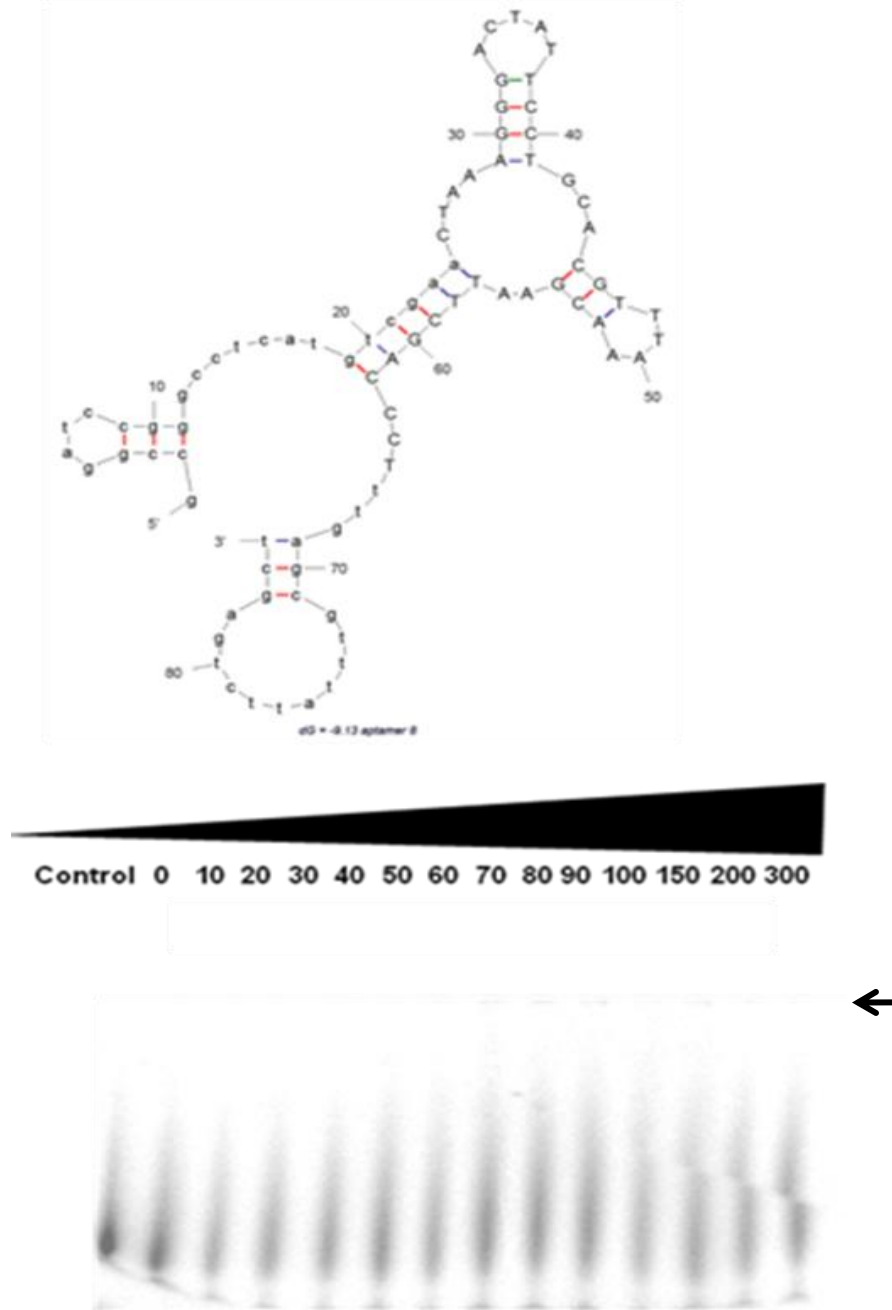


Figure A50. Preliminary DNA/H69 binding EMSA results for aptamer #8. DNA aptamer #8 is represented on an EMSA native gel using the same reaction conditions as in **Fig. 5.8**. The secondary *Mfold* structure prediction of aptamer #8 is pictured above EMSA with an increasing concentration (0 – 300 nM) incubated with 1 nM of H69. The arrow points to $[^{32}\text{P}]$ -H69 forming complexes with DNA aptamers (≥ 60 nM).

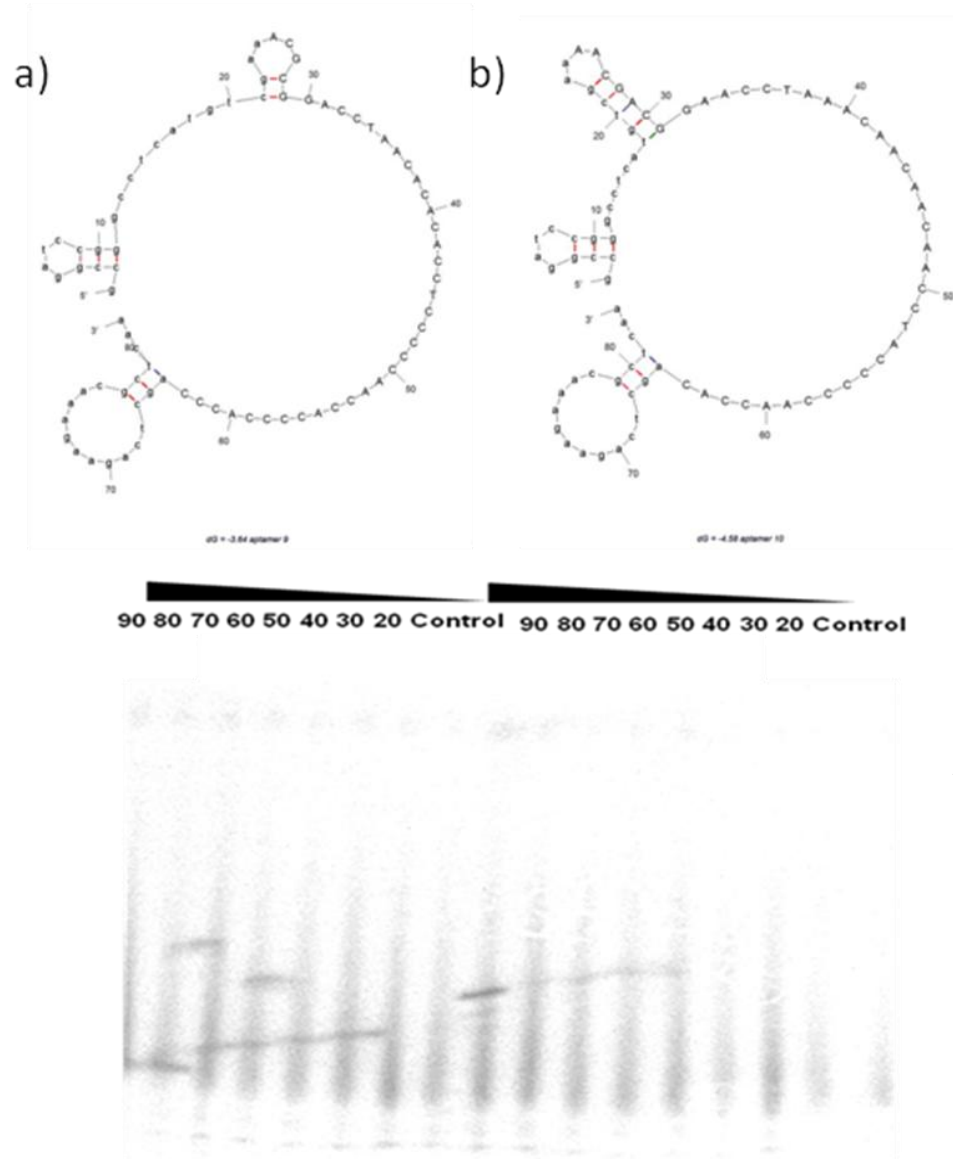
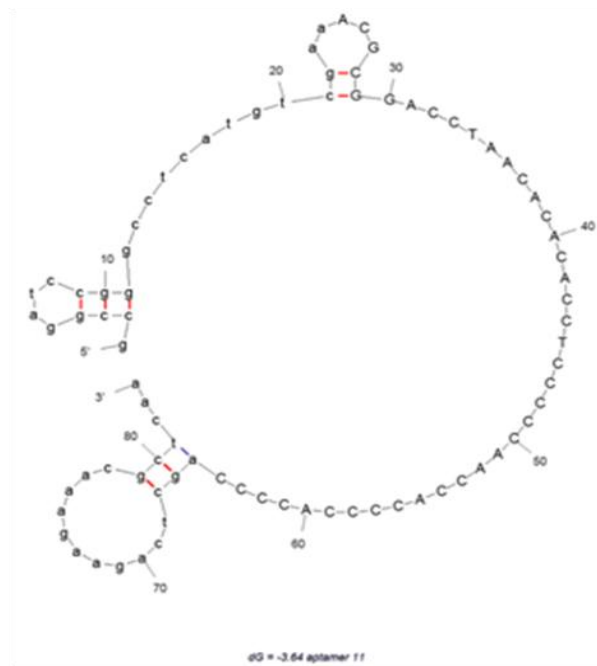


Figure A51. Preliminary DNA/H69 binding EMSA results for aptamers #9 and 10. DNA aptamers #9 (a) and 10 (b) by EMSA on a native gel were performed using the same reaction conditions as in Fig. 5.8. and (a) secondary *Mfold* structure prediction of aptamer #9 has an increasing concentration (0 nM - 90 nM) incubated with 1 nM of H69. Secondary *Mfold* structural prediction for aptamer #10 (b) has an increasing concentration range (0 nM – 90 nM) incubated with 1 nM of H69. A dark arrow indicates evidence of $[^{32}\text{P}]$ -H69 forming complexes with DNA aptamer #9 and 10 (≥ 20 nM for aptamer #9 and ≥ 50 nM for aptamer #10).



400 150 130 110 90 30 10 Control

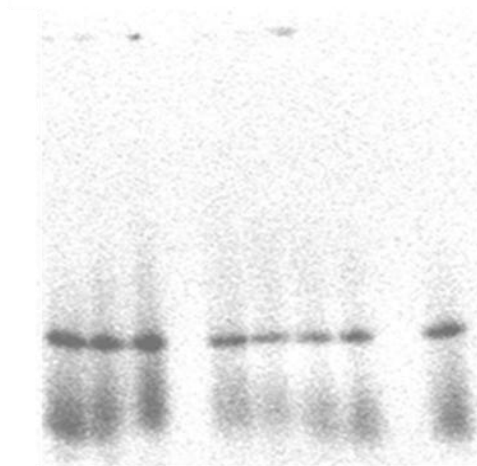


Figure A52. Preliminary DNA/H69 binding EMSA results for aptamer #11. DNA aptamer #11 is represented by EMSA on a native gel and performed using the same reaction conditions as in **Fig. 5.8**. Secondary *Mfold* structure prediction for aptamer #11 of increasing concentration (0 – 400 nM) was incubated with 1 nM of H69. A dark arrow is shown to indicate evidence of [³²P]-H69 forming complexes with DNA aptamers (≥ 30 nM).

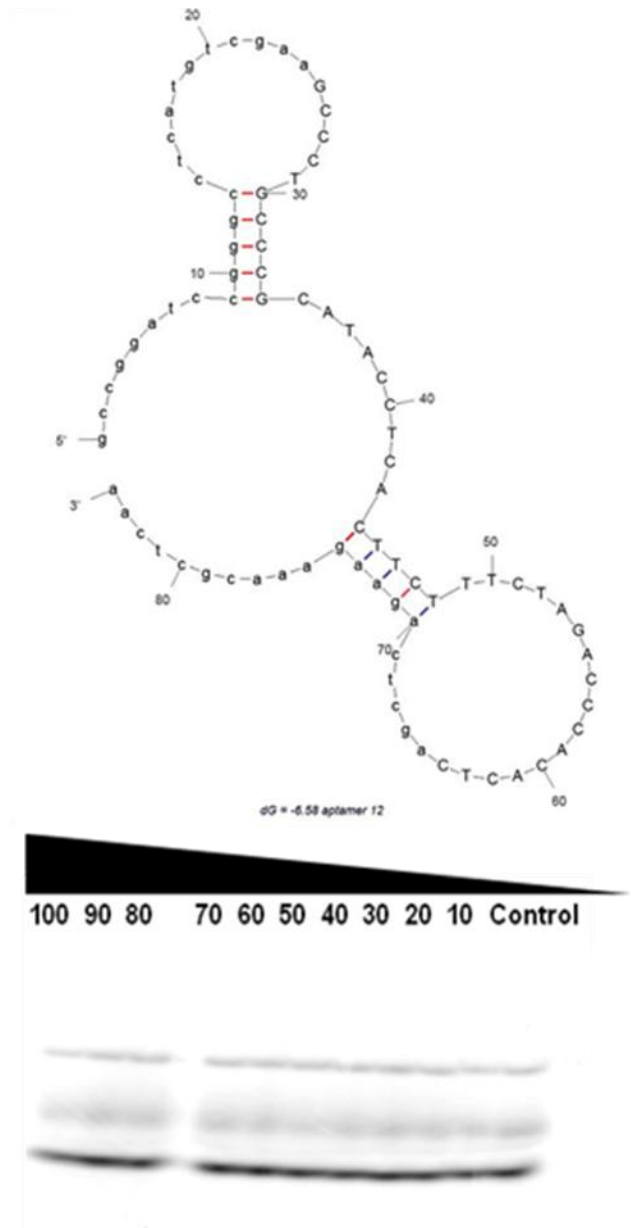


Figure A53. Preliminary DNA/H69 binding EMSA results for aptamers #12. Secondary *Mfold* structure prediction of aptamer #12 is represented above the EMSA gel analysis for aptamer #12 of increasing concentration (0 – 100 nM) incubated with 1 nM of H69 and reactions conditions were performed on a 10% non-denaturing polyacrylamide gel with 0.5× TBE running buffer and run for 1 h at 15 mA. H69 was denatured at 94 °C for 1 min and cooled to refold for 2 h at 37 °C. [32P] 5'-end-labeled wild-type H69 (1 nM) was preincubated at 37 °C for 15 min in buffer containing 50 mM Tris-HCl pH 7.5, 10 mM MgCl₂, 50 mM NaCl. No complexes with [32P] 5'-end-labeled wild-type H69 (1 nM) were observed within the range of DNA aptamer tested.

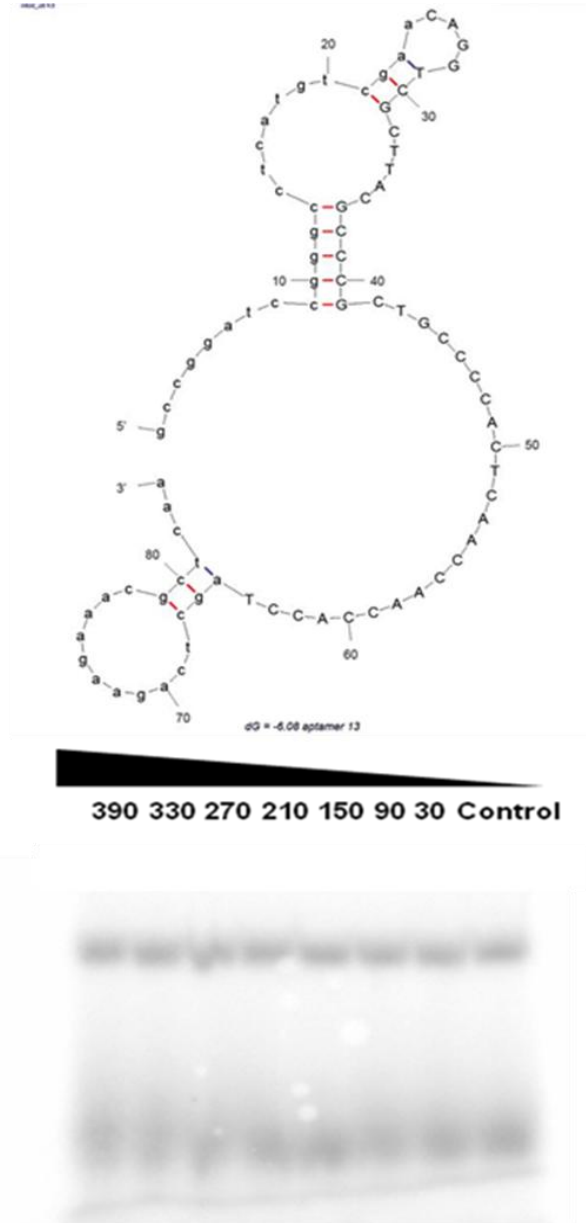
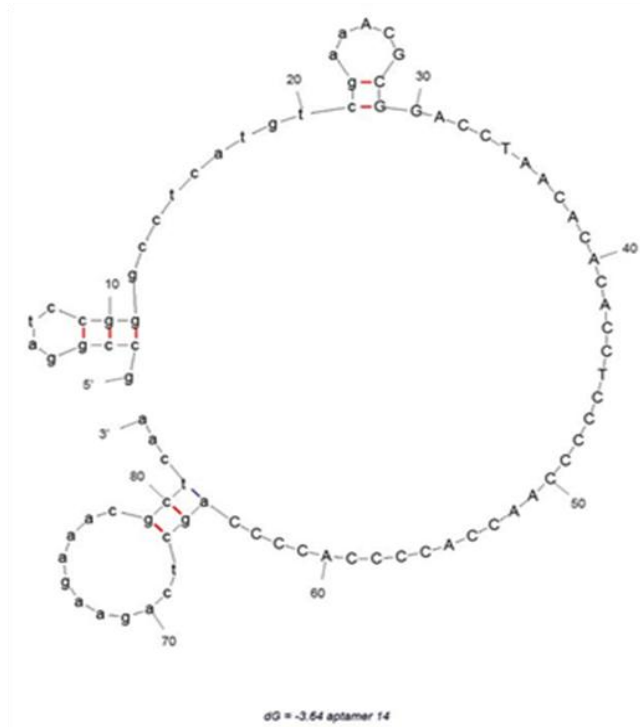


Figure A54. Preliminary DNA/H69 binding EMSA results for aptamer #13. DNA aptamer #13 secondary *Mfold* structure prediction is pictured above with increasing concentration of aptamer #13 (0 – 390 nM) incubated with 1 nM of H69. EMSA experimental conditions were performed on a 10% non-denaturing polyacrylamide gel with 0.5× TBE running buffer and run for 1 h at 15 mA. H69 was denatured at 94 °C for 1 min and cooled to refold for 2 h at 37 °C. [32P] 5'-end-labeled wild-type H69 (1 nM) was preincubated at 37 °C for 15 min in buffer containing 50 mM Tris-HCl pH 7.5, 10 mM MgCl₂, 50 mM NaCl. No complexes with [32P] 5'-end-labeled wild-type H69 (1 nM) were observed within the range of DNA aptamer tested.



500 480 460 400 380 360 320 240 0 Control

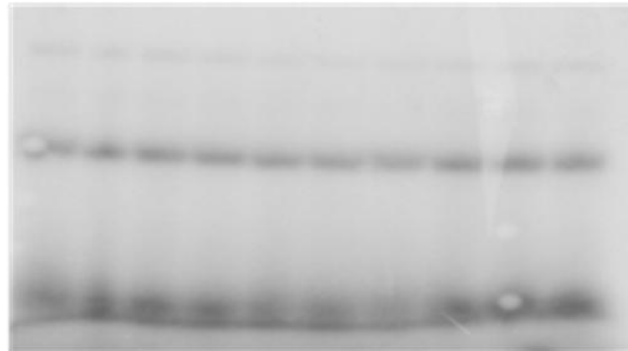


Figure A55. Preliminary DNA/H69 binding EMSA results for aptamer #14. Secondary *Mfold* structure prediction of aptamer #14 is pictured above EMSA gel analysis of increasing concentration of aptamer #14 (0 – 500 nM) incubated with 1 nM of H69 using 10% non-denaturing polyacrylamide gel with 0.5× TBE running buffer and run for 1 h at 15 mA. H69 was denatured at 94 °C for 1 min and cooled to refold for 2 h at 37 °C. [³²P] 5'-end-labeled wild-type H69 (1 nM) was preincubated at 37 °C for 15 min in buffer containing 50 mM Tris-HCl pH 7.5, 10 mM MgCl₂, 50 mM NaCl. No complexes with [³²P] 5'-end-labeled wild-type H69 (1 nM) were observed within the range of DNA aptamer tested.

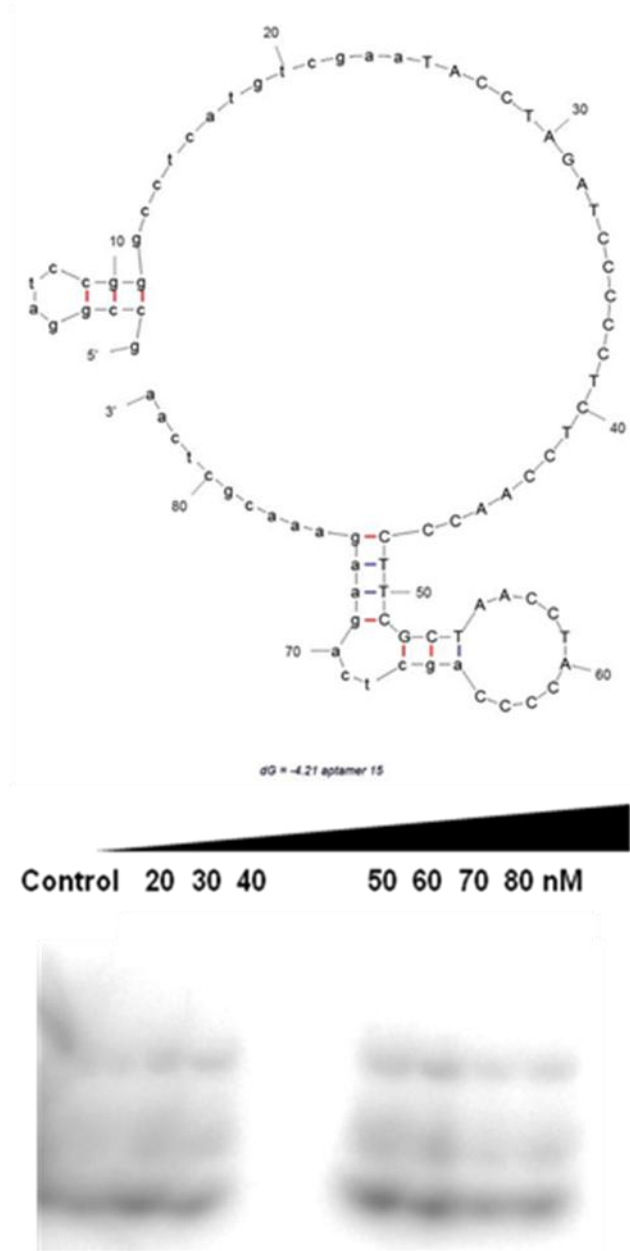


Figure A56. Preliminary DNA/H69 binding EMSA results for aptamer #15. Secondary *Mfold* structure prediction of aptamer #15 is pictured above EMSA gel analysis for aptamer #15 of increasing concentration (0 – 80 nM) incubated with 1 nM of H69 performed using 10% non-denaturing polyacrylamide gel with 0.5× TBE running buffer and run for 1 h at 15 mA. H69 was denatured at 94 °C for 1 min and cooled to refold for 2 h at 37 °C. [³²P] 5'-end-labeled wild-type H69 (1 nM) was preincubated at 37 °C for 15 min in buffer containing 50 mM Tris-HCl pH 7.5, 10 mM MgCl₂, 50 mM NaCl. No complexes with [³²P] 5'-end-labeled wild-type H69 (1 nM) were observed within the range of DNA aptamer tested.

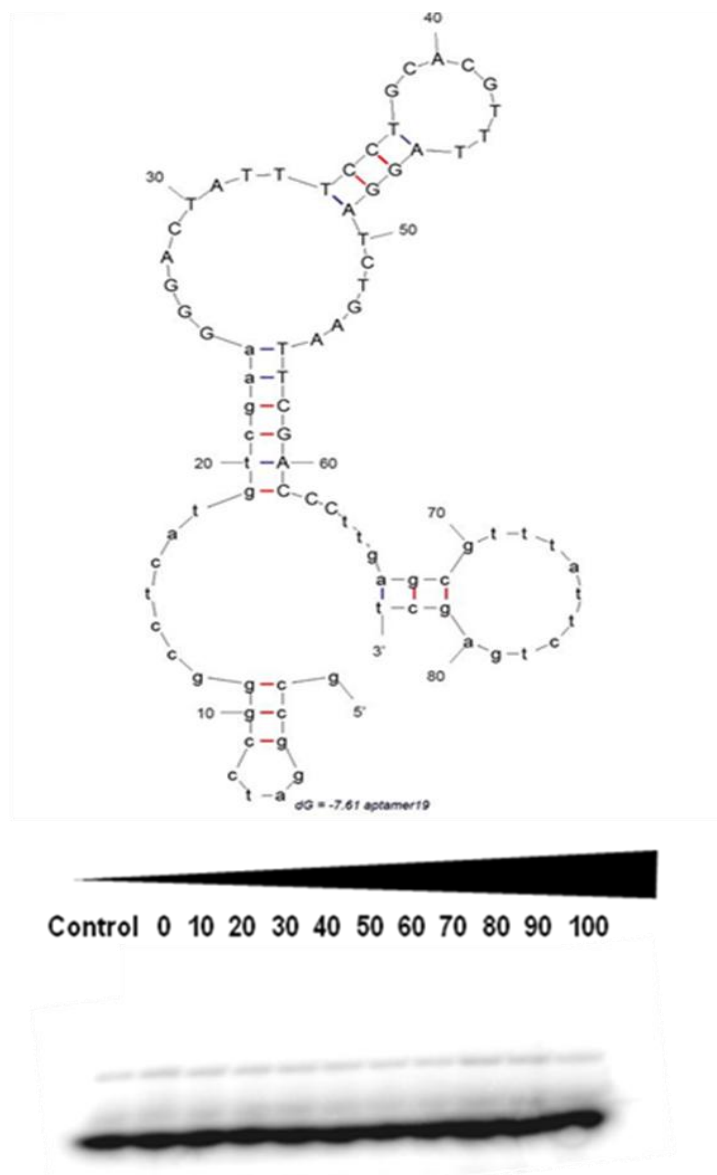


Figure A57. Preliminary DNA/H69 binding EMSA results for aptamer #19. Secondary *Mfold* structure prediction of aptamer #19 is pictured above EMSA gel analysis for aptamer #19 of increasing concentration (0 – 100 nM) incubated with 1 nM of H69 performed on a 10% non-denaturing polyacrylamide gel with 0.5× TBE running buffer and run for 1 h at 15 mA. H69 was denatured at 94 °C for 1 min and cooled to refold for 2 h at 37 °C. [³²P] 5'-end-labeled wild-type H69 (1 nM) was preincubated at 37 °C for 15 min in buffer containing 50 mM Tris-HCl pH 7.5, 10 mM MgCl₂, 50 mM NaCl. No complexes with [³²P] 5'-end-labeled wild-type H69 (1 nM) were observed within the range of DNA aptamer tested.

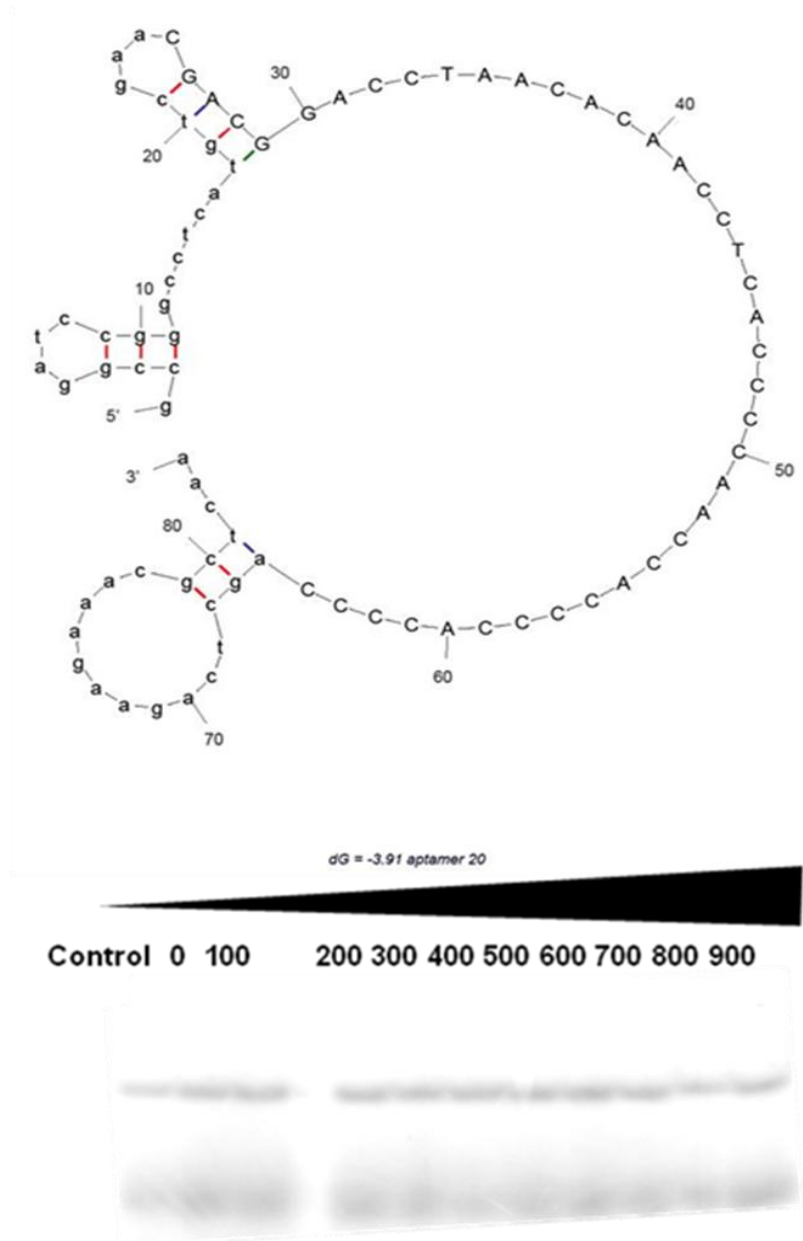


Figure A58. Preliminary DNA/H69 binding EMSA results for aptamer #20. Secondary *Mfold* structure prediction of aptamer #20 is pictured above EMSA gel analysis for aptamer #20 of increasing concentration (0 – 900 nM) incubated with 1 nM of H69 performed on a 10% non-denaturing polyacrylamide gel with 0.5× TBE running buffer and run for 1 h at 15 mA. H69 was denatured at 94 °C for 1 min and cooled to refold for 2 h at 37 °C. [³²P] 5'-end-labeled wild-type H69 (1 nM) was preincubated at 37 °C for 15 min in buffer containing 50 mM Tris-HCl pH 7.5, 10 mM MgCl₂, 50 mM NaCl. No complexes with [³²P] 5'-end-labeled wild-type H69 (1 nM) were observed within the range of DNA aptamer tested.

REFERENCES

1. Frangsmyr T., *Nobel Lectures, Chemistry 1981-1990*, World Scientific Publishing Co., Singapore, (1992).
2. Guerrier-Takada C., Gardiner K., Marsh T., Pace N., Altman S., "The RNA Moiety of Ribonuclease P is the Catalytic Subunit of the Enzyme," *Cell*, **35**, 849-57(1983).
3. Dahm R., "Friedrich Miescher and the Discovery of DNA," *Developmental Biology*, **278**, 274–88 (2005).
4. Furberg S., "The Crystal Structure of Cytidine," *Acta Crystallogr.*, **3**, 325-331 (1950).
5. Watson J.D. and Crick F.H.C., "A Structure for Deoxyribose Nucleic Acid," *Nature*, **171**, 737-73 (1953).
6. Franklin R. and Gosling R.G. "Molecular Configuration in Sodium Thymonucleate," *Nature*, **171**, 740-741 (1953).
7. P. O. P. Ts'o, *Bases, Nucleosides, and Nucleotides In: Basic Principles in Nucleic Acid Chemistry* (P. O. P. Ts'o, Ed.), vol. I, pp. 453-584. Academic Press, New York (1974).
8. Watson J.D., *The Double Helix: A Personal Account of the Discovery of the Structure of DNA* (1968).
9. Adams P.L. R., Knowler T. J., Leader P. D., *The Biochemistry of the Nucleic Acids*. 11th ed. (1998).
10. Kornberg A. *DNA Replication*, San Francisco. Freeman (1980).
11. Saenger W. *Principles of Nucleic Acid Structure*, Springer-Verlag, New York (1984).

12. H. P. M. de Leeuw, C. A. G. Haasnoot, and C. Altona, "Empirical Correlations between Conformational Parameters in β -D-furanoside Fragments Derived from a Statistical Survey of Crystal Structures of Nucleic Acid Constituents. Full Description of Nucleoside Molecular Geometries in Terms of Four Parameters," *Isr. J. Chem.*, **20**, 108 -126 (1980).
13. Tinoco I. Jr. and Bustamante C., "How RNA Folds," *J. Mol. Biol.*, **293**, 271–281 (1999).
14. Tian B., Bevilacqua C. P., Diegelman-Parente A., and Mathews B. M. "The Double-Stranded-RNA-Binding-Motif: Interference and Much More," *Nature Reviews Molecular Cell Biology*, **5**, 1013-1023 (2004).
15. Crick F. H. C., "Central Dogma of Molecular Biology," *Nature*, **227**, 561-563 (1970).
16. Kastner B., Stoffler-Meilicke M., and Stoffler G., "Arrangement of the Subunits in the Ribosome of *Escherichia coli*: Demonstration by Immunoelectron Microscopy," *Proceedings of the National Academy of Sciences of the United States of America*, **78**, 6652-6656 (1981).
17. Joachim F., "How the Ribosome Works," *American Scientist*, **86**, 428-439(1998).
18. Roberts, R. B. 1958. Introduction. In R. B. Roberts, *Microsomal Particles and Protein Synthesis*. New York: Pergamon Press.
19. Ben-Shem A., Jenner L., Yusupova G., Yusupov M. "Crystal Structure of the Eukaryotic Ribosome," *Science*, **26**, 1203-9 (2010).
20. Frank J. C., "Cryo-Electron Microscopy as an Investigative Tool: The Ribosome as an Example," *Bioessays.*, **23**, 725-32 (2001).
21. A. E. Dahlberg, "Site-Directed Mutagenesis of *Escherichia coli* Ribosomal RNA Structure", *Function, and Genetics of Ribosomes Springer Series in Molecular Biology* 686-698 (1986).

22. Stark H., "Three-Dimensional Electron Cryomicroscopy of Ribosomes," *Curr. Protein Pept. Sci.*, **1**, 79-91 (2002).
23. Moine H., Cachia C., Westhof E., Ehresmann B., Ehresmann C., "The RNA Binding Site of S8 Ribosomal Protein of *Escherichia coli*: Selex and Hydroxyl Radical Probing Studies," *RNA*, **3**, 255- 268 (1997).
24. Wilson D.N., Nierhaus K.H., "The Ribosome Through the Looking Glass," *Angew. Chem. Int. Ed. Engl.*, **30**, 3464-86 (2003).
25. Cooper G.C., Hausman R.E., *The Cell: A Molecular Approach*, Sinauer, vol. 297, pp. 339–44, 3rd ed. (2004).
26. Mueller F., Sommer I., Baranov P., Matadeen R., Stoldt M., Wöhnert J., Görlach M., van Heel M., Brimacombe R., "The 3D Arrangement of the 23S and 5S rRNA in the *Escherichia coli* 50S Ribosomal Subunit Based on a Cryo-Electron Microscopic Reconstruction at 7.5 Å Resolution," *J. Mol. Biol.*, **1**, 35-59 (2000).
27. Brenner S., Jacob F., and Meselson M., "An Unstable Intermediate Carrying Information from Genes to Ribosomes for Protein Synthesis," *Nature*, **190**, 576–581 (1961).
28. Cundliffe E., "Involvement of Specific Portions of rRNA in Defined Ribosomal Functions: A Study Utilizing Antibiotics," In *Structure, Function and Genetics of Ribosomes*, Hardesty, B. & Kramer, G., ed., pp. 586–604, Springer-Verlag, New York (1986).
29. Slonczewski J., Watkins F. J., *Microbiology: An Evolving Science*, New York, W.W. Norton (2009).
30. Yusupov M. M., Yusupova G. Z., Baucom A., Lieberman K., Earnest T. N., Cate J. H. D., and Noller H. F., "Crystal Structure of the Ribosome at 5.5 Å Resolution," *Science*, **292**, 883–896

- (2001).
31. Kavran J. M., Steitz T. A., "Structure of the Base of the L7/L12 Stalk of the *Haloarcula marismortui* Large Ribosomal Subunit: Analysis of L11 Movements," *J. Mol. Bio.*, **371**, 1047-1059, (2007).
 32. Ban N., Nissen P., Hansen J., Moore P. B., and Steitz T. A. "The Complete Atomic Structure of the Large Ribosomal Subunit at 2.4 Å Resolution," *Science*, **289**, 905–920 (2000).
 33. Yusupov M. M., Garber B. M., Vasiliev D. V., Spirin A. S., "Thermus Thermophilus Ribosomes for Crystallographic Studies," *Biochimie* **73**, 887–897 (1991).
 34. Noller H. F., Yusupov M., Yusupova G., Baucom A., Lieberman K., Lancaster L., Dallas A., Fredrick K., Earnest T. N., and Cate J. H. D., "Structure of the Ribosome at 5.5 Å Resolution and Its Interactions with Functional Ligands," *The Ribosome*, vol. 66. Cold Spring Harbor Laboratory Press, Cold Spring Harbor, New York, pp. 57-66 (2001).
 35. Ben-Shem A., Jenner L., Yusupova G., Yusupov M., "Crystal Structure of the Eukaryotic Ribosome," *Science*, **330**, 1203-9 (2010).
 36. Schmeing T. M., Voorhees R. M., Kelley A. C., Gao Y. G., Murp F. V., Weir J. R., and Ramakrishnan V., "The Crystal Structure of the Ribosome Bound to EF-Tu and Aminoacyl-tRNA," *Science*, **326**, 688-694 (2009).
 37. Blaha G., Stanley R. E., Steitz T. A., "Formation of the First Peptide Bond: The Structure of EF-P Bound to the 70S Ribosome," *Science*, **325**, 966-70 (2009).
 38. Schlutzen F., Tocilj A., Zarivach R., Harms J., Gluehmann M., Janell D., Bashan A., Bartels H., Agmon I., Franceschi F. and Yonath A., "Structure of Functionally Activated Small

- Ribosomal Subunit at 3.3 Å resolution," *Cell*, **102**, 615-623 (2000).
39. Rodnina M.V., Beringer M., Wintermeyer W. "How Ribosomes Make Peptide Bonds," *Trends Biochem. Sci.*, **32**, 20-6 (2007).
40. Noller F. H., "Ribosomal RNA and Translation," *Annu. Rev. Biochem.*, **60**, 191-227 (1991).
41. Bremer H., Dennis P. P. 1996. *Modulation of Chemical Composition and Other Parameters of the Cell by Growth Rate. In Escherichia coli and Salmonella: Cellular and Molecular Biology*, ed. FCNeidhardt, RCurtiss, JL Ingraham, ECCLin, KBLow, pp. 1553-69. Washington, DC, ASM (1996).
42. Forschhammer and Lindahl L., "Rate of Prokaryotic Cytoplasmic Protein Synthesis," *J. Mol. Biol.*, **55**, 563-568 (1971).
43. Alberts and Bruce. *Molecular Biology of the Cell*, New York: Garland Science. pp. 760 (2002).
44. Evarsson A., Brazhnikov E., Garber M., Zheltonosova J., Chirgadze Y., al-Karadaghi S., Svensson L. A., and Liljas A., "Three-Dimensional Structure of the Ribosomal Translocase: Elongation Factor G from *Thermus thermophilus*," *EMBO J.*, **13**, 36669-3677 (1994).
45. Wilson K. S. and Noller H. F., "Mapping the Position of Translational Elongation Factor EF-G in the Ribosome by Directed Hydroxyl Radical Probing," *Cell*, **92**, 131-139 (1998).
46. Agrawal R. K., Penczek P., Grassucci R. A., and Frank J., "Visualization of Elongation Factor G on the *Escherichia coli* 70S Ribosome: The Mechanism of Translocation," *Proc. Natl. Acad. Sci.*, **95**, 6134-6138 (1998).
47. Sherman, F., Stewart, J. W. and Tsunasawa, S., "Methionine or Not Methionine at the Beginning of a Protein," *Bioessays*, **3**, 27-31 (1985).

48. Berg J. M., Tymoczko J. L., Stryer L., *Biochemistry* (5th ed.). WH Freeman and Company. pp. 118–19 and 781–808 (2002).
49. Schluederger F., Tocilj A., Zarivach R., Harms J., Gluehmann M., Janell D., Bashan A., Bartels H., Agmon I., Franceschi F., “Structure of Functionally Activated Small Ribosomal Subunit at 3.3 Angstroms Resolution,” *Cell*, **102**, 615–623 (2000).
50. Moazed D., and Noller F. H., “Intermediate States in the Movement of Transfer RNA in the Ribosome,” *Nature*, **342**, 142–148 (1989).
51. Wimberly B. T., Brodersen D. E., Clemons W. M. Jr., Morgan-Warren R. J., Carter A. P., Vornrhein C., Hartsch T., and Ramakrishnan V., “Structure of the 30S Ribosomal Subunit,” *Nature*, **407**, 327–339 (2000).
52. Schmeing T. M., Seila A.C., Hansen J. L., Freeborn B., Soukup J. K., Scaringe S. A., Strobel S. A., Moore P. B., and Steitz T. A., “A Pre-translocational Intermediate in Protein Synthesis Observed in Crystals of Enzymatically Active 50S Subunits,” *Nat. Struct. Biol.* **9**, 225–230 (2002).
53. Rozenski, J., Crain, P. F. and McCloskey, J. A., The RNA Modification Database: (1999) Update. *Nucleic Acids Res.*, **27**, 196-197 (1999).
54. McCloskey J.A., and Rozenski J., “The Small Subunit rRNA Modification Database,” *Nucleic Acids Research*, **33**, Database issue D135-D138, (2005).
55. Agris P. F., “The Importance of Being Modified: Roles of Modified Nucleosides and Mg²⁺ in RNA Structure and Function,” *Prog. Nucleic Acid Res. Mol. Biol.*, **53**, 79-129 (1996).
56. Wang X., Lu Z., Gomez A., Hon G. C., Yue Y., Han D., Fu Y., Parisien M., Dai Q., Jia G., Ren B., Pan T., He C., “N6-methyladenosine-dependent Regulation of Messenger RNA Stability,”

- Nature*, **505**, 117-20 (2014).
57. Wolfram Saenger W., Verlag S., *Principles of Nucleic Acid Structure*. Chapter 7, 159 (1984).
58. Ballin J. D., Bharill S., Fialcowitz-White E. J., Gryczynski I., Gryczynski Z., Wilson G. M., "Site-specific Variations in RNA Folding Thermodynamics Visualized by 2-Aminopurine Fluorescence," *Biochemistry*, **46**, 13948-13960 (2007).
59. Ryder S.P., Strobel S.A., "Nucleotide Analog Interference mapping of the Hairpin Ribozyme: Implications for Secondary and Tertiary Structure Formation," *Methods*, **18**, 38-50, (1999).
60. Ofengand J. and Bakin A., "Mapping to Nucleotide Resolution of Pseudouridine Residues in Large Subunit Ribosomal RNAs from Representative Eukaryotes, Bacteria, Archaeobacteria, Mitochondria, and Chloroplasts," *J. Mol. Biol.*, **266**, 246-268 (1997).
61. Lane B. G., *Historical Perspectives on RNA nucleoside Modification*. In *Modification and Editing of RNA* (Grosjean, H. and Benne, R., eds.), pp. 20. ASM Press, Washington D.C. (1998).
62. Charette M., Gray M. W., "Pseudouridine in RNA: What, Where, How, and Why". *IUBMB Life* **49** (5): 341-51. PMID 10902565 (2000).
63. Davis F. F. and Allen W. F., "Ribonucleic Acids from Yeast which Contain a Fifth Nucleotide," *J. Biol. Chem.*, **227**, 907-915 (1957).
64. Cohn W. E., "Pseudouridine, a Carbon-Carbon Linked Ribonucleoside in Ribonucleic Acids: Isolation, Structure, and Chemical Characteristics," *J. Biol. Chem.*, **235**, 1488-1498 (1960).
65. Cunningham, P., Lee K., and Holland-Staley C. A., "Genetic Approaches to Studying Protein Synthesis: Effects of Mutations at Ψ 516 and A535 in *Escherichia coli* 16S rRNA," *J. Nutr.*,

131(2001).

66. Ferré-D'Amaré A. R. "RNA-Modifying Enzymes," *Curr. Opin. Struct. Biol.*, **13**, 49-55 (2003).
67. Shapiro R. and Chambers R. W., "Synthesis of Pseudouridine," *J. Am. Chem. Soc.*, **83**, 3920-3921, (1961).
68. Pang H., Ihara M., Kuchino Y., Nishimura S., Gupta R., Woese C. R., and McCloskey J. A. *J. Biol. Chem.*, **257**, 3589-3592, (1982).
69. Robins M. J., Naik S. R., *et al.* "Chemistry of Nucleosides and Nucleotides," *J. Org. Chem.*, **39**, 1891-1899, (1974).
70. Raychaudhuri S., Conrad J., Hall B. G., Ofengand J., "A Pseudouridine Synthase Required for the Formation of Two Universally Conserved Pseudouridines in Ribosomal RNA is Essential for Normal Growth of *Escherichia coli*," *RNA*, **4**, 1407-1417 (1998).
71. Hall R. H., "Isolation of 3-Methyluridine and 3-Methylcytidine from Soluble Ribonucleic Acid," *Biochem. Biophys. Res. Commun.*, **5**, 361-364 (1963).
72. Davis D. R. "Stabilization of RNA Stacking by Pseudouridine," *Nucleic Acids Res.*, **23**, 5020-5026 (1995).
73. Lane B. G., Ofengand J., Gray M. W., "Pseudouridine and O^{2'}-Methylated Nucleosides. Significance of their Selective Occurrence in rRNA Domains that Function in Ribosome-Catalyzed Synthesis of the Peptide Bonds in Proteins," *Biochimie*, **77**, 7-15 (1995).
74. Davis D. R., Poulter C. D., "1H-15N NMR Studies of *Escherichia coli* tRNAPhe from *hist* mutants: A Structural Role for Pseudouridine," *Biochemistry*, **30**, 4223-4231 (1991).

75. Arnez J.G., Steitz T. A., "Crystal Structure of Unmodified tRNA^{Gln} Complexed with Glutamyl-tRNA Synthetase and ATP Suggests a Possible Role for Pseudo-uridines in Stabilization of RNA Structure," *Biochemistry*, **33**, 7560–7567 (1994).
76. Lyons G. I., Alvarez S., Iwata-Reuyl D., and Crécy-Lagard V., "Biosynthesis of 7-Deazaguanosine-modified tRNA Nucleosides: A New Role for GTP Cyclohydrolase," *J. Bacteriol. Epub* **24**, 7876-84 (2008).
77. McCloskey A. J. and Nishimura S., "Modified Nucleosides in Transfer RNA," *Acc. Chem. Res.*, **10**, 403-410 (1977).
78. Agris P. F., "The Importance of Being Modified: Roles of Modified Nucleosides and Mg²⁺ in RNA Structure and Function," *Prog. Nucleic Acid Res. Mol. Biol.*, **53**, 79-129 (1996).
79. Bashan A., Agmon I., Zarivach R., Schluenzen F., Harms J., Berisio R., Bartels H., Franceschi F., Auerbach T., Hansen H. A. S., "Structural Basis of The Ribosomal Machinery for Peptide Bond Formation, Translocation, and Nascent Chain Progression," *Mol. Cell* **11**, 91–102 (2003).
80. Cannone J. J., Subramanian S., Schnare N. M., Collett R. J., D'Souza M. L., Du Y., Feng B., Nan Lin N., Lakshmi V. M., Müller M. K., Pande N., Shang Z., Yu N., and Gutell R. R., "The Comparative RNA Web" *BMC Bioinformatics*, **3**, 2 (2002).
81. Ofengand J., "Ribosomal RNA Pseudouridines and Pseudouridine Synthases," *FEBS Letter.*, **514**, 7-25 (2002).
82. Liiv, A., Karitkina, D., Maivali, U., and Remme J., "Analysis of the Function of *E. coli* 23S rRNA Helix-Loop 69 by Mutagenesis," *BMC Mol. Biol.*, **18**, 1471-2199 (2005).

83. Liang X. H., Liu Q., Fournier M. J. "rRNA Modifications in an Intersubunit Bridge of the Ribosome Strongly Affect Both Ribosome Biogenesis and Activity," *Molecular Cell*, **28**, 965-77 (2007).
84. Ali K. I., Lancaster L., Feinberg J., Joseph S., Noller F. H., "Deletion of a Conserved, Central Ribosomal Inter-subunit RNA Bridge," *Molecular Cell*, **23**, (2006).
85. Schuwirth, B.S., Borovinskaya, M.A., Hau, C.W., Zhang, W., Vila-Sanjurjo, A., Holton, J.M., Cate, J.H.D., "Structures of the Bacterial Ribosome at 3.5 Å Resolution," *Science*, **310**, 827–834 (2005).
86. Wilson, T.J., Ouellet, J., Zhao, Z.-Y., Harusawa, S., Araki, L., Kurihara, T., Lilley, D.M.J., "Nucleobase Catalysis in the Hairpin Ribozyme," *RNA*, **12**, 980–987 (2007).
87. Gabashvili I., Agrawal R., Spahn C. M. T, Grassucci R. A, Svergun D. I, Frank J., Penczek P. "Solution Structure of the *E. coli* 70S Ribosome at 11.5 Å Resolution," *Cell*, **100**, 537-549 (2000).
88. Gao H., Sengupta J., Valle M., Korostelev A., Eswar N., Stagg S. M., Roey P. V., Agrawal R. K., Harvey S. C., Sali A., Chapman M. S., Frank J., "Study of the Structural Dynamics of the *E. coli* 70S Ribosome Using Real-Space Refinement," *Cell*, **113**, 789-801 (2003).
89. Harms J., Schluenzen F., Zarivach R., Bashan A., Gat S., Agmon I., Bartels H., Franceschi F., and Yonath A., "High Resolution Structure of the Large Ribosomal Subunit from a Mesophilic Eubacterium," *Cell*, **107**, 679–688 (2001).
90. Selmer M., Dunham C. M., Murphy F. V. IV, Weixlbaumer A., Petry S., Kelley A.C., Weir J. R., Ramakrishnan V., "Structure of the 70S Ribosome Complexed with mRNA and tRNA," *Science*, **313**, 935–1942 (2006).

91. Wilson D. N., Schulzen F., Harms J. M., Yoshida T., Ohkubo T., Albrecht R., Buerger J., Kobayashi Y., Fucini P., "X-ray Crystallography Study on Ribosome Recycling: The Mechanism of Binding and Action of RRF on the 50S Ribosomal Subunit.," *Embo J.*, **24**, 251-260 (2005).
92. Hirashima A., Kaji A., "Factor Dependent Breakdown of Polysomes," *Biochem. Biophys. Res. Commun.*, **41**, 877–883 (1970).
93. Subramanian A.R., Davis B. D., "Release of 70S Ribosomes from Polysomes in *Escherichia coli*," *J. Mol. Biol.*, **74**, 45–56 (1973).
94. Peske F., Rodnina M. V., Wintermeyer W., "Sequence of Steps in Ribosome Recycling as Defined by Kinetic Analysis," *Mol. Cell.*, **18**, 403–412 (2005).
95. Kotra L. P., Haddad J., Mobashery S., "Aminoglycosides Binding to the Ribosome as Function as Bactericides," *Antimicrob. Agents Chemother.*, **44**, 3249–3256 (2000).
96. Francisco J. A., "The Mechanisms of Evolution," *Sci. Am.*, **65**, 239 (1978).
97. Schlunzen F., Zarivach R., Harms J., Bashan A., Tocilj A., Albrecht R., Yonath A., and Franceschi F. "Structural Basis for the Interaction of Antibiotics with the Peptidyl Transferase Centre in Eubacteria," *Nature*, **413**, 814–821 (2001).
98. Garrett A. R., *The Ribosome: Structure, Function, Antibiotics, and Cellular Interactions*. Washington, DC: ASM Press, (2000).
99. Bruce Chabner B., and Knollman B. *Goodman and Gilman's The Pharmacological Basis of Therapeutics*. 12th Ed. The McGraw-Hill (2011).
100. Anderson K., "Is Bacterial Resistance to Antibiotics an Appropriate Example of Evolutionary Change?" *Creation Research Society Quarterly*, **41**, 318–326 (2005).

101. <http://www.cdc.gov/drugresistance/threat-report-2013> monitor
102. National Research Council, Committee on Drug Use in Food Animals. "The Use of Drugs in Food Animals: Benefits and Risks," Washington (DC): National Academy Press; 1999.
103. Mellon M., Benbrook C., Benbrook K. L., "Hogging It: Estimates of Antimicrobial Abuse in Livestock," Cambridge (MA) Union of Concerned Scientists (2001).
104. Keep Antibiotics Working, "The Health Threat," www.keepantibioticsworking.com
105. <http://www.cdc.gov/drugresistance/threat-report-2013/pdf/ar-threats-2013-508.pdf> \l "page=51
106. "http://www.cdc.gov/drugresistance/threat-report-2013/pdf/ar-threats-2013-508.pdf" \l "page=53"
107. "http://www.fda.gov/downloads/AnimalVeterinary/GuidanceComplianceEnforcement/Guidance%20for%20Industry/UCM299624.pdf" \t
108. Roberts R. B., *Introduction in Microsomal Particles and Protein Synthesis*. New York: Pergamon Press, Inc. (1958).
109. Pai R. D., Zhang W., Schuwirth B. S., Hirokawa G., Kaji H., Kaji A., and Cate J. H., "Structural Insights into Ribosome Recycling Factor Interactions with the 70S Ribosome," *J. Mol. Biol.*, **376**, 1334–1347 (2008).
110. Graham W. D., Scheunemann A. E., and Agris P., "Binding of Aminoglycoside Antibiotics to Helix 69 of 23S rRNA," *FASEB J.*, **23**, 845 (2009).
111. Tuerk C., and Gold L., "Systematic Evolution of Ligands by Exponential Enrichment: RNA Ligands to Bacteriophage T4 DNA-polymerase," *Science*, **249**, 505-510 (1990).
112. Ellington A. D. and Szostak J. W., "*In vitro* Selection of RNA Molecules that Bind Specific

- Ligands. *Nature*, **346**, 818-822 (1990).
113. Prudent J. R., Uno T., Schultz P. G., "Expanding the Scope of RNA Catalysis," *Science*, **264**, 1924-1927 (1994).
114. Robertson D. L. and Joyce G. F., "Selection *In Vitro* of an RNA Enzyme that Specifically Cleaves Single-stranded DNA," *Nature Struct. Biol.*, **344**, 467-468 (1990).
115. Sefah K., Shangguan D., Xiong X., O'Donoghue M. and Weihong T., "Development of DNA Aptamers Using Cell-SELEX," *Nat. Protoc.*, **5**, 1169-1185 (2010).
116. Geiger A., Burgstaller P., Eltz von der H., Roeder A., and Famulok M., "RNA Aptamers that Bind L-Arginine with Sub-Micromolar Dissociation Constants and High Enantioselectivity," *Nucl. Acids Res.*, 1996, **24**, 1029–1036 (1996).
117. Irvine D., Tuerk C., and Gold L., "SELEXION. Systematic Evolution of Ligands by Exponential Enrichment with Integrated Optimization by Non-Linear Analysis," *J. Mol. Biol.*, **222**, 739-761 (1991).
118. Lauridsen L. H., Rothnagel J. A., and Veedu R. N., "Enzymatic Recognition of 2' Modified Ribonucleoside 5'-Triphosphates: Towards the Evolution of Versatile Aptamers," *ChemBioChem*, **13**, 19–25 (2012).
119. Sakamoto T., Oguro A., Kawai G., Ohtsu T., and Nakamura Y., "NMR Structures of Double Loops of an RNA Aptamer Against Mammalian Initiation Factor 4A," *Nucl. Acids Res.* **33**, 745-754 (2005).
120. Chang, K.Y., Tinoco, I., "Characterization of a Kissing Hairpin Complex Derived from the Human Immuno Deficiency Virus Genome," *Proc. Natl. Acad. Sci. USA*, **81**, 8705-8709 (1994).

121. Bartel D. P. and Szostak J. W., "Study of RNA-Protein Recognition by *In vitro* Selection," *In RNA-Protein Interactions*, 248-263, IRL Press (1994).
122. Bischofberger N. and Shea R. G., *Oligonucleotide-Based Therapeutics*. In *Nucleic Acid Targeted Drug Design* (Propst, C.L. and Perum, T.J., eds.), 579-613, Marcel Dekker, Inc (1992).
123. Gold, L., "Conformational Properties of Oligonucleotides," *Nucleic Acids Symposium Series*, **33**, 20-22 (1995).
124. Boiziau C., Dausse E., Yurchenko L. and Toulmé J., "DNA Aptamers Selected Against the HIV-1 Trans-Activation-Responsive RNA Element Form RNA-DNA Kissing Complexes," *The Journal of Biological Chemistry*, **274**, 12730-12737 (1999).
125. Jenison R. D., Gill S. C., Pardi A., Polisky B., "High-Resolution Molecular Discrimination by RNA," *Science*. **263**, 1425-9 (1994).
126. Nucleic Acid Aptamers for Diagnostics and Therapeutics: Global Markets Report Code: BIO071A, Published: March 2010.
127. Ng E. W., Shima D. T., Calias P., Cunningham E. T. Jr, Guyer D. R., Adamis A. P., "Pegaptanib Sodium for Ocular Vascular Disease," *Nat Rev Drug Discov.*, **5**, 123-32 (2006).
128. Hayat A., Marty J. L., "Aptamer Based Electrochemical Sensors for Emerging Environmental Pollutants," *J. Front. Chem.*, **2**, 41 (2014).
129. Brent B., "Aptagen Cultivates Next Move Alternative Business Model has Served it Well, But Now it is Gearing for Growth," *Central Penn Business Journal*, **17**, (2010).
130. Gold L. "Oligonucleotides as Research, Diagnostic, and Therapeutic Agents," *J. Biol. Chem.*, **270**, 13581-13584 (1995).

131. Amaya-Gonzalez S., de-los-Santos-Alvarez N., Miranda-Ordieres J. A., Lobo-Castanon J. A., "Aptamer-Based Analysis: A Promising Alternative for Food Safety Control," *Sensors*, **13**, 16292-16311 (2013).
132. Wlotzka B., "In vivo Properties of an Anti-GnRH Spiegelmer: An Example of an Oligonucleotide-Based Therapeutic Substance Class," *Proc. Natl. Acad. Sci. U.S.A.*, 8898-8902 (2002).
133. Bischofberger N. and Shea R. G., *Oligonucleotide-Based Therapeutics In Nucleic Acid Targeted Drug Design* (Propst, C.L. and Perum, T.J., eds.), 579-613, Marcel Dekker, Inc. (1992).
134. Zuker M., "Mfold Web Server for Nucleic Acid Folding and Hybridization Prediction," *Nucleic Acids Res.*, **31**, 3406-3415 (2003).
135. Goodman and Gilman's Manual of Pharmacology and Therapeutics (2008) The McGraw-Hill Companies, Inc. ISBN 978-0-07-144343-2.
136. Roberts R. B., *Introduction in Microsomal Particles and Protein Synthesis*. New York: Pergamon Press, Inc. (1958).
137. Pai R. D., Zhang W., Schuwirth B. S., Hirokawa G., Kaji H., Kaji A., and Cate J. H., "Structural Insights into Ribosome Recycling Factor Interactions with the 70S Ribosome," *J. Mol. Biol.*, **376**, 1334-1347 (2008).
138. Graham D., Scheunemann W., Elizabeth A., Agris P. "Binding of Aminoglycoside Antibiotics to Helix 69 of 23S rRNA," 23 Meeting Abstract Supplement 845.4 *FASEB J.* (2009).
139. Maivali U., Remme J., "Definition of Bases in 23S rRNA Essential for Ribosomal Subunit Association," *RNA*, **10**, 600-604 (2004).

140. Boiziau C., Dausse E., Yurchenko L. and Toulmé J. J., "DNA Aptamers Selected Against the HIV-1 trans-Activation-responsive RNA Element Form RNA-DNA Kissing Complexes," *The Journal of Biological Chemistry.*, **274**, 12730-12737 (1999).
141. Chui H. M., Meroueh M., Scaringe S.A., and Chow C. S., "Synthesis of a 3-Methyluridine Phosphoramidite to Investigate the Role of Methylation in a Ribosomal RNA Hairpin," *Bioorg. Med. Chem.*, **10**, 325-32 (2002).
142. https://tools.lifetechnologies.com/content/sfs/manuals/ta_man.pdf
143. Larkin A. M., Blackshields G., Brown P. N., *et al.*, "Clustal W and Clustal X version 2.0," *Bioinformatics*, **23**, 2947-2948 (2007).
144. Thompson J. D., Higgins D. G., Gibson T. J., "Clustal W: Improving the Sensitivity of Progressive Multiple Sequence Alignment through Sequence Weighting, Position-Specific Gap Penalties and Weight Matrix Choice." *Nucleic Acids Res.*, **22**, 4673– 4680 (1994).
145. Connors K. A., *Binding Constants: The Measurement of Molecular Complex Stability*, John Wiley & Sons, New York (1987).
146. Kaur M., Rupasinghe C. N., Klosi E., Spaller M.R., and Chow C. S., "Selection of Heptapeptides that Bind Helix 69 of Bacterial 23S Ribosomal RNA," *Bioorg. Med. Chem.*, **21**, 1240-7 (2013).
147. Sakakibara Y., Abeysirigunawardena C. S., Duc. E. A., Dremann D. N., Chow C. S., "Ligand- and pH-Induced Conformational Changes of RNA Domain Helix 69 Revealed by 2-Aminopurine Fluorescence," *Angew. Chem. Int. Ed.*, **51**, 12095-12098 (2012).
148. Hoogsteen K., "The Crystal and Molecular Structure of a Hydrogen-bonded Complex between 1-methylthymine and 9-methyladenine," *Acta Crystallographica*, **16**, 907–916

(1963).

149. Lee S. H. "Increased Urinary Level of Oxidized Nucleosides in Patients with Mild-To-Moderate Alzheimer's Disease," *Clin. Biochem.*, **40**, 936–938 (2007).
150. Sumita, M. Jiang J. SantaLucia J. Jr. Chow C. S., "Comparison of Solution Conformations and Stabilities of Modified Helix 69 rRNA Analogues from Bacteria and Human", *Biopolymers*, **97**, 94–106 (2012).

ABSTRACT**DNA APTAMERS SELECTED AGAINST WILD-TYPE HELIX 69 RIBOSOMAL RNA AND THEIR IMPLICATIONS IN COMBATING ANTIBIOTIC RESISTANCE**

by

SAKINA MIRIAM HILL**MAY 2015****Advisor:** Christine S. Chow, Ph.D.**Major:** Chemistry (Biochemistry)**Degree:** Doctor of Philosophy

Outbreaks of advanced antibiotic-resistant strains of microbes have increased the need to identify new viable molecular targets for the development of novel anti-infectives. For this purpose, helix 69 (H69, or $\Psi m^3\Psi\Psi$), a 19 nucleotide (19-nt) hairpin motif that is highly conserved throughout phylogeny and rich in modified nucleotides, including pseudouridine (Ψ) and 3-methylpseudouridine ($m^3\Psi$) was chosen as a potential target. Helix 69, which is located in domain IV of Escherichia coli 23S ribosomal RNA (rRNA), undergoes conformational changes when in close proximity to the decoding region of 16S rRNA and transfer RNAs (tRNAs) in the peptidyl-transferase center (PTC). The exact biological role(s) of H69 remain(s) unclear; however, its proposed importance within protein synthesis may support it as an ideal target to develop ligands with high binding specificity.

In this thesis work, DNA aptamer candidates with binding specificity for wild-type bacterial H69 were selected. The 84-nt long DNA aptamer (H69DNAapt18) that was identified from a DNA library with a 40-nt randomized region has the sequence 5'-CTCCCCGGGCACTATTTCTGGGACTAGTTCTGCAGGTT-3'. The initial library contained 5×10^{14} DNA sequences and was used in systematic evolution of ligands by exponential enrichment (SELEX) and exhibited a molecular diversity of reduction of $\sim 1 \times 10^2$ after 11 rounds of *in vitro* selection. A synthetic construct of H69 was biotinylated and used with optimized SELEX. After immobilization of the biotinylated target H69 to streptavidin-coated surfaces, DNA library candidates were challenged against H69 in multiple rounds of selection, recovered, and enriched by direct-bead polymerase chain reactions. Levels of bound DNA and diversity of the amplified library pools were monitored by UV-Visible spectroscopy and sequencing between rounds of SELEX (11 total). Select rounds were cloned and sequenced. Consensus sequences from select rounds of SELEX were identified by using Clustal W alignments, and optimal secondary structures were predicted by *Mfold* analysis. Analysis of 120 clones led to the identification of 20 sequences with consensus motifs. Notably, one of the selected DNA ligands (H69DNAapt18) contained a conserved 20-nt hairpin-loop motif with complementarity to the loop region of the targeted *E. coli* wild-type H69. Interestingly, this 20-nt hairpin motif of H69DNAapt18 retained its conserved 20-nt motif within the truncated 40-nt *Mfold* structural prediction representing only the randomized region of the 84-nt DNA library.

Attempts to determine binding affinities of select isolated DNA aptamer candidates to ^{32}P -radiolabeled H69 by electrophoretic mobility shift assays (EMSAs) were moderately successful,

with observation of RNA-DNA complexes with apparent dissociation constants (K_d s) in the high nM range. To better evaluate the affinity and selectivity of DNA aptamer #18, a fluorescently tagged H69-DNA aptamer #18 (FAM-H69DNAapt18) was used for a comparison binding study with wild-type H69 and unmodified rRNA constructs. Relative dissociation constants of FAM-H69DNAapt18 for H69 and RNAs other than H69, as determined by fluorescence titrations with small RNA constructs, are as follows: wild-type H69 < partially modified H69 < unmodified H69 < A-site RNA of 16S rRNA.

Overall, this study provides a reference point for the development of DNA aptamers that identify modified nucleosides and/or methylation sites in RNA, or could potentially function as novel therapeutics to help combat antibiotic resistance.

Keywords: 23S ribosomal RNA (rRNA); helix 69 (H69); modified nucleosides; pseudouridine (Ψ); 3-methylpseudouridine ($m^3\Psi$); peptidyl-transferase center (PTC); systematic evolution of ligands by exponential enrichment (SELEX); DNA aptamers; fluorescence spectroscopy; DNA/RNA complexes; dissociation constants (K_d s); anti-infectives; antibiotic resistance; novel antibacterial therapeutics; and bioprobes.

AUTOBIOGRAPHICAL STATEMENT

SAKINA M. HILL

EDUCATION

Wayne State University: Detroit, MI Ph.D. (2015) – NIH Research Fellow

Michigan Technological University: Houghton, MI (1999-2001) - Graduate Research Fellow

Alma College: Alma, MI Bachelors of Science (1997) - Dow Chemical Research Fellow

RESEARCH EXPERIENCE

- | | |
|--|------------------------------|
| Wayne State University, Department of Chemistry, Detroit, MI | Research Fellow |
| Dissertation research: Isolation and characterization of DNA aptamers for helix 69 | |
| Real DNA Solutions, LLC - Grosse Pointe, MI (2005-2015) | CEO/Owner |
| Development of DNA diagnostic products for legal applications. | |
| Veterans Affairs Medical Ctr., Detroit, MI (06/98-04/99) | Biological Technician |
| Mesothelioma lung cancer research and design and set-up of new governmental research lab. | |
| Michigan Tech University - Houghton, MI (09/99 - 09/00) | Research Assistant |
| <i>Lilium longiflorum</i> alkaline phytase molecular characterization. | |
| American Diagnostica - Greenwich, CT (12/97 - 04/98) | Lab Assistant |
| Research and development of blood clotting factor diagnostic kits | |
| Alma College, Department of Biochemistry, Alma, MI (1993-1996) | Research Assistant |
| <ul style="list-style-type: none"> • Environmental chemistry survey (Cairo, Egypt) • DNA sequence homology analysis of <i>Tribolium</i> flour-beetles genomes • Analytical chemical survey of Bass Lake (Shepard, MI) | |
| Dow Chemical Co. Specialty Chemicals S&D - Midland, MI (1996) | Summer Intern |
| Patent development of antimicrobial surfactant formulations for commercial applications | |
| Metropolitan Center for High Technology- Detroit, MI (1995) | Research Assistant |
| Heavy metal toxicity of monkey kidney cells. | |
| Dow Chemical Co. Polyurethanes R&D – Freeport, TX (1994) | Summer Intern |
| HFC-134a replacements of chlorofluorocarbons (CFCs) in polyurethane formulations. | |

TEACHING EXPERIENCE

- Wayne State University – Graduate teaching assistant (Biochemistry and Chemistry)**
- Michigan Technological University - Graduate teaching assistant (Chemistry)**
- EDUSTAFF, LLC - Substitute K-12 instructor (General Chemistry and Biology)**

RESEARCH TECHNIQUES

- Nucleic Acid Isolation and Purification and Polymerase Chain Reactions (PCR)
- Aptamer Development (SELEX)
- Molecular Cloning and Cell/Tissue Culturing and DNA Sequencing (CEQ)
- Alignment Algorithmic Programs: InsightII Homology, Finch and Clustal W
- Biotin Labeling, Radiolabeling and Electrophoretic Mobility Shift Assays (EMSA)
- Matrix-Assisted Laser Desorption/Ionization Mass Spectrometry (MALDI-MS)
- Product Development/Patent Development (*i.e.*, Antimicrobials, Diagnostic Kits)